CANOPY REFLECTANCE MODELING IN A TROPICAL WOODED GRASSLAND

Principal Investigator: David Simonett, Professor of Geography

Department of Geography, University of California, Santa Barbara, CA 93106

FINAL REPORT

NASA Award NAGW-788

June 13, 1988

Report prepared by Janet Franklin

CANOPY REFLECTANCE MODELING IN A TROPICAL WOODED GRASSLAND

(Report prepared by Janet Franklin)

Final Report NASA Award NAGW-788

ABSTRACT

The Li-Strahler canopy reflectance model, driven by Landsat Thematic Mapper (TM) data, provided regional estimates of tree size and density in two bioclimatic zones in West Africa. This model exploits tree geometry in an inversion technique to predict average tree size and density from reflectance data using a few simple parameters measured in the field (spatial pattern, shape, and size distribution of trees), and in the imagery (spectral signatures of scene components). Trees are treated as simply-shaped objects, and multispectral reflectance of a pixel is a function of the proportion of tree crown, shadow, and understory in the pixel. These, in turn, are a direct function of the number and size of trees, the solar illumination angle, and the signatures of crown, shadow and understory. Because the inversion is quite sensitive to correct determination of component signatures, predictions of size and spacing are not very accurate within small (e. g., 200-400 ha) areas. However, individual errors cancel when larger regions are considered, and the procedure has the potential to predict size and density of trees over large areas of open woodland with good accuracy.

Reflectance properties of the trees were measured in the study sites using a pole-mounted radiometer. The measurements showed that the assumptions of the simple Li-Strahler model are reasonable for these woodlands; canopy spectral components, shadowed and sunlit tree crown and understory, have distinct reflectance characteristics in red and infrared wavebands. The field radiometer measurements were used to calculate the normalized difference vegetation index (NDVI), and the integrated NDVI over the canopy was related to crown volume.

Predictions of tree size and density from the canopy model were used with allometric equations from the literature to estimate woody biomass and potential foliar biomass for the sites and for the regions. Estimates were compared with independent measurements made in the Sahelian sites, and to typical values from the literature for these regions and for similar woodlands. If combined with a vegetation stratification at the appropriate scale, this approach could provide regional estimates of woody biomass for fuelwood inventory. Estimates of foliage biomass could be used in forage production modeling and inventory. Both could be used in regional and global scale models of biogeochemical cycling.

In order to apply the inversion procedure regionally, an area must first be stratified into woodland cover classes, and dry-season TM data have also been used to generate a stratum map of the study areas with reasonable accuracy. The method used was unsupervised classification of multi-date principal components images. While initial classification results were poor, accuracy was comparable with results reported in the literature for Level III land cover classes when a lenient accuracy criterion was used. When sample points identified as being one density class higher or lower that classified were counted as correct, overall accuracy was around 90 percent, and class accuracy was greater than 80 percent for most classes. Contextual classification or spatial/spectral image segmentation will be more powerful techniques than per-pixel classification for stratification of complex vegetation patterns when they are commonly available as part of image processing systems. However, results based on conventional digital image processing techniques are nonetheless useful. The accuracy achieved is adequate for stratification of woody biomass at a regional scale.

PREFACE

February 11, 1796. About noon we saw at a distance the capital of Kaarta, situated in the middle of an open plain — the country for two miles around being cleared of wood by the great consumption of that article for building and fuel... (Park 1893)

The city of Kaarta was located in the Sahel, in what is now northwestern Mali. This quote illustrates that land degradation caused by human land use patterns is not just a modern problem. However, human development and technology have reached the scale where the global climate, and even the survival of the planet is threatened. Now more than ever before there is a need for accurate baseline data on the type and condition of landcover for large areas of the earth (NASA 1983, Houghton et al. 1983, Woodwell 1984). Terrestrial biota greatly affect the climate, energy budget, hydrologic cycle and biogeochemistry of the Earth, and are in turn affected by these processes. Quantifying the effects of human impact on the biosphere requires a greatly improved understanding of the influence of human-induced changes in land cover (such as deforestation, "desertification," and conversion of land to agricultural and urban uses) on the spatial and temporal dynamics of terrestrial vegetation. This understanding may in turn help resource planners improve land use practices in areas where degradation of range and farmland and loss of fuelwood contributes to problems of starvation and disease.

Global land-cover information is traditionally derived from small-scale vegetation maps and FAO statistics, and more recently from satellite imagery (Tucker et al. 1985, Justice et al. 1985, Matthews 1983). These estimates vary considerably, due to lack of consistency between data sources, particularly concerning classification and methodology (Ajtay et al. 1979, Matthews 1983). The accurate assessment of land cover and biophysical parameters of woody vegetation, such as productivity, biomass, albedo, canopy height (surface roughness), surface temperature, and evapotranspiration, are important for determining the relationship between the land surface and the atmosphere and for driving models of climate, energy balance and biogeochemical cycling (Botkin *et al.* 1984, Hobbie *et al.* 1984).

Degradation of arid and semi-arid ecosystems has accelerated in recent years due to increased human use for fuel and food production, coupled with climatic fluctuation. Degradation is defined as a reduction in perennial phytomass and ecosystem productivity, elimination of woody cover, soil exposure, compaction, and erosion, and loss of stored nutrients and carbon (Dregne 1983, Petrov 1976, Vinogradov 1980, Reining 1978, and Hare

1983). This has occurred in sub-Saharan Africa, particularly the Sahel, in the last two decades.

In the development of remote sensing techniques for vegetation assessment, the spectral vegetation indices and transforms that have been applied successfully to estimate vegetation amount in agricultural and grassland ecosystems do not work as well in forests and semi-arid woodlands, bush, and shrublands, because the bulk of the biomass is not green biomass but in the woody structures. Absorption and shadowing by woody parts and the amount of bare soil visible has a complicated effect on greenness measures. Thus, it is important to account for the ecosystem architecture. Further, the information classes in remotely sensed scenes of arborescent landscapes are composed of spectral mixtures of objects (such as trees, shrubs, grass, and soil) and form a mosaic at the scale of satellite sensor resolution.

We have tested a geometric/optical canopy reflectance model which exploits the canopy geometry in an inversion technique to predict tree height and density. This model was applied in a savanna ecosystem, an ecosystem of great importance in terms of global ecology and human utilization.

This report summarizes the research supported primarily by NASA under Grant NAGW-788. Additional support was provided through a NASA Training Grant (NGT 05-010-804), and a UCSB General Affiliates Dissertation Year Fellowship. Each section describes a separate experiment or phase of the research. The figures, tables and references for each part appear at the end of that section. We have tried keep the redundancy among sections to a minimum, but there will be some repetition of introductory material. Section 1 also comprised the Final Report for NASA Training Grant NGT 05-010-804, and has been accepted for publication by *IEEE Transactions on Geoscience and Remote Sensing*, with Janet Franklin, and Alan Strahler as authors, and with NASA's support acknowledged. This report also serves as the doctoral dissertation submitted by Janet Franklin to the Department of Geography, University of California at Santa Barbara.

References

Ajtay, G. L, Ketner, P., and Duvigneaud, P., "Terrestrial primary production and phytomass," in *The Global Carbon Cycle*, ed. B. Bolin, E.T. Degens, S. Kempe and P. Ketner, pp. 129-181, SCOPE 13, John Wiley and Sons, New York, 1979.

Botkin, D. B., Estes, J. E., MacDonald, R. M., and Wilson, M. V., "Studying the Earth's vegetation from space," *BioScience*, vol. 34, pp. 508-514, 1984.

Curran, P., "Multispectral remote sensing of vegetation amount," *Progress in Physical Geography*, vol. 4, pp. 315-341, 1980.

Dregne, H. E., *Desertification of Arid Lands*, Elsevier, New York, 1983. 242 pp.

Hare, F. K., "Climate on the desert fringe," in *Mega-Geomorphology*, ed. R. Gardener and H. Scoging, pp. 134-151, Clarendon Press, Oxford, 1983.

Hobbie, J., Cole, J., Dungan, J., Houghton, R. A., and Peterson, B., "Role of the biota in the global CO_2 balance: The controversy," *BioScience*, vol. 34, pp. 492-498, 1984.

Houghton, R. A., Hobbie, J. E., Melillo, J. M., Moore, B., Peterson, B. J., Shaver, G. R., and Woodwell, G. M., "Changes in the carbon content of the terrestrial biota and soils between 1860 and 1980: A net release of carbon to the atmosphere," *Ecological Monographs*, vol. 53, pp. 235-262, 1983.

Jensen, J., "Biophysical remote sensing," *Annals of the Association of American Geographers*, vol. 73, pp. 111-132, 1983.

Justice, C. O., Townshend, J. R. G., .Holben, B. N, and .Tucker, C. J, "Analysis of the phenology of global vegetation using meteorological satellite data," *International Journal of Remote Sensing*, vol. 6, pp. 1271-1318, 1985.

Matthews, E., "Global vegetation and land use: New high-resolution data bases for climatic studies," *Journal of Climate and Applied Meteorology*, vol. 22, pp. 474-487, 1983.

NASA, "Land-Related Global Habitability Science Issues," NASA Technical Memorandum 85841, National Aeronautics and Space Administration, July, 1983.

Park, M., *Travels in the interior of Africa*, Cassell and Co., Paris, 1893.

Petrov, M. P., "Problems preventing the development of deserts and semideserts and their conservation," *Problemy Osvoeniya Pustyn*, vol. 3-4, 1976.

Reining, P., *Handbook of Desertification Indices*, Am. Assoc. Adv. Science, Washington, D.C., 1978.

Tucker, C. J., Townshend, J. R. G., and Goff, T. E, "African land-cover classification using satellite data," *Science*, vol. 277, pp. 369-375, 1985.

Vinogradov, B. V., "Indicators of desertification and their aerospace monitoring," *Problemy Osvoeniya Pustyn*, vol. 4, pp. 14-23, 1980.

Woodwell, G. M., *The Role of Terrestrial Vegetation in the Global Carbon Cycle*, p. 247, Wiley, New York, 1984.

ACKNOWLEDGEMENTS

We would like to thank Li Xiaowen for his continuing efforts to modify the formulation of his model for our applications, for advise and recommendations regarding the model, and for allowing us to use unpublished data. We are indebted to Alan Strahler, Joel Michaelsen, Jeff Dozier and Julia Jones, who provided sound advice many steps along the way, and who greatly improved this report with their comments. We would also like to thank Aaron Goldschmidt, Chen Jian, Doug Grice, Frank Davis and David Lawson for their contributions.

The fieldwork in the Gourma was conducted with the permission and support of ILCA/Mali, Dr. Abdelkader Diallo, Director. We are grateful to Pierre Hiernaux and his colleagues at ILCA/Mali, particularly Lassine Diarra, Mohamed Idriss Cissé, Aboubakrine Mahamar and Issouf Maiga, for their cooperation, collaboration and support in the field. Dramane Diarra and Dramane Dembéle also assisted with the field work in Mali. The fieldwork in the Region of Ségou was conducted with authorization of the National Ministry of Education, Mali. We would like to thank Roy Cole for facilitating my field work in Ségou Region. The hospitality extended to us by Moussa Traoré and his family was a true lesson in how human beings should behave towards one another.

We would like to express our appreciation to Chris Justice and the GIMMS personnel at NASA Goddard for their cooperation and support, and to Bob Murphy, Jim Tucker, and Jim Smith for sponsoring Janet Franklin as a NASA Graduate Student Researcher. Stephen Prince and Niall Hannan of Queen Mary College, University of London, have been a joy to collaborate with.

Table of Contents

Chapter 1

INVERTIBLE CANOPY REFLECTANCE MODELING OF VEGETATION STRUCTURE IN SEMIARID WOODLAND

Abstract

The Li-Strahler canopy reflectance model, driven by Landsat Thematic Mapper (TM) data, provided regional estimates of tree size and density within twenty percent of sampled values in two bioclimatic zones in West Africa. This model exploits tree geometry in an inversion technique to predict average tree size and density from reflectance data using a few simple parameters measured in the field (spatial pattern, shape, and size distribution of trees) and in the imagery (spectral signatures of scene components). Trees are treated as simply shaped objects, and multispectral reflectance of a pixel is assumed to be related only to the proportions of tree crown, shadow, and understory in the pixel. These, in turn, are a direct function of the number and size of trees, the solar illumination angle, and the spectral signatures of crown, shadow and understory. Given the variance in reflectance from pixel to pixel within a homogeneous area of woodland, caused by the variation in the number and size of trees, the model can be inverted to give estimates of average tree size and density. Because the inversion is sensitive to correct determination of component signatures, which is a difficult procedure at best, predictions of size and spacing are not very accurate within small (e. g. 10-100 ha) areas. However, individual errors cancel when larger regions are considered, and the procedure may predict size and density of trees over large areas of open woodland with good accuracy.

I. INTRODUCTION

REMOTELY sensed data are commonly used to produce thematic land-cover maps, but also can provide quantitative information on biophysical variables, such as vegetation structure, amount, productivity, (reviewed in [1] and [2]), photosynthesis, and transpiration [3] [4]. These biophysical characteristics of vegetation and their spatial and temporal distribution are critical inputs to ecological models that describe the interaction between the land surface and climate, energy balance, and hydrologic and biogeochemical cycles [5] [6] [7] [8] [9] [10] [11]. Remote sensing provides the only tool that can measure these variables for large areas [12] [13] [14]. In this paper we use a canopy reflectance model and multispectral satellite data to estimate canopy structure in sparse woodland, a vegetation type of great spatial extent and importance.

A family of mathematical models of the reflectance of a plant canopy composed of discontinuous woody cover allows the direct estimation of plant size and density from remotely sensed reflectance data [15]. These Li-Strahler models are geometric in character, treating trees (plants) as solid, discrete, three-dimensional objects on a contrasting background. They use geometric optics to estimate the proportion of each pixel in tree canopy, shadow, and background. In the simplest model, tree density is assumed to be sufficiently low that the overlapping of trees and shadows may be ignored. Using this simple model, Li and Strahler [15] predicted tree size and density from Landsat MSS data within ten percent of actual values for sparse pine forest in northern California.

We have extended this model and tested it using Landsat Thematic Mapper (TM) data in a different environment where the basic assumptions of the model hold, but the parameters must be modified. The model was tested in sparse woodland and wooded grassland in the Sahelian and Sudanian bioclimatic zones in West Africa.

II. BACKGROUND

In plant canopy reflectance modeling, radiative transfer theory and geometric optics are used to predict the reflectance of a plant canopy as a function of the biophysical properties of the canopy elements, such as the size, shape, spatial distribution and optical properties of plants or plant parts. If a reflectance model can be mathematically inverted, the biophysical properties of the plant stand can be

inferred from spectral reflectance measurements. The simple Li-Strahler model describes reflectance as a function of vegetation structure for a canopy composed of large woody plants distributed at low density on the landscape. The model represents an early formulation of a general modeling approach which explicitly treats the interaction of three-dimensional illuminated discrete objects with the spatial sampling interval imposed by a digital image [16] [17] [18] [19] [20] [21] [22]. In the simple model it is assumed that the canopy is imaged by a multispectral scanner with pixel size several times larger than tree size, but with resolution fine enough that the sampling unit interacts with the size and placement of the trees. Thus, the model predicts variance as well as average reflectance. It uses covariance statistics from estimated mixtures of scene components across pixels for inversion to predict average tree size and density in a stand. While other canopy models are invertible, most predict the bidirectional reflectance distribution function (BRDF) of a canopy, and in inversion use field or aircraft radiometric measurements from varying look angles to predict some property of the vegetation, such as Leaf Area Index (LAI) [23] [24] [25] [26] [27], or leaf reflectance [28]. The Li-Strahler model is different from these other models in that it explicitly considers discretely distributed trees.

A. Formulation of the Canopy Model

The simple Li-Strahler model is discussed in detail elsewhere [15] [29] and will be reviewed in this section for clarity. The only modification to the simple model is the change in the shape parameter. The model assumes that a woodland stand can be modeled geometrically as a group of solid objects (trees) with simple shapes, casting shadows on a contrasting background (understory, grass or soil). Furthermore:

— A tree crown is a simple geometric form. In the sparse woodland, we use an ellipsoid on a stick (Fig. 1) for trees of all sizes.

— Tree counts vary from pixel to pixel as a Poisson function with a fixed density, i. e., the spatial pattern is random at the scale of sensor resolution.

— The size distribution function of trees is known, so that C_{r2}, the coefficient of variation of squared crown radius, can be determined for the stand.

— The tree crown and its associated shadow have spectral signatures that are distinct from that of the background.

The reflectance of a pixel is modeled as a linear combination of the signatures of scene components (illuminated tree crown, illuminated background, shadowed tree, and shadowed background) weighted by their relative areas. Pixels from an area of homogeneous tree cover can be used to estimate average reflectance of a stand of a given density. Interpixel variance exists because the number of trees per pixel and their size distribution vary. In the simple model, we ignore overlapping of trees and shadows, which would also produce pixel-to-pixel variance. Other proportion estimation models similarly predict cover as a function of brightness in canopies with incomplete cover [30] [31] [32] [33] [34] [35]. This effect has been modelled by Otterman [36] [37]. However, the Li-Strahler model solves for tree size and density using the distribution functions and statistical independence of these two parameters.

1) Model Parameters: The variables describing the stand are:

A Area of a pixel.

n Number of trees in a pixel.

N Average density of trees per m^2 in a stand ($= \overline{n}\,/A$).

r^2 Squared crown radius of tree.

R^2 Average r^2 for a pixel.

$\mathbf{R}^2$ Average R^2 for all pixels in a stand.

C_{r^2} Coefficient of variation of squared crown radius determined for stand.

m $= N\ \mathbf{R}^2$.

Note that since $\pi\ \mathbf{R}^2$ is the average area of a crown, $m\,\pi$ is the proportion of woody cover in the stand.

As a three dimensional object, the ellipsoid on a stick casts a shadow on the background. To quantify the area of canopy and shadow, a geometric factor, Γ, is used. Γ is defined such that $m\,\Gamma$ is the proportion of a pixel covered by tree crown and shadow (i. e., the tree cover adjusted to include shadowing). Based on the geometry of an ellipsoid illuminated at solar zenith angle θ (Fig. 1),

$$\Gamma = \pi + \frac{\pi}{\cos\theta'} - A_0$$

where

$$A_0 = \begin{cases} 0\,, & \text{if } (b\ +\ h\,)\tan\theta > r\left(1 + \dfrac{1}{\cos\theta'}\right), \\ r^2\left(\beta - \tfrac{1}{2}\sin 2\beta\right)\left(1 + \dfrac{1}{\cos\theta'}\right) & \text{else} \end{cases}$$

and

$$\beta = \cos^{-1}\left[\left(1 + \frac{h}{b}\right)\left(\frac{1 - \cos\theta'}{\sin\theta'}\right)\right],$$

and

$$\theta' = \tan^{-1}\left(\frac{\tan\theta}{(r/b)}\right).$$

While we tested the model in areas of flat terrain, it is a simple modification to adjust the shadowing geometry for a sloping surface [38]. If A_g, A_c, A_z, and A_t are the areas of sunlit background and crown, and shadowed background and crown within the pixel, then

$$A_c + A_t + A_z = m\,\Gamma$$

and

$$A_g = 1 - m\,\Gamma.$$

The signature of pixel i in band j, S_{ij}, is then modeled as

$$S_{ij} = (A_g \cdot G_j) + (A_c \cdot C_j) + (A_z \cdot Z_j) + (A_t \cdot T_j) \quad (1)$$

where G, C, Z and T are the reflectance signatures for a unit area of sunlit background and crown, and shadowed background and crown, respectively. Equation (1) can be written

$$S_{ij} = A_g \cdot G_j + (1 - A_g) \cdot X_0$$

where X_0 is the average reflectance of a tree and its associated shadow.

Fig. 2 (modified from [15]) shows an idealized plot of the four spectral components on greenness (i.e., infrared to red contrast) and brightness spectral axes. A bright soil background (G) has high brightness and low greenness, and sunlit canopy (C) has high greenness and is less bright than the background. Shadowed canopy (T) and background (Z) are less bright and less green. The composite tree signature X_0 falls within the triangle CTZ. When cover is low, the pixel signature S varies along the line GX_0 with distance from G proportional to tree cover (m). However, as cover increases, the proportion of

shadowed background decreases and the relative proportion of sunlit crown increases. This occurs because shadows fall on the near-vertical sides of trees instead of the background, and are thus less visible from nadir. At full canopy closure, only sunlit and shadowed crowns are present. The composite tree signature is then X_∞, which falls on the line TC. As coverage increases, the signature will thus diverge from the line GX_0 toward X_∞, and the simple (linear) model is no longer appropriate.

Substituting the expressions for A_g and $(1 - A_g)$, dropping the subscripts in (1) for convenience, and solving for m we have for each pixel

$$m = \frac{G - S}{\Gamma(G - X_0)} . \tag{2}$$

From (2) we can derive the variance of m :

$$V(m) = \frac{V(S)}{\Gamma[(G - X_0)]^2} . \tag{3}$$

where $V(S)$ is the variance in reflectance for all pixels in the stand.

For multiple spectral bands m should be the same if determined from any band. However, variance in the signatures and stand parameters will cause m to vary, and thus m can be taken as a weighted average or selected as the median value.

2) Model Sensitivity: The sensitivity of this model to noise in S and the component signatures, and to errors in estimation of parameters, can be shown by taking the partial derivative of m with respect to these variables.

$$\frac{\partial m}{\partial S} = \frac{-1}{\Gamma(G - X_0)}$$

$$\frac{\partial m}{\partial G} = \frac{S - X_0}{\Gamma(G - X_0)^2} \approx \frac{1}{\Gamma(G - X_0)} \quad \text{(because when cover is low } S \approx G \text{)}$$

$$\frac{\partial m}{\partial X_0} = \frac{G - S}{\Gamma(G - X_0)^2} = \frac{m}{G - X_0}$$

$$\frac{\partial m}{\partial \Gamma} = \frac{S - G}{\Gamma^2(G - X_0)} = \frac{-m}{\Gamma}$$

When the spectral contrast between background and tree is high, sensitivity to noise in S, G and X_0 will be reduced, because $(G - X_0)$ is in the denominator. When density is low (m is small), noise or error in estimating X_0 and Γ are less important than the contrast between tree and background $(G - X_0)$, because m is in the numerator.

3) Inversion of the Model: If size and density are independent, then the expressions for the mean and variance of independent products can be applied ([15] p. 709). If $V(R^2) = V(r^2)/n \approx V(r^2)/N$, then

$$V(m) \approx (N + C_{r2}\,N + C_{r2})(\mathbf{R}^2)^2 = (M + C_{r2}\,M + C_{r2}\,\mathbf{R}^2)\mathbf{R}^2 \tag{4}$$

where M is the average m in the stand. Solving for $\mathbf{R}^2$, we obtain:

$$\mathbf{R}^2 = \frac{[(1 + C_{r2})^2\,M^2 + 4V(m)C_{r2}]^{1/2} - (1 + C_{r2})M}{2C_{r2}}. \tag{5}$$

Applying the approximation $\sqrt{1+x} \approx 1 + x/2$, we obtain:

$$\mathbf{R}^2 \approx \frac{V(m)}{(1 + C_{r2})M}. \tag{6}$$

This should be reasonably accurate if $V(m)$ is fairly large. Finally, substituting (2) and (3), the expressions for mean and variance of m, into (5) or (6), $\mathbf{R}^2$ and N can be found from the reflectance values of the pixels in a stand.

III. Study Sites in Mali

The Li-Strahler model was originally developed and tested for sparse pine woodland in northeastern California. However, there are many other landscapes for which the assumptions of the model hold: *Acacia* and broadleaf savanna or woodland in Africa also consist of trees at low density, with a uniform, contrasting understory of grass or soil at some point in the annual cycle. Further, the plants can be regarded as having simple shapes, invariant with size, and with little overlap, thus casting shadows that can be predicted from tree geometry and sun angle. Savanna canopies are more translucent than conifers, having lower LAI, and cast weaker shadows. The simple model is still applicable because the components' signatures are calibrated from the imagery, although the contrast between G and X_0 will be reduced in this woodland type.

Woodland and savanna, or wooded grassland, will be defined as the subtropical and tropical vegetation formations where the grass stratum is continuous, trees and shrub cover is greater than five percent and less than eighty percent, where fire occurs, and where the growth is closely associated with alternating wet and dry seasons [39]. We chose to test the model for woodland sites in Africa because of the global extent and importance of this physiognomic type. Woodland and wooded grassland cover ten to twenty percent of the land surface, greater than any other surface cover type (except desert and ice) [40]. Dry woodlands and wooded savanna (with tree cover greater than ten percent) are presently estimated to cover 486.4 million ha or 22.2 percent of the continent of Africa, including 8.6 million ha in Mali [41]. Woodlands are often monospecific (one or two dominant types of trees) or nearly so, of low density, have a uniform herbaceous understory, and occur over extensive areas of flat terrain.

We tested the model in study sites in the Sahelian and Sudanian bioclimatic zones in Mali, West Africa (Fig. 3). The Sahel is usually defined with reference to mean annual isohyets and corresponds to the 200-600 mm annual precipitation zone [42] [43] [44] [45] [46]. The vegetation of the Sahel ranges from an open annual grassland with less than ten percent woody cover in the north to perennial grasses with 25 percent or more tree cover in the south. In the Sahelian zone in northern Mali, four test sites were located in the Gourma region, three from among those being monitored by ILCA/Mali (The International Livestock Centre for Africa) in collaboration with the GIMMS Project (Global Inventory, Monitoring and Modeling System; National Aeronautics and Space Administration, Goddard Space Flight Center) [47] [48] [49] [50]. The fourth site was added in this study. Although tree cover is generally low in the Sahel, woodlands are locally dense in low-lying inundated areas, and all of our sites were located in these dense woodland stands (thirty to sixty percent cover). Three of these sites are dominated by *Acacia seyal* Del., one by *Acacia nilotica* (L.) Willd. ex Del. (all nomenclature follows [51]).

The Sudanian zone is the region to the south of the Sahel, lying between about 11° and 13° N in West Africa, where the rainfall is 600 to 1000 mm, the rainy season lasts 4 to 5 months, and there is permanent agriculture. The vegetation is a mosaic of open crop/woodland or savanna, with trees up to 15 m tall, some closed woodland, and edaphic bush thickets and grasslands [52]. The Sudanian test sites are located within the administrative region of Ségou, Mali. The crop/woodland type of vegetation is formed

when crops are grown under a woodland of useful trees that are preserved when land is cleared [53]. Three sites are dominated by *Butyrospermum parkii* (G. Don) Hepper and three by *Acacia albida* Del. All sites are located in the house fields, cultivated areas near the village where shrubs and weeds are cleared regularly.

We emphasize that these sites were carefully chosen based on prior field investigations, reconnaissance, and photo interpretation, to be representative homogeneous woodland stands of a certain minimum size and range of cover. Without any modification, the simple model must be applied to a stand of uniform density and composition. Therefore, the landscape must be stratified prior to regional application of the model.

IV. METHODS

Tree shape parameters and tree cover, size and density were measured in the field to parameterize and test the model. Sites ranged in size from about 9 to 90 ha (100 to 1000 TM pixels), with most sites about 20 to 40 ha (200 to 500 pixels). This corresponds roughly to the size of the 1 km diameter circular plots used by Hiernaux and Justice [49] in their AVHRR (Advanced Very High Resolution Radiometer) study.

Four to eight fixed-radius plots were located systematically within sites (at regular intervals on a rectangular grid or line) in order to sample all parts of the stand, and not bias the location of the plots. Plot radius was fixed within, but variable among sites, and was established by taking preliminary density measurements and choosing a radius that would include approximately fifty trees per site (see Fig. 4 for an example of plot size). Tree height (H), crown diameter ($= 2r$), and height to widest crown diameter were measured for all trees in each plot.

Average h and b (see Fig. 1) were calculated for the site, and were used with the sun angle for the TM scene to calculate Γ from the geometry of an ellipsoid on a stick. The model parameter C_{r2} was calculated from sample data for the sites. Size distribution was examined by inspecting histograms of tree size (expressed both as crown size and height) for all sites. Spatial pattern was established by mapping point patterns of 200-900 trees from low-altitude aerial photographs in sample quadrats within test sites for which there was good photo coverage (sites 2, 15 and 20), and analyzing using quadrat analysis [15]

[54] and second-order analysis of intertree distances [55].

Observed cover for the sites was estimated from the sample plot data. Independent cover estimates for some of the plots from line transect (from [48] and [50]) and photointerpreted point intercept on a grid (by the authors; see [56] for methods) were also used to test the model. These compared favorably with the field measurements, within the expected range of variance (see [22] Table I).

TM data were used to test this model. Early dry season imagery was chosen to enhance the contrast between trees (still green for most species) and background (a dry herbaceous layer, or bare soil). The TM scene for the Sahelian sites was acquired 9 September 1984 at the end of a very poor rainy season [49] [57], but just after a local rainfall event in the study area [47]. A second Sahelian scene, acquired 7 May 1985 at the end of the dry season, was also used to test the model. The scene for the Sudanian sites dates from 17 November 1984, after the harvest, so the fields beneath the tree canopy have been cleared. The mean and variance of reflectance for all pixels (S and $V(S)$) were computed for each spectral band in the test sites.

The component signatures required by the model are simply the relative brightnesses of the components (background, tree and shadows) compared to the mean brightness of the stand, not the absolute radiance or reflectance. The signatures were established from the satellite data, because it would have been very difficult to calibrate them accurately from field radiometer measurements in a heterogeneous environment, and to project them through a modelled atmosphere. Signatures for background and canopy (G and X_0) were initially computed from small training areas in the image, using aerial photographs as a guide. Areas of no tree cover in or near sites were used to estimate G, and pixels with high tree cover were used to estimate X_0. Comparable and satisfactory results were obtained by automatically choosing the extreme pixel values from the histogram of the brightness values in the site as the G and X_0 signatures. It was possible to predict G and X_0 using the model in these sites for which N and $\mathbf{R}^2$ were known, and compare predicted values to those observed in training sites or the histograms.

The model was tested by providing the stand parameters (Γ and C_{r^2}) and the spectral parameters (G, X_0, S and $V(S)$), predicting $\mathbf{R}^2$ and N for each site, and comparing to actual $\mathbf{R}^2$ and N from field measurements. Observed and predicted values were compared by simple regression. The model was

tested for all visible and infrared TM bands (1-5 and 7; see Table I for wavelength bands) and then for a subset of bands, TM 3, 4 and 7. Band 3 was chosen because in our experience red reflectance is strongly related to tree cover [58] [59], Band 4 because of its relationship to green vegetation amount [60], and Band 7 because it had the highest variance in the sites, and has also been shown to be related to tree cover [61]. These bands are from different regions of the spectrum and tend to be uncorrelated. Finally, the model was tested using transformed spectral channels, the NDVI (Normalized Difference Vegetation Index [62] [63]) representing image greenness, and the first principal component representing image brightness.

V. Results

A. Stand Parameters

The tree shape measurements for the sites (height, $\overline{H}$, and crown radius, $\overline{r}$) and the derived model parameters Γ and C_{r2} are shown in Table II. The trees in the Sudanian sites are taller, with relatively narrower crowns, and in the Sahelian sites, the trees are shorter with relatively wider crowns. In site 15 the trees are essentially balls of foliage sitting on the ground, and Γ is smaller than for site 101 because even though the average crown is smaller in 101, it is elevated off the ground and more shadow is visible. The average Γ for the Sahelian sites is 5.1. The Sudanian sites have larger Γ because the TM scene was imaged later in the fall so the solar angle is greater. Average Γ for the Sudanian sites is 7.1.

Tree size distributions for all sample populations were slightly to extremely right-skewed. This concurs with other studies of the West African savanna (summarized in [64]). Log-transforms produced normal-looking distributions. Fig. 5 presents two examples of size parameters (crown area and height) as log-normalized. Thus, if field measurements were not available, the assumption of a lognormal size distribution is valid for these sites, and the formula for C_{r2} for a lognormal distribution could be used. However, for these sites C_{r2} was calculated directly from sample data, and ranges from .26 to .77 (Table II). There is no apparent difference in the C_{r2} values between the two regions; however, the value is sensitive to the presence of a few very large crowns in the sample population (as in sites 2 and 15).

Fig. 6 shows the point locations and results of second order analysis for one of the sites. In all sites there is generally an inhibition distance of five to ten meters, below which the probability of finding two

trees is very low, but at relevant sensor resolution (20 to 50 m) a Poisson model is adequate. This is supported by the quadrat analysis (Table III). At larger distances (50 to 100 m) a Poisson model still fits in many of the sites, including the sparser stands (site 2) at densities where the Poisson model broke down in our earlier studies of California pine stands [15].

The actual tree size (expressed as squared crown radius), density, and cover for the sample sites are shown in Table IV. Sahelian sites have small trees at higher density. Sudanian sites have very large trees at low density, and generally lower cover.

In order to compare observed size, density and cover with predicted values obtained by model inversion, estimates of sample variance in these quantities are required. These estimates help to indicate how much of the difference between the predicted and observed values results from sample variance rather than disagreement between model and measurement. For r^2, variance is simply determined using the many individual tree count measurements for all plots taken at a site. However, for N, the sample size within a site was small, ranging from four to eight. To determine whether or not sample variance should be based on within-site measurements, or are sufficiently similar between sites or regions that pooled estimates should be used, we conducted three analyses of variance (ANOVAs) (Table V). The ANOVAs showed significant difference at region and site levels, indicating that pooling was inappropriate. Accordingly, the standard deviations shown in Table IV are based on within-site measurements.

B. Effect of Model Approximations

Equation (6) was almost always the best predictor, although in a few cases Equation (5) was better. Therefore, (6) was accepted as being a reasonable approximation ($V(m)$ was fairly large), and in all analyses, the results from this approximation are presented.

C. Early vs. Late Dry Season Imagery

For the Sahelian study region, we hypothesized that the September 1984 image (recorded following a rainfall event) would have a green herbaceous layer of varying density or standing water in sites 15, 20 and 21, causing low separability of component signatures, and that late dry-season (May 1985) imagery would work better in the model. This is true for site 20, the only site for which G_{obs} (brightest pixel in stand) is *darker* than G_{pred} (probably due to herbaceous growth or inundated soil in the site). However,

the May 1985 late dry season imagery did not consistently predict cover better than the 1984 imagery for the Sahelian sites (see Fig. 7). It is difficult to discern a pattern with only four points; however, it appears that as long as there is some spectral contrast between background and tree, the model can be inverted. It can be seen in Fig. 8 (shown for 1984 data) that for sites 15 and 101, G and X_0 don't separate well in greenness (NDVI), but the contrast is better in brightness, and the predictions of the model are reasonable.

D. Effect of Stand Parameters

We used the average values of C_{r2} (.45) and Γ (7.1 for Sudanian scene, 5.1 for Sahelian), and there was no systematic change in the accuracy of predictions. There is little change in the predicted values of R^2 and N, and no systematic error caused by holding the stand variables constant. Predicted cover values only changed by three to four percent, improving or degrading the prediction by only that much (Table VI).

E. Effect of Shape Model

In order to evaluate the effects of shape on the inversion procedure, we developed an alternative formulation of Γ for the shape of a hemisphere on a stick. At least some of the trees in each plot could be considered to fit this shape reasonably well. To test this change, we calculated Γ for the sites using the hemisphere model to see if it performed better or worse than that of an ellipsoid. There was no consistent difference in the results using the hemisphere shape. As Γ increases, predicted R^2 increases (and predicted N doesn't change), so, as Γ increases results should improve in cases where cover was underestimated, and vice versa. Since there were cases where cover was over- and underestimated, there was no overall improvement in model results (see Table VI).

F. Component Signature Estimation

Using unadjusted component signatures, density (N) is overestimated and size (R^2) is underestimated for all sites and all bands. This is because the brightest pixel reflectance in the stand (or signatures from training sites) are overestimates of the background signature G. If G is overestimated, the model predicts too many trees, and if N goes up, R^2 must go down, so size is underestimated. When observed and predicted G and X_0 were regressed, the coefficient of determination ($\mathbf{r}^2$) values were very

high (.96-.99). The distributions of G_{pred}/G_{obs} and X_{0pred}/X_{0obs} were very peaked (see Fig. 9), so the average (median) values of G_{pred}/G_{obs} and X_{0pred}/X_{0obs} in each region were used to scale G and X_0 (.90 and 1.15 in the Sudanian sites, .98 and 1.05 in the Sahelian sites). Thus, G is slightly darker than the brightest pixel and X_0 slightly brighter than the darkest in all spectral channels including the near-infrared (Band 4), and in composite image brightness (the first principal component of the spectral data). This pattern is reversed in composite image greenness (the NDVI in this analysis). When G and X_0 are adjusted using these simple scaling factors, the results improved, especially for predictions of cover and density. This adjustment was necessary for obtaining reasonable predictions, even though it only changed the signatures by a few DNs ("digital numbers" or brightness levels, quantized to 256 levels for TM data) because of the extreme sensitivity of the model to the component signatures, especially to the background signature G.

G. Multispectral Predictions

We tested the model for single spectral bands for all sites (each band is assumed to be an independent predictor). When observed and predicted size and density were compared for all sites and all single bands, the results were highly variable. However, the results substantially improved when the median predictions from among the bands was compared to the observed value. The median improved the correlation between observed and predicted values because the scaling of G sometimes caused spurious results for a band. For example, if scaled G (G_{pred}) was closer than S to X_0, the result was a negative R^2 prediction, or an extremely large predicted N. The results were also calculated for the median prediction from Bands 3, 4, and 7, bands which are not strongly correlated (Fig. 7 and Table VI). Results are slightly better for the six band median. Fig. 7 (e) and (f) also shows that although the variance in observed N and R^2 (estimated from the plot data) is large in some cases, it is not as great in the "variance" in the multispectral predictions (shown as the range of the three-band prediction).

H. Transformed Spectral Channels

Successful inversion of the model requires good spectral separability of G and X_0 (Fig. 2); thus, we explored the use of multiband transforms to define G and X_0. For this analysis, we selected the first principal component of the images as a brightness channel, and used the NDVI as a greenness channel.

Although NDVI is not necessarily orthogonal to the first principal component, it is well known to respond to green vegetation in a fashion independent of image brightness. Averaging the predictions of size and density obtained from these two transformed bands did not produce a better result than the median of Bands 3, 4 and 7 (Table VI), but the results are helpful for graphic interpretation because they correspond to the idealized spectral channels used by Li and Strahler in their original formulation of the model. The effect of scaling G is to create a linear relationship between G, S and X_0. Fig. 8 shows the position of G, X_0 and S for the Sahelian sites (15, 20, 21, 101) for both observed and predicted (adjusted) values of G and X_0. Separation between G and X_0 is best for sites 20 and 21, and cover, size and density are predicted more accurately for these sites than for sites 15 and 101 where separation is poorer. The patterns are similar for the Sudanian sites.

I. Regional Estimates

When the observed and predicted tree size and density are averaged for all sites in a region, the results clearly differentiate the two distinctive regions. As Table VII shows, the tree dimensions and distribution are very different in the two regions and the averaged predictions for size and density are very close to the observed averages for the regions. T-tests show that the regions have significantly different average size and density (all at least at the 0.0005 level). Observed and predicted values for each region are not significantly different; however, it should be noted that the sample size for the t-test is small.

VI. Summary and Discussion

The models doesn't predict tree size very well for the ten test sites ($\mathbf{r}^2 = .20$). Size is both under- and overestimated. The model predicts density and cover better ($\mathbf{r}^2$ is .62 to .78) in these test sites, where cover ranges from approximately ten to forty percent. It is a reasonable assumption that $V(m)$ (variance in cover among pixels) is large at this sampling scale (30 m TM pixels), and Equation (6) can be used to approximate $\mathbf{R}^2$ for these samples (100-1000 pixels).

The results support our prediction that the model is sensitive to the choice of the G signature and to the separability of G and X_0. When G is overestimated, tree size is systematically underestimated, and density overestimated. Scaling G dramatically improved results. Sites and spectral bands with good separability between G and X_0 generally showed better predictions (sites 1, 20, 21, Bands 3, 5, 7),

although there were exceptions. Also in support of our predictions for these sites with low cover (small m), the model is not sensitive to variance or error in estimating tree shape and size parameters (Γ and C_{r2}). Using a different shape model that slightly changed Γ, or using standardized Γ and C_{r2} had very little effect on the overall results.

Best results were obtained by using all spectral channels for the predictions, and selecting the median value from among them. This is because scaling the component signatures can cause spurious results for an individual band. The best results come from selecting the median predictions from all six visible and infrared TM bands. Neither parameter was systematically over- or underestimated for the sites. Reasonable predictions of tree size and density were also obtained using three largely uncorrelated bands (3, 4 and 7). Actually, correlation among the spectral bands should be an advantage, not a problem, given the formulation of the model. It is not a system of equations requiring independent variables for its solution, but rather the bands are instrumental variables that help to separate the signal from the noise.

The sites that were not predicted well are helpful in illustrating the limits of the simple model. Cover is underestimated in site 20, which has the highest cover value. As cover increases, trees and shadows do, in fact, overlap. X_0 will approach X_∞ as shown in Fig. 2. Therefore, our estimate of X_0 is too dark, and for a given brightness, tree cover will be underestimated. Either tree size is underestimated when variance is low, or density is underestimated when variance is higher. However, in this site the actual cover may also be overestimated by our plot data (see Fig. 7 (d) and Table IV).

For several of the sites (2, 4, 5, 7), tree density is as low as one to three trees per pixel. In this case, the predictions of the model will be strongly influenced by variations in the background (G). This will contribute to errors in the prediction of both N and $\mathbf{R}^2$. Also, X_0 will be incorrectly estimated at low density, causing errors in the prediction of $\mathbf{R}^2$. This can be seen in site 7. The darkest pixel in the stand doesn't represent X_0 because it contains background. Therefore X_0 is too bright and R^2 is overestimated. If X_0 is assigned a lower brightness, closer to the values for the other *Butyrospermum parkii* sites ($X_0 = .98\ X_0$), the predicted value is much closer to observed (see Fig. 7 (c)).

In site 2, density is overestimated and cover underestimated. This may be because scaled G is still brighter than the actual background signature, although when inspecting the imagery for the stand, there are not any anomalously bright pixels included in the training data. However, our photointerpreted cover for the stand is much greater than is calculated from the plot data, and closer to the value predicted from the model. In this case the observed values for tree size and density may be low, due to sample variance or errors in the field measurements.

We conclude that at this scale, in small sites on the order of 0.5 km^2, variations in the understory signature and other stand parameters cause site-specific predictions, particularly of tree size, to be poor. This is not surprizing, as many of the factors contributing to reflectance are not accounted for in the simple model, nor were they controlled for in this study. One of the most important is the heterogeneity in the background reflectance caused by differences in soil color, variable leaf litter cover, and slopes or microrelief causing local differences in surface illumination. These would all contribute to interpixel variance. On the other hand, the atmospheric haze so prevalent over the Sahel would tend to reduce interpixel variance. Nevertheless, when our predictions were averaged within the Sudanian and Sahelian regions, regional differences in the structure of these woodland types were accurately detected and quantified by the inversion procedure.

Therefore, this procedure could be used most effectively as part of a multistage inventory to estimate the average size and density of woody plants directly over large areas in woodlands ranging from ten to forty percent cover. In an automated procedure, G and X_0 could be selected from the histograms for twenty or thirty sites in a stratified region. C_{r2} and Γ can be chosen *a priori* for a vegetation type. We would expect a good prediction of tree size and density for a stratum within a region based on the average from these sites. We feel that the model could be inverted using Landsat MSS data in this landscape because stands are sufficiently large that even at 80 m resolution there are enough pixels (100 or more) to estimate variance.

Because size and spacing are often related to leaf and woody biomass, this technique could also provide woodland biomass estimates over large areas [65]. Besides their obvious relationship to standing biomass, important enough in itself, height and spacing could be used to determine surface roughness and

other parameters important to land-surface climatological models [11]. Also, regional-scale ecological models of ecosystem photosynthetic production and biogeochemical cycling may require input parameters of vegetation structure of the type obtainable through our inversion procedure [4] [66]. This is especially true in open woodland where tree canopy is not homogeneous, and its interaction with radiation and the atmosphere near the ground cannot be approximated by homogeneous plane-parallel models.

Finally, the inversion procedure may help monitor desertification — the spread of desert-like conditions into arid and semi-arid lands, such as the Sahel, caused by drought and overexploitation of vegetation and soil in the region [67]. In general, drought reduces density by killing individual trees (observed by Poupon [68]), while over-use of trees (coppicing and woodcutting for fuel and fodder) reduces crown area, while number of individuals may actually increase [69]. These two phenomenon could be distinguish in a regional context using the inversion procedure, which could be applied to historical Landsat data to examine changes in the recent past.

REFERENCES

[1] P. Curran, "Multispectral remote sensing of vegetation amount," *Prog. Phys. Geography*, vol. 4, pp. 315-341, 1980.

[2] J. Jensen, "Biophysical remote sensing," *Ann. Assoc. Amer. Geographers*, vol. 73, pp. 111-132, 1983.

[3] P. J. Sellers, "Canopy reflectance, photosynthesis and transpiration," *Int. J. Remote Sensing*, vol. 6, pp. 1335-1372, 1985.

[4] P. J. Sellers, "Canopy reflectance, photosynthesis, and transpiration. II. The role of biophysics in the linearity of their interdependence," *Remote Sensing Envir.*, vol. 21, pp. 143-183, 1987.

[5] R. A. Houghton, J. E. Hobbie, J. M. Melillo, B. Moore, B. J. Peterson, G. R. Shaver, and G. M. Woodwell, "Changes in the carbon content of the terrestrial biota and soils between 1860 and 1980: A net release of carbon to the atmosphere," *Ecological Monographs*, vol. 53, pp. 235-262, 1983.

[6] G. M. Woodwell, *The Role of Terrestrial Vegetation in the Global Carbon Cycle*, 247 pp., Wiley, New York, 1984.

[7] T. H. Rosswall, "The biogeochemical nitrogen cycle," in *Some Perspectives on the Major Biogeochemical Cycles*, ed. G. E. Likens, pp. 25-49, John Wiley and Sons, Chichester, 1981.

[8] Y. Mintz, *The Global Climate*, Bracknell, United Kingdom, 1984.

[9] S. I. Rasool, "On dynamics of desert and climate," in *The Global Climate*, ed. J. T. Houghton, pp. 107-120, Cambridge University Press, Cambridge, 1983.

[10] C. J. Tucker, I. Y. Fung, C. D. Keeling, and R. H. Gammon, "Relationship between atmospheric CO_2 variations and a satellite-derived vegetation index," *Nature*, vol. 319, pp. 195-198, 1986.

[11] P. J. Sellers, Y. Mintz, Y. C. Sud, and A. Dalcher, "A simple biosphere model (SiB) for use within general circulation models," *J. Atmos. Sci.*, vol. 43, pp. 505-531, 1986.

[12] National Academy of Sciences (NAS) Committee of Planetary Biology, "Remote Sensing of the Biosphere," Space Sciences Board Commission on Physical Sciences, Mathematics and Resources, National Research Council, National Academy Press, Washington, D.C., 1986.

[13] NASA, "Land-Related Global Habitability Science Issues," NASA Technical Memorandum 85841, National Aeronautics and Space Administration, July, 1983.

[14] D. B. Botkin, J. E. Estes, R. M. MacDonald, and M. V. Wilson, "Studying the Earth's vegetation from space," *BioScience*, vol. 34, pp. 508-514, 1984.

[15] X. Li and A. H. Strahler, "Geometric-optical modeling of a conifer forest canopy," *IEEE Trans. Geosci. Remote Sensing*, vol. GE-23, pp. 705-721, 1985.

[16] X. Li and A. H. Strahler, "Geometrical-optical bidirectional reflectance modeling of a coniferous forest canopy," *IEEE Trans. Geosci. Remote Sensing*, vol. GE-24, pp. 906-919, 1986.

[17] A. H. Strahler, C. E. Woodcock, and J. Smith, "On the nature of models in remote sensing," *Remote Sensing Envir.*, vol. 20, pp. 121-139, 1986.

[18] C. E. Woodcock and A. H. Strahler, "The factor of scale in remote sensing," *Remote Sensing Envir.*, vol. 21, pp. 311-332, 1987.

[19] C. E. Woodcock, A. H. Strahler, and D. L. B. Jupp, "The use of variograms in remote sensing," *Remote Sensing Envir.*, Scene models and simulated images, 1988. Accepted for publication.

[20] C. E. Woodcock, A. H. Strahler, and D. L. B. Jupp, "The use of variograms in remote sensing II: Real digital images," *Remote Sensing Envir.*, 1988. Accepted for publication.

[31] A. J. Richardson, E. C. Weigand, H. Gausman, J. Cuellar, and A. Gerberman, "Plant, soil and shadow reflectance components of row crops," *Photogrammetr. Eng. Remote Sensing*, vol. 41, pp. 1401-1407, 1975.

[32] R. D. Jackson, R. J. Regirato, P. J. Pinter Jr., and S. B. Idso, "Plant canopy information extraction from composite scene reflectance of row crops," *Appl. Optics*, vol. 18, pp. 3775-3782, 1979.

[33] F. J. Heimes and J. A. Smith, "Spectral variability in mountain terrain," Final Report, Rocky Mountain Forest and Range Experiment Station U. S. Forest Service Cooperative Agreement 16-625-CA, 1977.

[34] R. D. Graetz and M. R. Gentle, "The relationships between reflectance in the Landsat wavebands and the composition of an Australian semi-arid shrub rangeland," *Photogrammetr. Eng. Remote Sensing*, vol. 48, pp. 1721-1730, 1982.

[35] R. P. Pech, R. D. Graetz, and A. W. Davis, "Reflectance modelling and the derivation of vegetation indices for an Australian semi-arid shrubland," *Int. J. Remote Sensing*, vol. 7, pp. 389-403, 1986.

[36] J. Otterman, "Albedo of a forest modeled as a plane with dense vertical protrusions," *J. Climate Appl. Meteorol.*, vol. 22, pp. 297-307, 1984.

[37] J. Otterman, "Bidirectional and hemispherical reflectivities of a bright soil plane and a sparse dark canopy," *Int. J. Remote Sensing*, vol. 6, pp. 897-902, 1985.

[38] X. Li, "An invertible coniferous forest canopy reflectance model," Masters Thesis, Department of Geography, University of California, Santa Barbara, 1981. 167 pp.

[39] F. Bourlière and M. Hadley, "Present-day Savannas: An Overview," in *Tropical Savannas*, ed. F. Bourlière, pp. 1-18, Elsevier Scientific Publishing Company, Amsterdam, 1983.

[40] G. L Ajtay, P. Ketner, and P. Duvigneaud, "Terrestrial primary production and phytomass," in *The Global Carbon Cycle*, ed. B. Bolin, E.T. Degens, S. Kempe and P. Ketner, pp. 129-181, SCOPE 13, John Wiley and Sons, New York, 1979.

[41] J. P. Lanley and J. Clement, "Tropical Forest Resources Assessment Project (in the framework of GEMS - Global Environmental Monitoring System)," in *Forest Resources of Tropical Africa, Part 1-Regional Synthesis*, UN FAO/UNEP (United Nations Food and Agricultural Organization/ United

Nations Environmental Programme), Rome, 1982.

[42] A. Aubréville, *Climats, Foret et Desertification de l'Afrique Tropicale*, 351 pp., Soc. Ed. Geogr. Marit-et Cd., Paris, 1949.

[43] G. Boudet, *Rapport sur la Situation Pastorale dans les Pays du Sahel*, 45 pp., UN FAO/EMASAR, IEMVT, Rome, 1975.

[44] H. N. Le Houerou, "The rangelands of the Sahel," *J. Rangeland Management*, vol. 33, pp. 41-46, 1980.

[45] F. W. T. Penning de Vries and M. A. Djitéye, *La Productivité des Paturâges Sahéliens: Une Etude de l'Exploitation de cette Ressource Naturelle*, Centre for Agricultural Publishing and Documentation, Wageningen, Holland, 1982.

[46] H. Breman and C. T. de Witt, "Rangeland productivity and exploitation in the Sahel," *Science*, vol. 221, pp. 1341-1347, 1983.

[47] P. Hiernaux and L. Diarra, "Pour une technique de télédetection appliquée au sui de l'evolution de la végétations sahélienne," Programme des Zones Aride et Semi-aride, Document du Programme, Centre International pour l'Elevage en Afrique (CIPEA), Bamako, Mali, 1986.

[48] L. Diarra and P. Hiernaux, "Evolution de la végétation sahélienne après la sécheresse bilan du suivi des sites du Gourma en 1986," Programme des Zones Aride et Semi-aride, Document du Programme, Centre International pour l'Elevage en Afrique (CIPEA), Bamako, Mali, 1987.

[49] P. H. Y. Hiernaux and C. O. Justice, "Suivi du développement végétal au cours de l'été 1984 dans le Sahel Malien," *Int. J. Remote Sensing*, vol. 7, pp. 1515-1531, 1986.

[50] P. Hiernaux, M. I. Cissé, and L. Diarra, "Bilan d'une saison d'es pluies 1984 très déficitaire dans la Gourma (Sahel Malien). Première campagne de suivi et télédetection expérimentale, Annexe: Fiches descriptives des sites," Programme des Zones Aride et Semi-aride, Document du Programme, Centre International pour l'Elevage en Afrique (CIPEA), Bamako, Mali, 1984.

[51] J. Hutchinson, J. M. Dalziel, and Hepper, *Flora of West Tropical Africa*, Crown Agents for Oversea Governments and Administrations, London, 1963.

[52] R. Schnell, *Introduction á la Phytogéographie des Pays Tropicaux: 8. La Flore et la Végétation de l'Afrique Tropicale,* Gauthiers-Villars, Paris, 1977.

[53] M. Nielsen, *Introduction to the Flowering Plants of West Africa,* University of London Press, London, 1965.

[54] J. Franklin, J. Michaelsen, and A. H. Strahler, "Spatial analysis of density dependent pattern in coniferous forest stands," *Vegetatio,* vol. 64, pp. 29-36, 1985.

[55] A. Getis, "Interaction modeling using second-order analysis," *Environment and Planning A,* vol. 16, pp. 173-183, 1984.

[56] P. L. Warren and C. Dunford, "Vegetation sampling with large scale aerial photography," *Remote Sensing Newsletter,* vol. 83, pp. 1-6, University of Arizona, 1983.

[57] J. R. G. Townshend and C. O. Justice, "Analysis of the dynamics of African vegetation using the normalized difference vegetation index," *Int. J. Remote Sensing,* vol. 7, pp. 1435-1445, 1986.

[58] T. L. Logan and A. H. Strahler, "Optimal Landsat transforms for forest applications," *Proc. Sixteenth Int. Symp. Remote Sensing Environment,* pp. 455-468, Ann Arbor, Michigan, 1982.

[59] J. Franklin, "Thematic Mapper analysis of coniferous forest structure and composition," *Int. J. Remote Sensing,* vol. 7, pp. 1287-1301, 1986.

[60] C. J. Tucker, "Red and photographic infrared linear combinations for monitoring vegetation," *Remote Sensing Envir.,* vol. 8, pp. 127-150, 1979.

[61] D. N. H. Horler and F. J. Ahern, "Forestry information content of Thematic Mapper data," *Int. J. Remote Sensing,* vol. 7, pp. 405-428, 1986.

[62] B. N. Holben, C. J. Tucker, and C. J. Fan, "Spectral assessment of soybean leaf area and leaf biomass," *Photogrammetr. Eng. Remote Sensing,* vol. 46, pp. 651-656, 1980.

[63] C. J. Tucker, B. N. Holben, J. H. Elgin, and J. E. McMurtrey, "Remote sensing of total dry-matter accumulation in winter wheat," *Remote Sensing Envir.,* vol. 11, pp. 171-189, 1981.

[64] J. C. Bille, "Mesure de la production primaire appetée des ligneux," in *Browse in Africa, the Current State of Knowledge,* ed. H. N. Le Houerou, pp. 183-193, International Livestock Centre for Africa, Addis Ababa, Ethiopia, 1980.

[65] J. Franklin and P. Hiernaux, "Estimating leaf and wood biomass in Sahelian and Sudanian woodlands using a remote sensing model," *in preparation*, 1988.

[66] G. P. Robertson and T. Rosswall, "Nitrogen in West Africa: The regional cycle," *Ecological Monographs*, vol. 56, pp. 43-57, 1986.

[67] J. A. Mabbutt, "Perspectives on desertification," *Economic Geography*, vol. 53, pp. 429-432, 1977.

[68] H. Poupon, "Evolution d'un peuplement d'*Acacia senegal* (L.) Willd dans une savane sahélienne au Sénégal de 1972 à 1976," *Cah. O.R.S.T.O.M., sér. Biologie*, vol. 12, pp. 283-291, 1977.

[69] P. Hiernaux, "L'inventaire du potentiel fourrager des arbres et arbustes d'une region du Sahel Malien. Méthods et premiers résultats," in *Browse in Africa, the Current State of Knowledge*, ed. H. N. Le Houerou, pp. 195-201, International Livestock Centre for Africa, Addis Ababa, Ethiopia, 1980.

Table I

TM SPECTRAL BANDS

TM band	Wavelength (μm)
1	0.45-0.52
2	0.52-0.60
3	0.63-0.69
4	0.76-0.90
5	1.55-1.75
7	2.08-2.35

Table II

TREE SHAPE MEASUREMENTS FOR STUDY SITES

Site	Species	n	Height (m)		Crown Radius (m)		Γ	C_{r^2}
			mean	σ	mean	σ		
SUDANIAN SITES								
1	*Vitellaria paradoxa*	35	8.35	2.44	3.67	1.19	7.00	.5164
2	*Vitellaria paradoxa*	50	8.61	2.94	4.13	1.60	6.67	.7780
3	*Acacia albida*	32	11.07	1.96	4.15	1.02	7.28	.2612
4	*Acacia albida*	63	13.17	3.01	5.57	2.06	7.10	.5682
5	*Acacia albida*	60	11.58	2.58	4.91	1.72	7.07	.5616
7	*Vitellaria paradoxa*	50	12.60	2.71	4.72	1.36	7.55	.2969
SAHELIAN SITES								
15	*Acacia nilotica*	56	5.64	1.59	3.56	1.25	4.72	.6816
20	*Acacia seyal*	87	5.27	1.66	3.06	1.08	5.00	.4385
21	*Acacia seyal*	75	4.88	1.53	2.50	0.88	5.30	.5151
101	*Acacia seyal*	105	5.02	1.16	2.45	0.90	5.30	.5797

Table III

QUADRAT ANALYSIS: FIT TO POISSON DISTRIBUTION

Quadrat Size	n quadrats	n points	mean	χ^2	df
Site 15 (*Acacia nilotica*)					
10	784	587	0.7	4.7	3
20	196	587	3.0	4.7	9
25	121	567	4.7	8.0	12
30	81	547	6.8	3.1	13
35	64	587	9.2	9.1	18
40	49	587	12.0	20.9	24
50	25	466	18.6	~ 10	27
Site 20 (*Acacia seyal*)					
20	182	838	4.6	10.0	10
25	121	877	7.2	24.8	18
30	81	850	10.5	25.9	19
35	56	780	13.9	~ 15	28
40	42	757	18.0	~ 51*	30
Site 2 (*Vitellaria paradoxa*)					
10	625	223	0.36	3.1	0
20	144	212	1.47	0.3	4
30	64	213	3.3	3.9	7
40	36	213	5.9	5.8	14
50	25	223	8.9	6.4	17
60	16	213	13.1	11.3	26

* significantly different at .05 level

Table IV

ACTUAL TREE SIZE, DENSITY, AND COVER

Site	(Crown radius)^2 (m^2)			Density (ha^{-1})			Cover (%)	
	mean	σ	n	mean	σ	n	sampled	photo
SUDANIAN SITES								
1	14.85	10.67	35	45.74	13.84	4	22	
2	19.58	17.27	50	30.36	6.65	6	19	27
3	18.25	9.33	32	35.72	7.44	4	21	
4	35.18	26.52	63	21.40	12.23	8	24	
5	27.02	20.25	60	12.74	8.37	6	11	
7	24.05	13.11	50	10.61	3.08	6	08	
SAHELIAN SITES								
15	14.21	11.73	56	71.30	40.53	4	32	23
20	10.53	6.97	87	168.07	24.63	3	56	39
21	7.03	5.04	75	149.21	26.29	4	33	44
101	6.82	5.19	105	133.69	154.55	4	29	

Table V

ANOVA OF DENSITY IN SAMPLE SITES

Source of Variation	F	p
Regions vs. plots within regions	1357.51	0.0000
Sudanian Sites, sites vs. plots within sites	61.82	0.0000
Sahelian Sites, sites vs. plots within sites	4.51	0.02
Sahelian Sites, without site 101	36.48	0.0001

Table VI

SUMMARY OF MODEL RESULTS
REGRESSION, OBSERVED VS. PREDICTED STAND PARAMETERS

Trial	a	b	r^2
COVER			
Six Bands Median	.674	+.036	.74
Bands 3, 4, 7 Median	.922	+.094	.62
Standard Γ and C_{r2}	.038	+.682	.72
Hemisphere shape model	.039	+.652	.76
TREE SIZE (R^2)			
Six Bands Median	.586	+8.352	.28
Bands 3, 4, 7 Median	.756	+7.449	.16
Standard Γ and C_{r2}	.348	+6.511	.18
Hemisphere shape model	.399	+5.207	.18
Brightness and NDVI	.270	+13.170	.04
DENSITY (N)			
Six Bands Median	.822	+15.280	.72
Bands 3, 4, 7 Median	.807	+17.992	.75
Standard Γ and C_{r2}	.810	+7.887	.78
Hemisphere shape model	.807	+17.992	.75
Brightness and NDVI	.591	+36.750	.17

Table VII

AVERAGED REGIONAL ESTIMATES OF TREE SIZE ANDDENSITY

Region	n	R^2				N			
		Observed		Predicted		Observed		Predicted	
		mean	σ	mean	σ	mean	σ	mean	σ
Sudanian	6	23.16	7.30	27.42	10.24	26.10	13.69	38.22	25.80
Sahelian	8	9.65	3.23	12.89	5.25	130.57	38.83	123.97	44.40

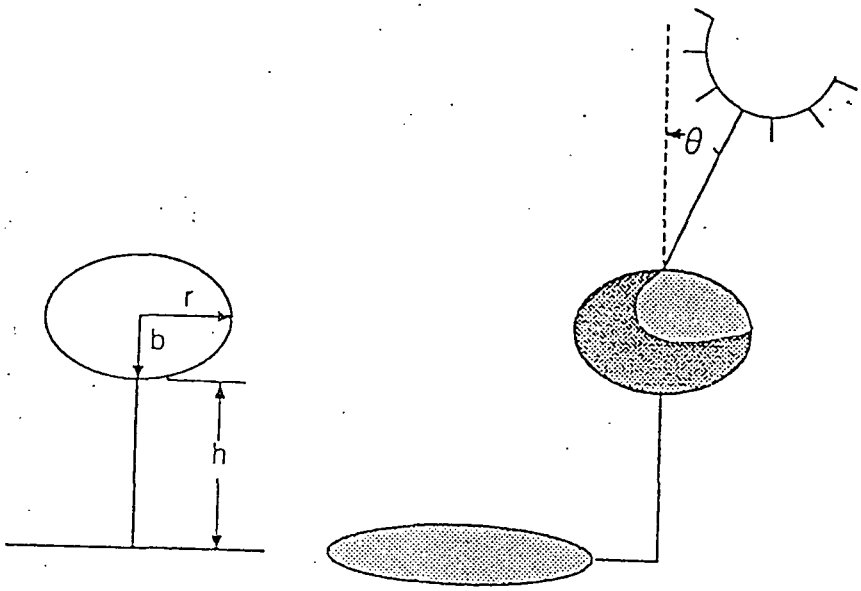

Fig. 1 — Tree shape and illumination geometry for an ellipsoid on a stick.

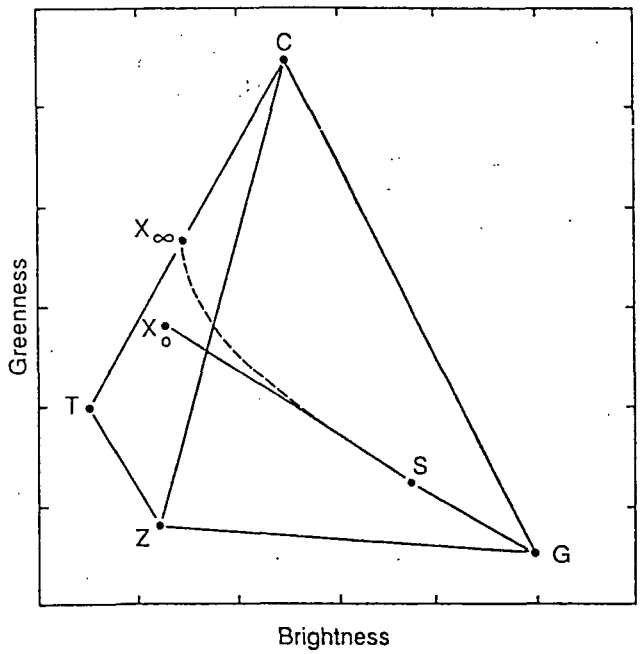

Fig. 2 — Idealized plot of spectral components on brightness and greenness spectral axes.

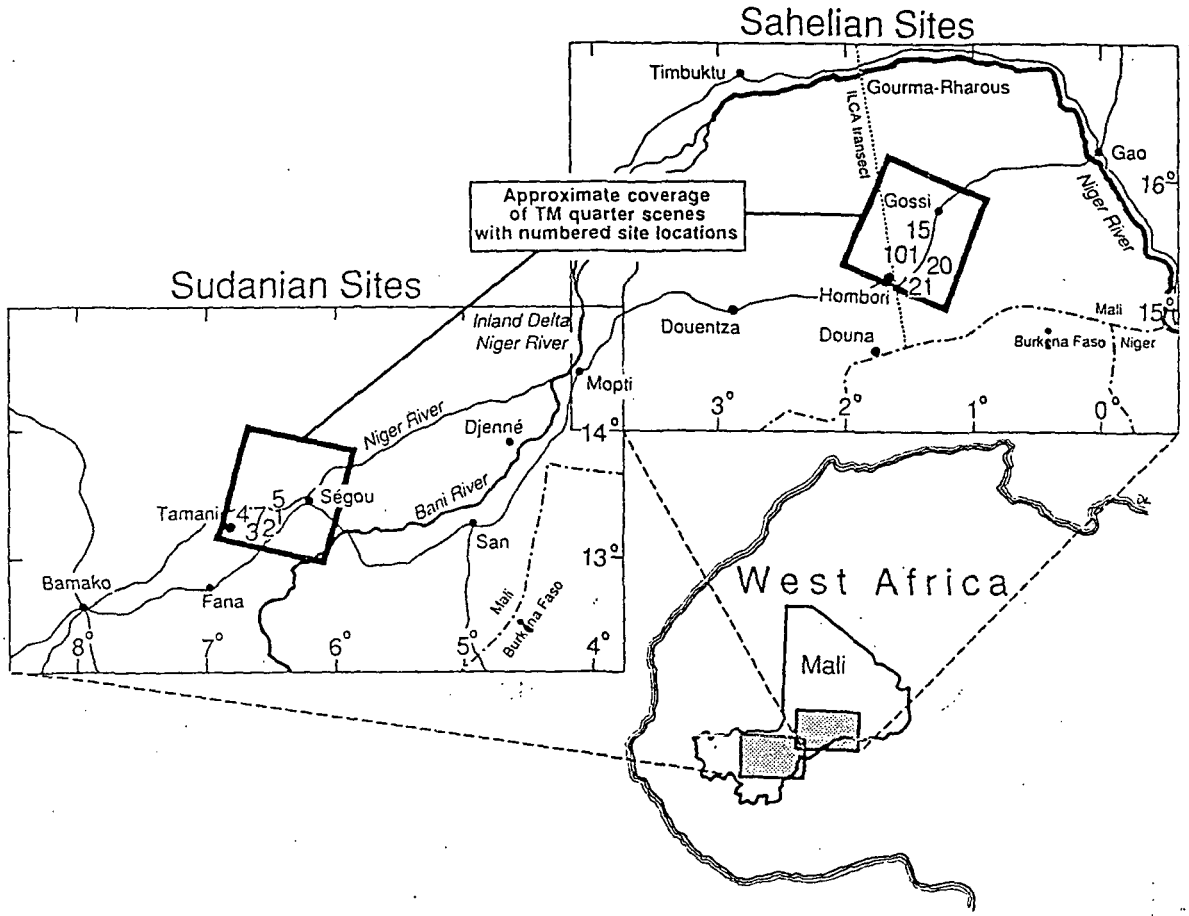

Fig. 3 — Location of test sites in West Africa.

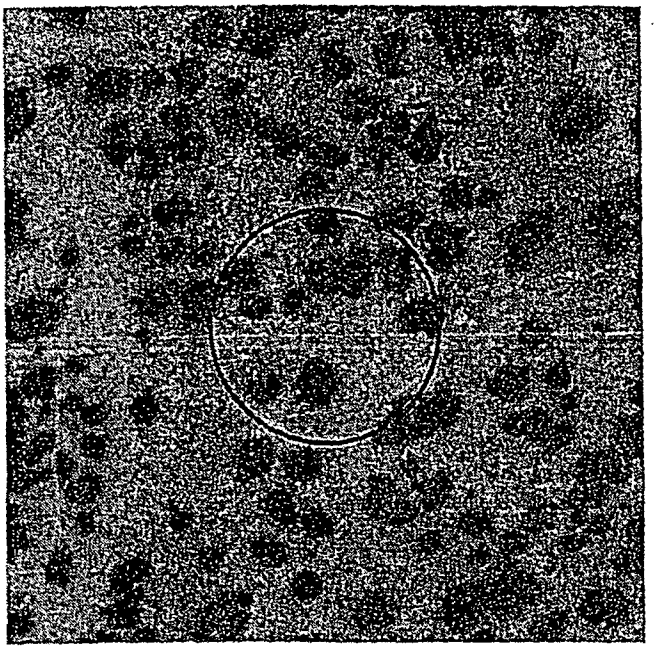

Fig. 4 — A portion of site 15 shown on an aerial photograph with plot size (25 m radius) indicated by the circle.

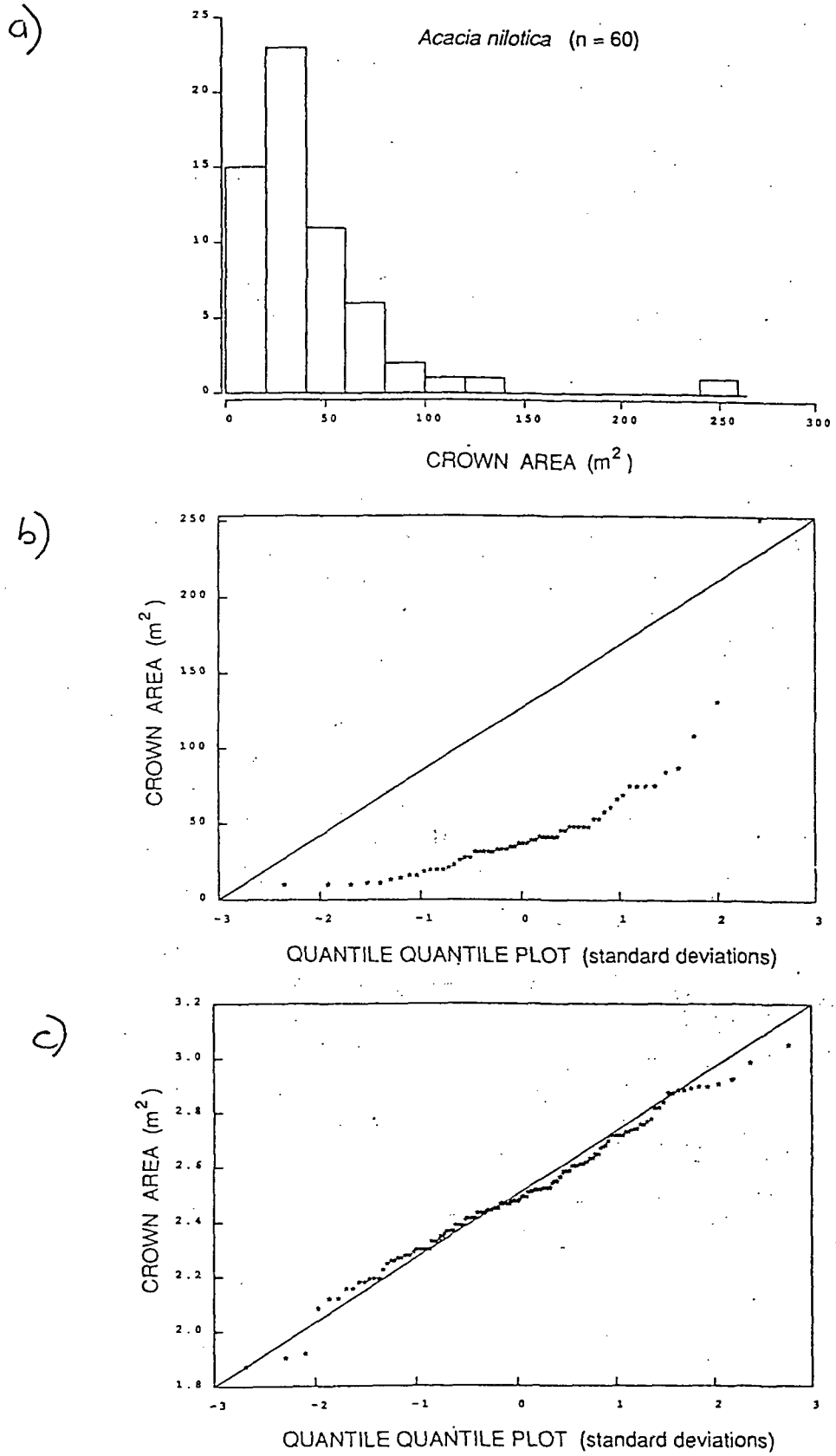

Fig. 5 — Histograms of size distributions for (a) *Acacia nilotica* (crown area) and (d) *Acacia albida* (height). The quantile-quantile (Q-Q) plots represent the data plotted against corresponding quantiles of the normal distribution (units are standard deviations). If the points fall in a straight line, they are normally distributed. (b), (e) raw values; (c), (f) lognormal values.

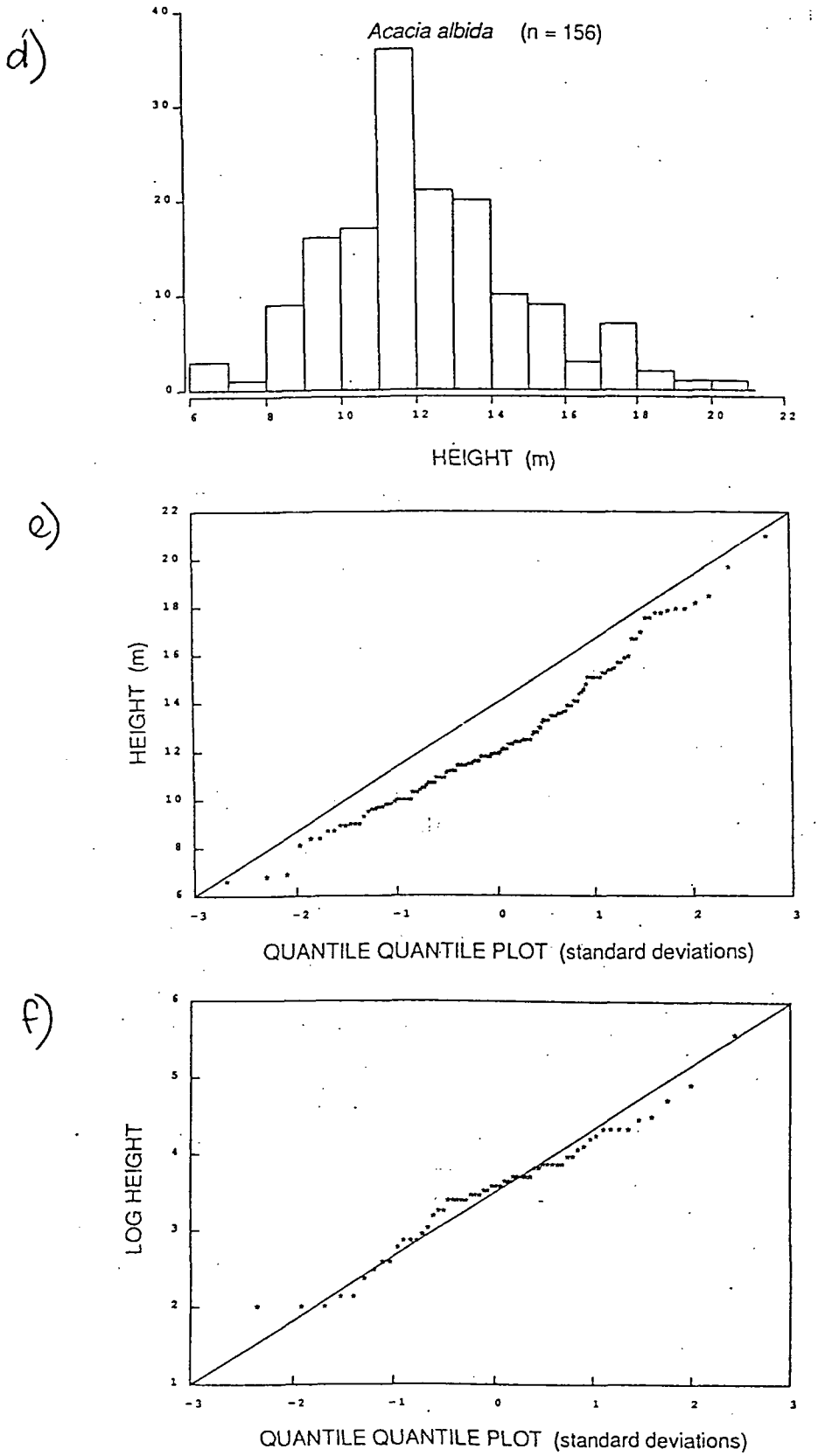

Fig. 5 — (cont.) Histograms of size distributions for (a) *Acacia nilotica* (crown area) and (d) *Acacia albida* (height). The quantile-quantile (Q-Q) plots represent the data plotted against corresponding quantiles of the normal distribution (units are standard deviations). If the points fall in a straight line, they are normally distributed. (b), (e) raw values; (c), (f) lognormal values.

a)

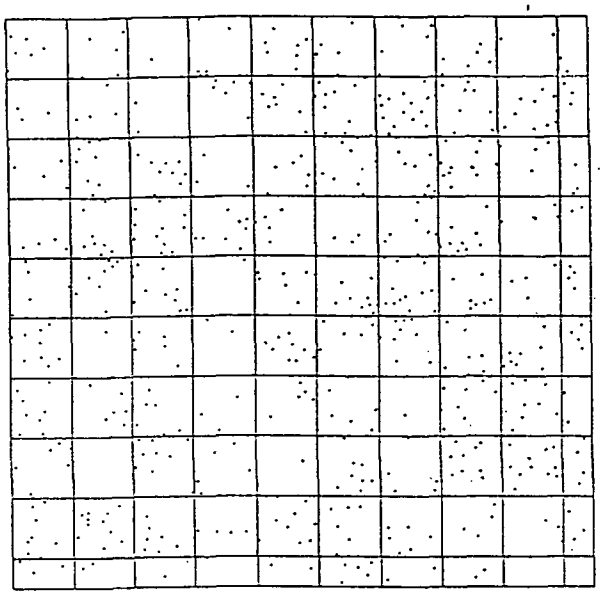

b)

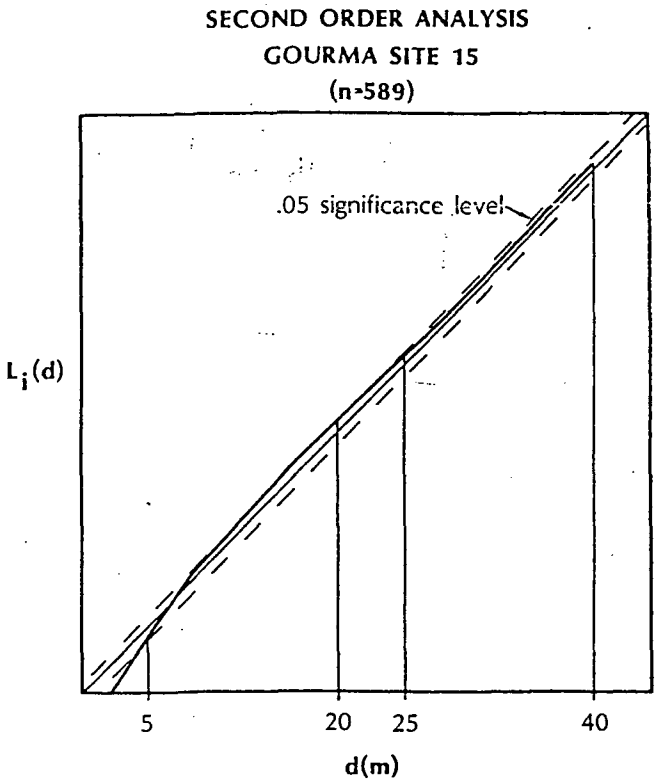

Fig. 6 — (a) Point locations of trees, Gourma Site 15 with grid of 30 m quadrats overlain. (b) Cumulative frequency of observed interpoint distances ($L_i[d]$). The diagonal is the expected frequency for a Poisson distribution, and the lines surrounding it are the .05 significance level.

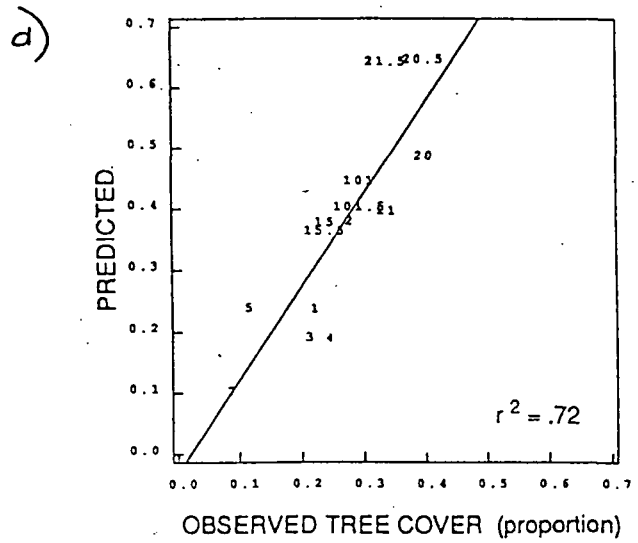

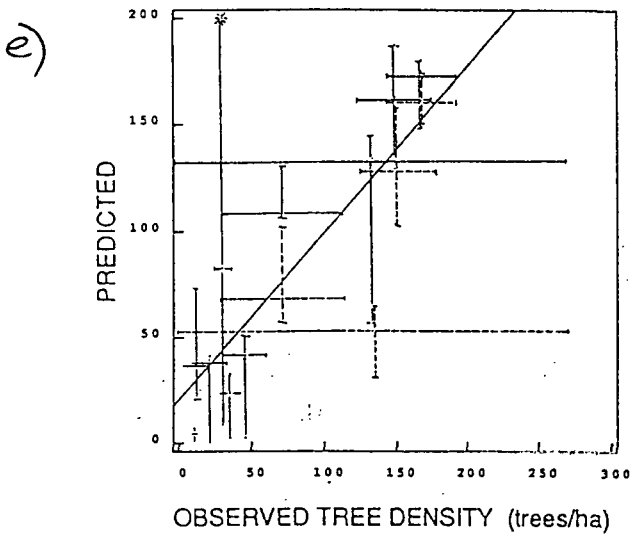

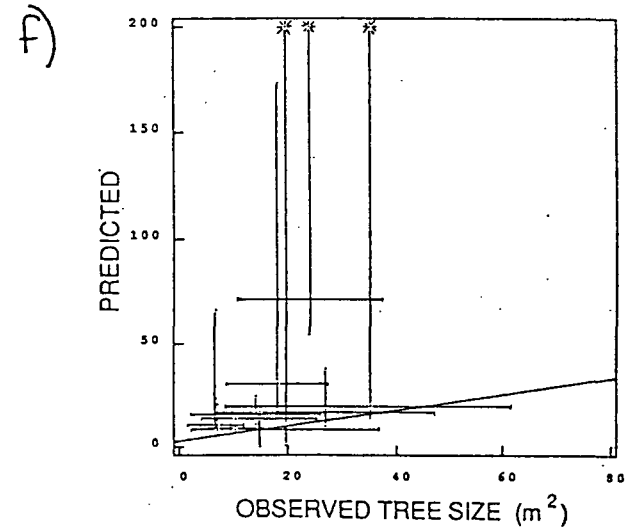

Fig. 7 — (cont.) Observed vs. predicted stand parameters for Band 3, 4, 7 median, (a) cover, (b) density (N), (c) size (R^2), (d) cover substituting photointerpreted values for sites 2, 15, 20, (e) density with sample variance (± one standard deviation) and range of predicted values plotted, (f) size with sample variance (± one standard deviation), and range of predicted values plotted. A star (*) indicates predicted values in one band that is much greater than the range of the y-axis shown. Points are labeled by site number; numbers followed by .5 are based on 1985 TM data. All other points are based on 1984 spectral data.

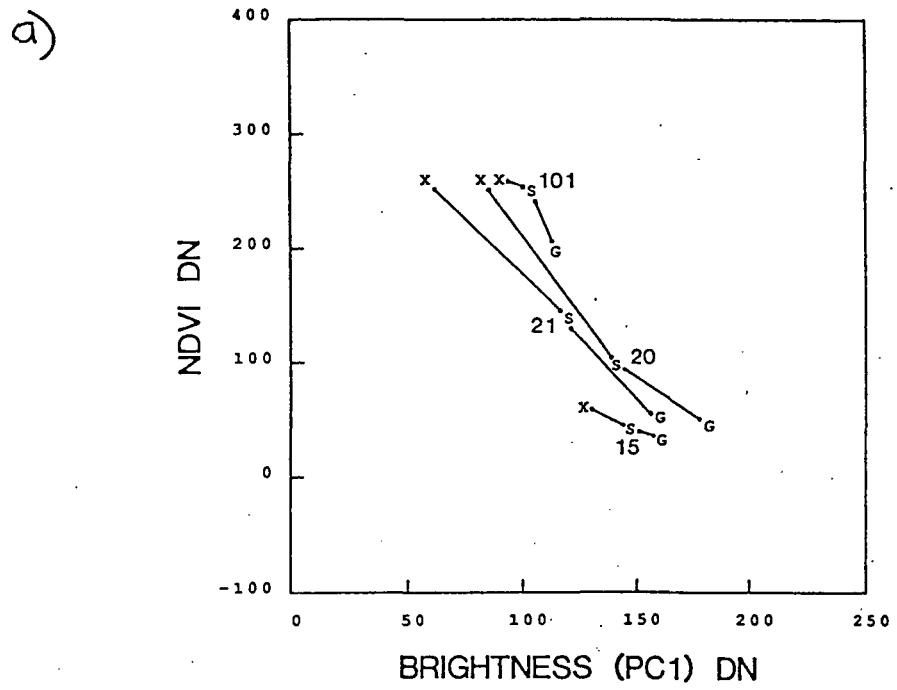

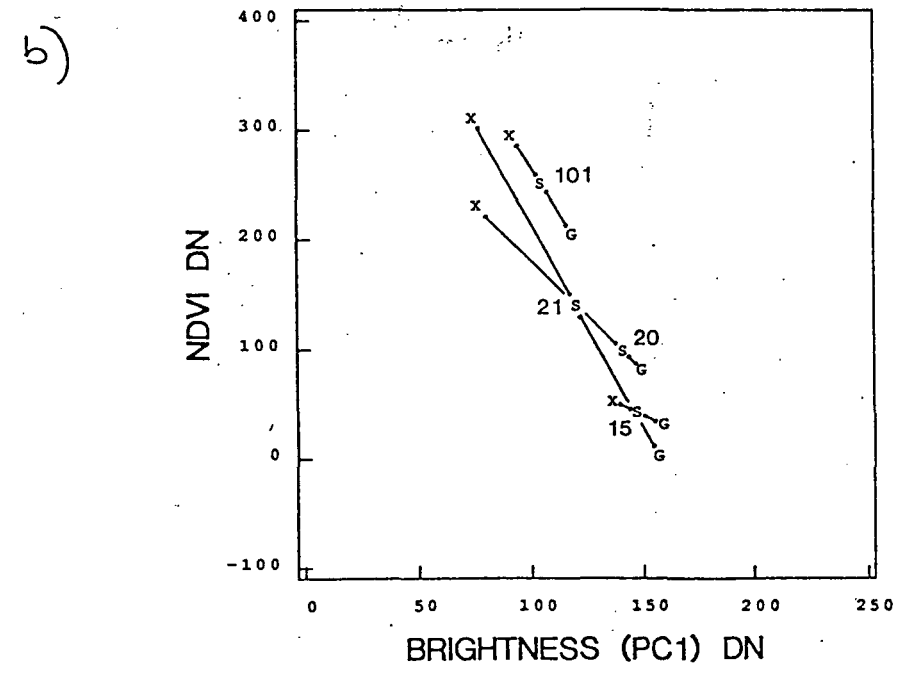

Fig. 8 — Component signatures for background (G), tree (X_0) and stand reflectance (S) plotted on brightness (PC1) and greenness (NDVI) transformed spectral axes, (a) observed G and X_0 and, (b) predicted G and X_0 for Sahelian sites, 1984 spectral data.

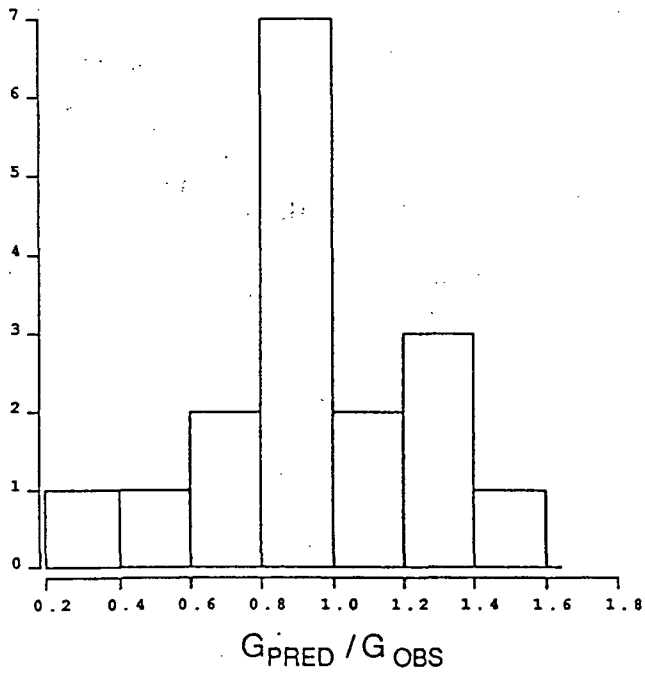

Fig. 9 — Histogram of G_{pred}/G_{obs} values for Sahelian sites, all TM Bands.

Chapter 2

REFLECTANCE PROPERTIES OF WEST AFRICAN SAVANNA TREES FROM FIELD RADIOMETER MEASUREMENTS

Abstract

Reflectance properties of savanna trees were measured using a pole-mounted radiometer for four Sahelian and two Sudanian species in West Africa. The measurements showed that canopy spectral components, viz shadowed and sunlit tree crown and background, have distinct reflectance characteristics in red and infrared wavebands as modelled by Li and Strahler (1986). Sunlit canopy is the greenest component, and sunlit background (consisting of bare soil with some brown herbaceous matter) the brightest. Shadowed crown is the darkest component, and is greener than shadowed background. The field radiometer measurements were used to calculate the normalized difference vegetation index (NDVI), and the integrated NDVI over the canopy was related to crown volume.

1. Introduction

Models of radiative transfer and of biophysical properties (reflectance, photosynthesis) that treat vegetation as a horizontally homogeneous photosythesizing medium may be appropriate for the field layer of a vegetation canopy (Suits 1972, Smith 1983, Sellers 1987), but, the three-dimensional geometry of the vegetation must be considered for the tree layer (Kimes and Kirchner 1982, Otterman 1984 and 1985, Li and Strahler 1985 and 1986). This is particularly necessary when analyzing radiative transfer in savanna vegetation for the purpose of inferring biophysical properties from remotely sensed data (Prince 1987), because both the tree and field layer are important in influencing reflectance, and in terms of ecosystem productivity (Bourlière and Hadley 1983). The transmission of radiation through semiarid savanna tree canopies is presaged by the observation that there is an unexpectedly good relationship between field-layer primary production and spectral vegetation indices derived from satellite data, despite savanna tree cover of up to 30 percent (Prince and Astle 1986, Prince and Tucker 1986).

We measured canopy reflectance in the red and infrared wavebands for typical, individual savanna trees because we were interested in the effect of the average tree canopy and its shadowing on reflectance. A canopy reflectance model for sparse woodland that treats trees as opaque Lambertian solids with distinct spectral properties for shadowed and sunlit tree canopy and background has been developed (Li and Strahler 1985). While this model can be empirically calibrated using component signatures obtained from satellite reflectance data, we wanted to establish that these spectral components exist and are distinct when measured in the field.

The effect of shadowing geometry and background (soil) or understory properties on canopy reflectance, particularly the bidirectional reflectance distribution function and greenness indices, has been modeled and measured in crops (Suits 1981, Verhoef and Bunnik 1976, Huete *et al.* 1985, Norman *et al.* 1983, Ranson *et al.* 1985), and forests (Heimes and Smith 1980, Kimes *et al.* 1986, Ranson *et al.* 1986, Kleman 1986, Li and Strahler 1985 and 1986, Ranson and Daughtry 1987, Jupp *et al.* 1986, Walker *et al.* 1986). However, the spectral components as defined by Li and Strahler (1986), (i. e., shadowed and illuminated canopy and background) have not been measured separately in the field. Measurements of canopy layer interception have been made which demonstrate that a large amount of the incident solar and sky radiation is transmitted through a typical savanna canopy, primarily due to the low leaf area index (LAI) of semiarid savanna tree canopies (Prince 1987).

Thus, the opaque solid assumption of the Li and Strahler model appears unrealistic for this application. In order to reconcile these approaches, and to define the spectral properties of the equivalent opaque solid objects, we have examined the effect of these canopies on the red and near infrared components of the incident radiation.

Specifically, we are concerned about the effect of the tree layer on satellite measurements of the properties of the field layer and of the entire community. An understanding of the reflectance of individual trees as three-dimensional objects that are self-shadowing and cast shadows on a background is important for a better understanding of the relationship between ratio vegetation indices and orthogonal transforms of red and infrared spectral bands and green vegetation (Tucker 1979, Jackson 1983, Perry and Lautenschlager 1984, Asrar *et al.* 1985) in woodlands and savannas.

The infrared/red indices have been found to be asymptotically related to green vegetation amount, and a radiative transfer model shows that infrared reflectance is linearly related to intercepted photosynthetically active radiation (Sellers 1987). However, many studies, including our own, have shown that, particularly in canopies with incomplete cover, woody vegetation amount (measured as cover, woody biomass or timber volume) is better correlated with red absorption than with near-infrared reflectance (Franklin 1986, Logan and Strahler 1982, Logan 1983, Frank 1985, Olsson 1984, Colwell 1981). This is primarily due to the three-dimensional shadowing geometry of the woody plants.

The savanna trees we measured generally have very open canopies (low LAI and thin branches), and do not cast very deep shadows. Prince's (1987) data suggests that they will transmit a great deal of radiation to the ground and back to the sky. In spite of this, the tree canopy and the shadow it casts are distinct in panchromatic aerial photography, even when the tree is in a leafless condition. Therefore, we wanted to measure the bispectral reflectance properties of the tree canopy and its shadow and to determine its effect on the background reflectance properties.

2. Methods

The study sites were in the Sahelian and Sudanian bioclimatic zones (as defined in Aubréville 1949) in Mali, West Africa. The measurements were taken for a total of 32 trees, twelve *Balanites aegyptiaca* (L.) Del., five *Acacia seyal* Del., three *Acacia senegal* (L.) Willd., six *Combretum glutinosum* Perrott, three

Butyrospermum parkii (G. Don) Hepper, and three *Acacia albida* Del. (nomenclature follows Hutchinson *et al.* 1963 and Von Maydell 1983). The *B. aegyptica*, *A. seyal*, *A. senegal* and *C. glutinosum* were located in or near Site 20 (15° 16' N, 1° 32' W) of the study area described in Hiernaux and Justice (1986). The *A. albida* were located in Site 4 (13° 19′ N, 6° 38′ W) of the study area described in Franklin and Strahler (1988), and the *B. parkii* were located in the same study region, near Site 7 (13° 15′ N, 6° 35′ W). We chose trees short enough to measure with hand-held equipment, and with relatively even (isotropic) canopies because measurements were made on only a single transect through the center of the tree (see below).

Butyrospermum parkii is a deciduous member of the Sapotaceae, with rather large sclerophyllous (leathery) leaves which it loses in the dry season. This tree typifies those found in the cultivated Sudanian zone in West Africa (Nielsen 1965). *Acacia albida* is one of the most common Sahelian-Sudanian zone trees, which can attain great size (20-30 m in height). It is a microphyllous *Acacia*, which (atypically) remains leafless in the rainy season and produces new leaves, and flowers, in the early dry season (September-October). *Butyrospermum parkii* and *Acacia albida* had the greatest leaf area (by visual estimation) of the trees we measured. *Acacia seyal* and *Acacia senegal* are also microphyllous, but are much smaller trees. They both occupy clay loam plains that are normally flooded during the rainy season, although *A. senegal* is more typically found on sandy soils with good drainage. When the measurements were taken, all trees were in leaf, but the *Acacia seyal* is characterized by sparse leaf coverage. *Balanites aegyptiaca* and *Combretum glutinosum* are common Sahelian-Sudanian small trees or large shrubs with irregularly shaped canopies (see Figure 1). *Balanites aegyptiaca* has small leaves, but has green (photosynthesizing) current-year twigs and spines. *Combretum glutinosum* has somewhat glaucous leaves.

We measured the radiance of individual tree canopies using an Exotech radiometer with a 15° field of view (FOV) in two wavelength bands corresponding to Landsat Thematic Mapper (TM) Bands 3 (.63-.69 μm) and 4 (.76 - .90 μm), red (R) and near infrared (NIR) radiance. The radiometer was mounted on a pole with an adjustable length of up to 6 m, and held by hand 1 m above the canopy pointing downward while we measured reflectance upwelling from above the tree canopy. We then measured reflectance upwelling from the ground below the canopy (at 1.5 m). Data were collected at 1 m intervals on a six- to ten-m transect in the principal plane of the sun. We measured from the sunlit to the shadowed side of the tree, and using this design radiance

could be measured in all four components (sunlit and shadowed canopy and background).

We also measured irradiance using the Exotech radiometer in hemispherical mode on the ground below the canopy at the same points on the transect. However, these measurements were subject to variation due to gaps in the canopy. Thus, we modified this technique in the second season by taking radiance measurements with the 15° FOV instrument pointed downward from 1 m height at a Kodak gray card placed on the ground. The known reflectance factors for the gray card in the two wavelength bands (18.36 percent and 19.47 percent, respectively) were used to calculate irradiance. Although this method ignores possible non-Lambertian surface effects of the gray card, paired hemispherical and gray card measurements taken in the open were well-correlated. From these paired measurements, we derived the same reflectance factors that were given as the gray card specifications.

Red and infrared reflectance were then calculated from radiance using the following relation: $R = L/E$, where R is reflectance, L is the radiance of the target, and E is irradiance. The hemispherical irradiance measurements taken in the open the sunlit end of the transect were used to approximate irradiance conditions during all measurements. From red and infrared reflectance, we calculated the normalized difference vegetation index (NDVI), which is defined as $(NIR - R)/(NIR + R)$. All measurements were taken in November 1986 and October 1987 under a clear sky between 10 a.m. and 2 p.m. local time. An entire set of measurements for a tree took less than twenty minutes, so the effect of changing sun angle was minimal. No changes in atmospheric conditions (cloudiness) were observed during a set of measurements.

There was no green herbaceous layer at the time of these measurements and the field layer was a heterogeneous mixture of sunlit light-colored dry soil and dry herbaceous material, shadows from sources other than the measure tree (plow furrows and other microrelief), and some green herbs and subshrubs near the transect.

Acacia albida and *Butyrospermum parkii* are typically 7 to 12 m tall, so we were forced to choose immature individuals for sampling, and the spectral characteristics of their crowns may not be representative of the population as a whole. This seemed particularly likely for the sampled *Butyrospermum parkii* because the individuals we measured appeared to have lower leaf density than mature individuals. *Acacia albida* canopies, on the other hand, looked representative of the local population despite the small size of the sampled trees. *Acacia seyal* and *Balanites aegyptiaca* are smaller and the individuals that we selected were of typical size and

morphology for the region. Ideally the sampling interval along the transect would have been shorter because the trees were quite small, but it was not possible to position the radiometer at shorter intervals using a hand-held pole. In spite of these limitations, general patterns emerge.

3. Results

Solar zenith angles were between 23° and 52° for all measurements (see table 1). Tree dimensional measurements are also shown in table 1. These are height (total height of the tree), height-to-width (height the widest part of the crown) and width of the crown. From these and a simple geometric shape model for the trees (Franklin and Strahler 1988) the amount of the transect in sunlit and shadowed crown and background can be estimated. Silhouettes of some of the canopies are shown in figure 1. Reflectance was averaged by species in case where the individual trees did not differ greatly in diameter, and the averaged reflectances are show in figures 2 through 4. Averaging may have masked some meaningful variability, and some patterns observed in the composite may be artifacts of averaging trees with slightly different leaf area, crown diameter and shape. Examples of the reflectance plots for a few individual trees are shown in figure 5, to illustrate the variability due to the heterogeneous canopy.

Some discussion of the generalized pattern of reflectance and irradiance that we observed may be helpful. First, consider the red band. In the red, the tree crown will be relatively dark due to strong absorption by leaves. Soil will be lighter, and the sky hemisphere will have some brightness due to scattering in the red. In the case of downward measurements above the canopy (figure 2), red reflectance is high over sunlit background, decreases as the radiometer's FOV encounters the canopy, decreases further over shadowed canopy, and increases slightly over shadowed background. In the near-infrared, the scene will appear somewhat different. Because transmission and scattering by the crown is strong, it will appear as a light object against a black sky background. Soil will appear dark in contrast to the crown. The generalized pattern for this type of scene shows near-infrared reflectance to be high over sunlit background, increase over sunlit canopy, decrease over shadowed canopy, and decrease further over shadowed background.

The result of these different patterns for the red and infrared wavebands is that NDVI increases over the canopy, but the pattern is shifted slightly shadow-ward from the crown. This is because infrared reflectance

increases as soon as the canopy is encountered on the sunlit side, whereas red reflectance does not decrease until further along the transect, owing to the open nature of the canopy at its edge. On the shadowed side, although the infrared reflectance is decreasing, the red reflectance remains low, and the ratio therefore remains high for a short distance into the shadow. The result of this shift is that the integrated area under the NDVI curve approximates the leaf area or green biomass of the tree crown fairly well.

This general picture holds well for crowns with reasonable leaf area. However, if leaf area is very low, as is the case with many of the trees measured in this study, the pattern will be somewhat different. Although infrared reflectance increases when the sunlit side of the crown is encountered, it drops off more quickly over the canopy due to fewer leaves and absorption by brown twigs and branches. Also, the shadow cast by the tree in the red is not as deep, and red reflectance may start to rise again past the center of the tree. Consequently, the NDVI increases over the canopy, but this increase is shifted towards the sunlit side of the tree as compared to the pattern for the denser canopy.

The averaged reflectances above the canopy for each species are shown in figure 2 (a-h). *Balanites aegyptiaca* (figure 2e) shows the first pattern described most clearly because, although it has few leaves, it has a dense, compact canopy with green stems and spines. *Butyrospermum parkii* and *Acacia albida* (figure 2f and g) had more heterogeneous canopies with some openings, and the red reflectance was not as depressed in the shadowed background, consequently the rise in the NDVI follows the tree outline more closely. This is intermediate between the two patterns we described. *Acacia senegal* and *Combretum glutinosum* (figure 2b, c and d) illustrate the second pattern, with NIR falling off past the leading edge of the tree, and the peak in NDVI shifted towards the sunlit edge. *Acacia seyal* had so few leaves that for some trees there was hardly any increase in infrared reflectance, although there was a decrease in red reflectance over sunlit canopy, and consequently a slight increase in the NDVI (figure 2a). For tree 13 (figure 2h) red absorption was minimal but a slight rise in infrared reflectance caused there to be an NDVI signal.

The typical downward-looking pattern under a dense canopied tree at 1.5 m (figure 3a-g) illustrates the effect of tree canopy shadowing on the red and near infrared radiances and the NDVI for a background consisting of bright soil with virtually no green plants. At first, NIR increases slightly as the radiometer sees NIR radiation scattered onto the ground near the tree augmenting the solar beam. The NIR falls as the radiometer field

of view begins to include the NIR shadow, which is deeper as canopy attenuation increases. As the beam path length through the canopy decreases, the depth of the the shadow decreases and NIR rises as the radiometer FOV emerges from the shadow. The situation for the red is similar, except that there is less initial scattering to supplement the solar and sky irradiance at the sunward edge of the tree. The result is a slight rise in NDVI that is centered around the shadowed edge of the tree. This pattern is again seen most clearly for *Balanites aegyptiaca* (figure 3e). The results are similar but noisier for *Combretum glutinosum*, *Butyrospermum parkii*, *Acacia albida* and *A. seyal* owing to the open nature of the crowns.

The irradiance measured under the canopy (figure 4a-h) is high in both bands in the open, then decreases in equal proportions under the sunlit canopy and shadowed canopy to a minimum in the shadow of the canopy. Both bands rise again as the edge of the shadow is neared, because of the increase in diffuse irradiance. The relative enrichment of infrared irradiance, due to scattering by the canopy, causes a slight rise in the NDVI of incident radiance. The NIR signal under the canopy is somewhat noisier than the red due to gaps and openings in the canopy, and greater transmission by the canopy in the NIR. This can be seen in the hemispherical irradiance plots for *Acacia albida*, *Butyrospermum parkii* and *A. seyal* (figure 4f, g and h). This is why irradiance was calculated from radiance of a known target in the 1987 season. The predicted pattern for a dense canopy is illustrated best by *Balanites aegyptiaca* (figure 4e), and also by *Acacia senegal* and *Combretum glutinosum* (figure 4b and c). For *Acacia seyal* (figure 4a) the pattern is slightly different because the crown is so open. Because the canopy of tree 13 (figure 4h) strongly reflected NIR, and red was absorbed more strongly in the shadow than over the canopy, the irradiance shows a drop in NDVI under the canopy, and an increase in the shadow. The slight rise in NDVI is located on the sunlit edge of the crown.

The above-canopy measurements discussed earlier show the strongest response of NDVI to the presence of vegetation canopy. This provides and opportunity to try to relate NDVI, as integrated across the entire crown, with leaf area. Figure 5 shows scatterplots of integrated NDVI over the crown versus crown volume for all trees, and for subsets of species. To calculate integrated NDVI, the red and infrared reflectances over bare soil were subtracted from each of the measurements over the canopy. Then NDVI was then calculated, and these values were summed. For crown volume, the volume of a sphere with radius r of each crown (half of the width, from table 1) was scaled by the proportion of that sphere filled with foliage. This scalar was estimated

by choosing a subsample of the trees, laying a grid over a high-contrast horizontal photograph of the crown (as in figure 1), and estimating the proportion of a circle of radius r covered with crown by dot count. An average value was chosen for each species. The values used were 1.0 for *Balanites aegyptiaca*, 0.40 for *Acacia seyal*, 0.45 for *A. senegal*, 0.50 for *Combretum glutinosum* and *Acacia albida*, and 0.75 for *Butyrospermum parkii*. A value of 0.20 was used for trees 13 and 14, because these *A. seyal* had very few leaves in the 1986 season. These estimates of volume actually include twigs and branches, as well as leaves, but they are reasonable approximations in the absence of measurements of leaf area.

Tree 9 had a very low NDVI compared to the other *Balanites aegyptiaca*, and is considered to be an outlier. A linear regression calculated for the remaining trees yielded an r^2 of 0.50. It would be better to look at this relationship for individual species. The large differences in leaf morphology and canopy structure make interspecific comparisons difficult, especially given our proxy measure of leaf area. Unfortunately, our sample size for each species was quite small. The relationship between integrated NDVI and volume was poor for *Balanites aegyptiaca*. This was probably because the canopies were extremely irregular in shape, and our estimate of crown volume was probably not well-related to leaf area for that species. Scatterplots for *Combretum glutinosum*, and *Acacia albida* and *Butyrospermum parkii* grouped together are also shown in figure 5 with r^2 of 0.75 and 0.81 respectively.

4. Discussion

An important conclusion from this work is the verification of the four-component model — i. e., shadowed and sunlit tree crown and background exhibit different reflectance characteristics in the wavebands measured. Although the transitions are not as abrupt as Li and Strahler's (1986) simple model assumes, the observed pattern could be predicted from more sophisticated models that consider the transmission of radiation through the tree canopy (Prince 1987, Li and Strahler 1988) and the non-Lambertian infrared scatter from the canopy. Li and Strahler's (1986) assumptions are born out in that the shadowed crown (their component T) is the darkest component, and that it is greener (has greater infrared to red contrast†) than shadowed background (Z). Figure

† We are using the term "greener" here in the sense of the greeness component of Kauth and Thomas (1976).

6 shown the generalized reflectance and irradiance patterns, and the location of the four spectral components on the x axis.

Our measurements also show that the NDVI, which is most affected by diverging red and infrared values, is relatively insensitive to self-shadowing of the savanna tree canopies examined using measurements of irradiance from below the canopy. When viewed from above however, an area of elevated NDVI is detected which is proportional to the volume of the canopy, but is shifted shadow-ward slightly in the case of dense crowns, and shifted sunward for sparse crowns. The NDVI, measured above or below the canopy, does not remain constant for sunlit and shadowed background consisting of bare soil, but rather rises slightly in the shadow. This is due to the influence of the canopy which causes some scattering of NIR. This effect was also noted by Diarra and Hiernaux (1986) for the sites in the Gourma region, Mali.

All canopies measured here were very open and sparse (low leaf area) and in denser canopies the observed effects can be expected to be more pronounced. The NDVI tends to saturate at an LAI around 7 or 8 (Spanner *et al.* 1984, Holben *et al.* 1980) or at green biomass of about 700 g/m^2 dry weight (Tucker 1979). For comparison, our *Acacia seyal* and *Balanites aegyptica* measurements were taken in a site with about 100 g/m^2 tree foliage biomass (maximum standing crop; Diarra and Hiernaux 1987) at roughly 50 percent crown closure, which gives approximately 200 g/m^2 within the tree canopy. In a Guinea savanna woodland Menaut and César (1982) measured an LAI of 1 with canopy cover of 45 percent or approximately an LAI of 2 within the tree canopy.

While our results show that the NDVI is responding to photosynthetic biomass, it is also responding to shadowed bare ground. Therefore, estimates of total photosynthetic biomass of the tree and grass layer may be affected by the shadows cast on the ground by the trees, particularly at low sun angle or large satellite view angle. As solar zenith angle increases, the path length though the canopy increases, so that shadows not only lengthen, they deepen. This would increase the effect of shadows on the composite scene reflectance.

Our results are somewhat limited by the difficulties of data acquisition in remote study areas, but they do indicate the effects of tree reflectance properties on measurements of spectral radiance. This has important implications for remote sensing models of composite scene reflectance, particularly three-dimensional discrete object models, and for vegetation monitoring using the NDVI.

References

Asrar, G., Kanamasu, E. T., Jackson, R. D., and Pinter, P. J. Jr., "Estimation of total above-ground phytomass production using remotely sensed data," *Remote Sensing of Environment*, vol. 17, pp. 211-220, 1985.

Aubréville, A., *Climats, Foret et Desertification de l'Afrique Tropicale*, p. 351, Soc. Ed. Geogr. Marit-et Cd., Paris, 1949.

Bourlière, F. and Hadley, M., "Present-day Savannas: An Overview," in *Tropical Savannas*, ed. F. Bourlière, pp. 1-18, Elsevier Scientific Publishing Company, Amsterdam, 1983.

Colwell, J. E., "Landsat feature enhancement or, can we separate vegetation from soil?," *Proceedings of the 15th International Symposium on Remote Sensing of Environment*, pp. 599-621, Ann Arbor, Michigan, 1981.

Diarra, L., Cissé, M. I., and Hiernaux, P., "Evolution de la vegetation sahelienne après la sécheresse bilan du suivi de sites du Gourma en 1985," Programme des Zones Aride et Semi-aride, Document du Programme, Centre International pour l'Elevage en Afrique (CIPEA), Bamako, Mali, 1986.

Diarra, L. and Hiernaux, P., "Evolution de la végétation sahélienne après la sécheresse bilan du suivi des sites du Gourma en 1986," Programme des Zones Aride et Semi-aride, Document du Programme, Centre International pour l'Elevage en Afrique (CIPEA), Bamako, Mali, 1987.

Frank, T. D., "Differentiating semiarid environments using Landsat reflectance indexes," *Professional Geographer*, vol. 37, pp. 36-46, 1985.

Franklin, J., "Thematic Mapper analysis of coniferous forest structure and composition," *International Journal of Remote Sensing*, vol. 7, pp. 1287-1301, 1986.

Franklin, J. and Strahler, A. H., "Invertible canopy reflectance modeling of vegetation structure in semiarid savanna," *IEEE Geoscience and Remote Sensing*, 1988. Accepted for publication.

Heimes, F. J. and Smith, J. A., "Spectral variability in mountain terrain," Final Report, Rocky Mountain Forest and Range Experiment Station U. S. Forest Service Cooperative Agreement 16-625-CA, 1977.

Hiernaux, P. H. Y. and Justice, C. O., "Suivi du développement végétal au cours de l'été 1984 dans le Sahel Malien," *International Journal of Remote Sensing*, vol. 7, pp. 1515-1531, 1986.

Holben, B. N., Tucker, C. J., and Fan, C. J., "Spectral assessment of soybean leaf area and leaf biomass," *Photogrammetric Engineering and Remote Sensing*, vol. 46, pp. 651-656, 1980.

Huete, A. R., Jackson, R. D., and Post, D. F., "Spectral response of a plant canopy with different soil backgrounds," *Remote Sensing of Environment*, vol. 17, pp. 37-53, 1985.

Hutchinson, J., Dalziel, J. M., and Hepper,, *Flora of West Tropical Africa*, Crown Agents for Oversea Governments and Administrations, London, 1963.

Jackson, R. D., "Spectral indices in n-space," *Remote Sensing of Environment*, vol. 13, pp. 409-421, 1983.

Jupp, D. L. B., Walker, J., and Penridge, L. K., "Interpretation of vegetation structure in Landsat MSS imagery: A case study in disturbed semi-arid eucalypt woodlots. Part 2. Model-based analysis," *Journal of Environmental Management*, vol. 23, pp. 35-57, 1986.

Kauth, R. J. and Thomas, G. S., "The tasseled cap — a graphic description of the spectral-temporal development of agricultural crops a ss seen by Landsat," *Proceedings of the Symposium on Machine Processing of Remotely Sensed Data*, pp. 4B41-4B51, Purdue University, West Lafayette, Indiana, 1976.

Kimes, D. S. and Kirchner, J. A., "Radiative transfer model for heterogeneous 3-D scenes," *Applied Optics*, vol. 21, pp. 4119-4129, 1982.

Kimes, D. S., Newcomb, W. W., Nelson, R. F., and Schutt, J. B., "Directional reflectance distributions of a hardwood and pine forest canopy," *IEEE Transactions on Geoscience and Remote Sensing*, vol. GE-24, pp. 281-293, 1986.

Kleman, J., "The spectral reflectance of stands of Norway Spruce and Scotch Pine measured from a helicopter," *Remote Sensing of Environment*, vol. 20, pp. 253-265, 1986.

Li, X. and Strahler, A. H., "Geometric-optical modeling of a conifer forest canopy," *IEEE Transactions on Geoscience and Remote Sensing*, vol. GE-23, pp. 705-721, 1985.

Li, X. and Strahler, A. H., "Geometrical-optical bidirectional reflectance modeling of a coniferous forest canopy," *IEEE Transactions on Geoscience and Remote Sensing*, vol. GE-24, pp. 906-919, 1986.

Li, X. and Strahler, A. H., "Modeling the gap probability of a discontinuous vegetation canopy," *IEEE Transactions on Geoscience and Remote Sensing*, vol. GE-25, pp. 161-170, 1988.

Logan, T. L., "Regional biomass estimation of a coniferous forest environment from NOAA AVHRR satellite imagery," Ph.D. dissertation, Department of Geography University of California, Santa Barbara, California, 1983. 263 pp.

Logan, T. L. and Strahler, A. H., "Optimal Landsat transforms for forest applications," *Proceedings of the Sixteenth International Symposium on Remote Sensing of Environment*, pp. 455-468, Ann Arbor, Michigan, 1982.

Menaut, J. C. and César, J., "The structure and dynamics of a West African savanna," in *Ecology of Tropical Savannas*, ed. B. J. Huntley and B. H. Walker, pp. 80-100, Springer-Verlag, New York, 1982.

Nielsen, M., *Introduction to the Flowering Plants of West Africa*, University of London Press, London, 1965.

Norman, J. M., Welles, J. M., and Walter, E. A., "Contrasts among bidirectional reflectance of leaves, canopies and soils," *IEEE Transactions on Geoscience and Remote Sensing*, vol. GE-23, pp. 659-667, 1985.

Olsson, K., "Remote sensing for fuelwood resources and land degradation studies in Kordofan, the Sudan," Ph.D. Dissertation., The Royal University of Lund, Department of Geography, Lund, Sweden , 1985. 182 pp.

Otterman, J., "Albedo of a forest modeled as a plane with dense vertical protrusions," *Journal of Climate and Applied Meteorology*, vol. 22, pp. 297-307, 1984.

Otterman, J., "Bidirectional and hemispherical reflectivities of a bright soil plane and a sparse dark canopy," *International Journal of Remote Sensing*, vol. 6, pp. 897-902, 1985.

Perry Jr., C. R. and Lautenschlager, L. F., "Functional equivalence of spectral vegetation indices," *Remote Sensing of Environment*, vol. 14, pp. 169-182, 1984.

Prince, S. D., "Measurement of canopy interception of solar radiation by stands of trees in sparsely wooded savanna," *International Journal of Remote Sensing*, vol. 8, pp. 1747-1766, 1987.

Prince, S. D. and Astle, W. L., "Satellite remote sensing of rangelands in Botswana. I. Landsat MSS and herbaceous vegetation," *International Journal of Remote Sensing*, vol. 7, pp. 1533-1553, 1986.

Prince, S. D. and Tucker, C. J., "Satellite remote sensing of rangelands in Botswana. II. NOAA AVHRR and herbaceous vegetation," *International Journal of Remote Sensing*, vol. 7, pp. 1555-1570, 1986.

Ranson, K. J. and Daughtry, C. S. T., "Scene shadow effects on multispectral response," *IEEE Transactions on Geoscience and Remote Sensing*, vol. GE-25, pp. 502-509, 1987.

Ranson, K. J., Daughtry, C. S. T., and Biehl, L. L., "Sun angle, view angle, and background effects on spectral response of simulated balsam fir canopies," *Photogrammetric Engineering and Remote Sensing*, vol. 52, pp. 649-658, 1986.

Ranson, K. J., Daughtry, C. S. T., Biehl, L. L., Bauer, M. E., and canopies, Sun-view angle effects on reflectance factors of corn, *Remote Sensing of Environment*, vol. 18, pp. 147-161, 1985.

Sellers, P. J., "Canopy reflectance, photosynthesis, and transpiration. II. The role of biophysics in the linearity of their interdependence," *Remote Sensing of Environment*, vol. 21, pp. 143-183, 1987.

Smith, J. A., "Matter-energy interactions in the optical region," in *Manual of Remote Sensing*, ed. D. S. Simonett, 2nd edition, vol. 1, pp. 61-113, American Society of Photogrammetry, Falls Church, Virginia, 1983.

Spanner, M. A., Teuber, K. B., Acevedo, W., Peterson, D. L., Running, S. W., Card, D. L., and Mouat, D. A., "Remote sensing of the leaf are index of temperate coniferous forests," *Proceedings of the Machine Processing of Remotely Sensed Data Symposium*, pp. 301-309, West Lafayette, Indiana, 1984b.

Suits, G. H., "The calculation of the directional reflectance of a vegetation canopy," *Remote Sensing of Environment*, vol. 2, pp. 117-125, 1972.

Suits, G. H., The extension of a uniform canopy reflectance model to include row effects, Environmental research Institute of Michigan, Ann Arbor, Michigan, 1981.

Tucker, C. J., "Red and photographic infrared linear combinations for monitoring vegetation," *Remote Sensing of Environment*, vol. 8, pp. 127-150, 1979.

Verhoef, W. and Bunnik, N. J. J., "The spectral directional reflectance of row crops. Part 1: Consequences of non-lambertian behavior for automatic classification. Part 2: Measurements on wheat and simulations by means of a reflectance model for row crops.," Netherlands Interdepartmental Working Groups on the Application of Remote Sensing, Delft, 1976.

Von Maydell, H. J., *Arbres and Arbustes du Sahel*, 1983.

Walker, J., Jupp, D. L. B., Penridge, L. K., and Tian, G., "Interpretation of vegetation structure in Landsat MSS imagery: a case study in disturbed semi-arid eucalypt woodlots. Part 1. Field data analysis," *Journal of Environmental Management*, vol. 23, pp. 19-23, 1986.

Table 1

Number	Species	Height (m)	Tree Width (m)	Width (m)
Solar zenith angle, $\theta = 39°$				
1	*Balanites aegyptica*	3.1	2.5	2.3
2	*Balanites aegyptica*	4.1	2.7	3.2
3	*Balanites aegyptica*	3.1	1.5	3.2
4	*Balanites aegyptica*	4.0	2.8	3.6
5	*Balanites aegyptica*	2.3	1.7	2.1
6	*Balanites aegyptica*	2.8	1.4	2.4
Solar zenith angle, $\theta \approx 30°$				
7	*Balanites aegyptica*	4.0	-	3.5
8	*Balanites aegyptica*	3.5	-	3.7
9	*Balanites aegyptica*	3.5	-	4.0
10	*Balanites aegyptica*	4.0	-	3.7
11	*Balanites aegyptica*	3.5	-	3.5
12	*Balanites aegyptica*	3.0	-	2.6
Solar zenith angle, $\theta \approx 30°$				
13	*Acacia seyal*	2.90	2.1	3.3
14	*Acacia seyal*	3.81	2.4	4.9
15	*Acacia seyal*	4.0	-	5.5
16	*Acacia seyal*	1.5	-	3.7
17	*Acacia seyal*	3.1	-	4.3
Solar zenith angle, $\theta \approx 25°$				
18	*Acacia senegal*	2.7	-	3.2
19	*Acacia senegal*	2.4	-	3.5
20	*Acacia senegal*	3.0	-	3.5
Solar zenith angle, $\theta \approx 38°$				
21	*Combretum glutinosum*	3.0	-	3.2
22	*Combretum glutinosum*	2.6	-	2.5
23	*Combretum glutinosum*	3.6	-	5.0
24	*Combretum glutinosum*	2.1	-	3.8
25	*Combretum glutinosum*	3.7	-	6.0
26	*Combretum glutinosum*	3.5	-	2.7
Solar zenith angle, $\theta = 52°$				
27	*Vitellaria paradoxa*	4.3	2.7	3.8
28	*Vitellaria paradoxa*	3.8	2.7	2.9
29	*Vitellaria paradoxa*	5.0	3.2	4.2
Solar zenith angle, $\theta = 36°$				
30	*Acacia albida*	4.88	4.1	4.2
31	*Acacia albida*	6.25	3.8	5.5
32	*Acacia albida*	5.49	3.8	4.2

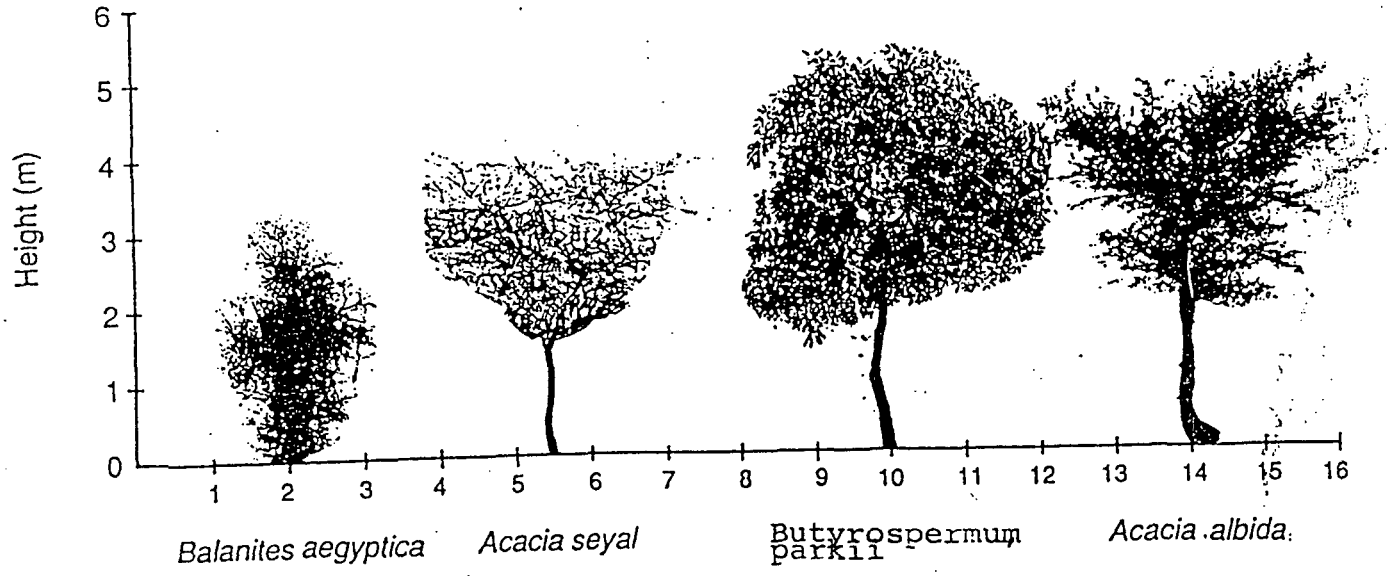

Figure 1. Silhouettes of several of the tree canopies included in the study from high-contrast photographs.

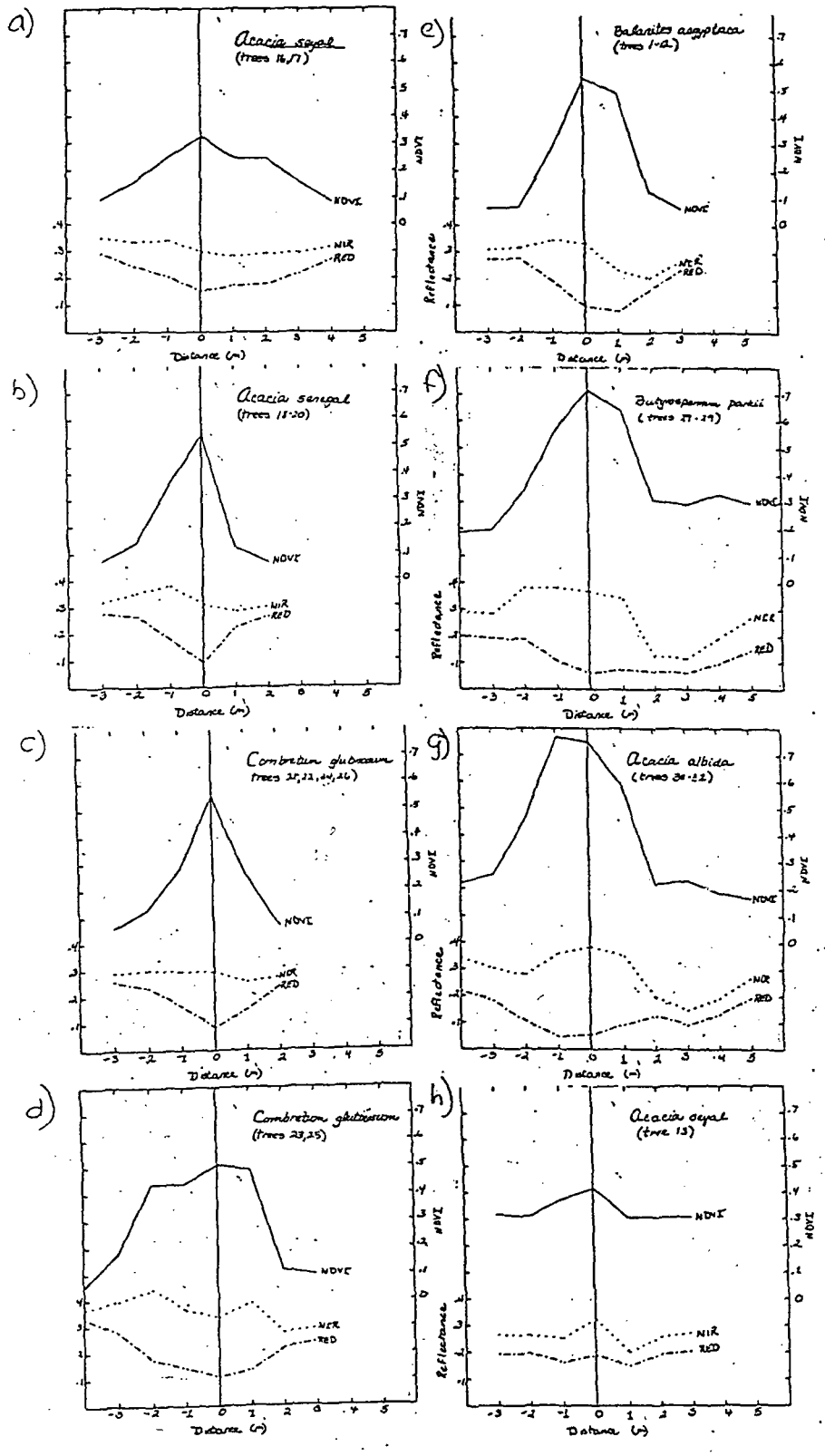

Figure 2. Reflectance of a tree canopy, 1 m above the tree, down-looking (15 ° field of view), in TM Bands 3 (.63-.69 μm) and 4 (.79-.90 μm), and calculated NDVI for trees averaged by species. a. *Acacia seyal* (trees 16-17), b. *Acacia senegal* (trees 18-20), c. *Combretum glutinosum* (trees 21, 22, 24 and 26), d. *Combretum glutinosum* (trees 23 and 25), e. *Balanites aegyptiaca* (trees 1-12), f. *Butyrospermum parkii* (trees 27-29), g. *Acacia albida* (trees 30-32), h. *Acacia seyal* (tree 13).

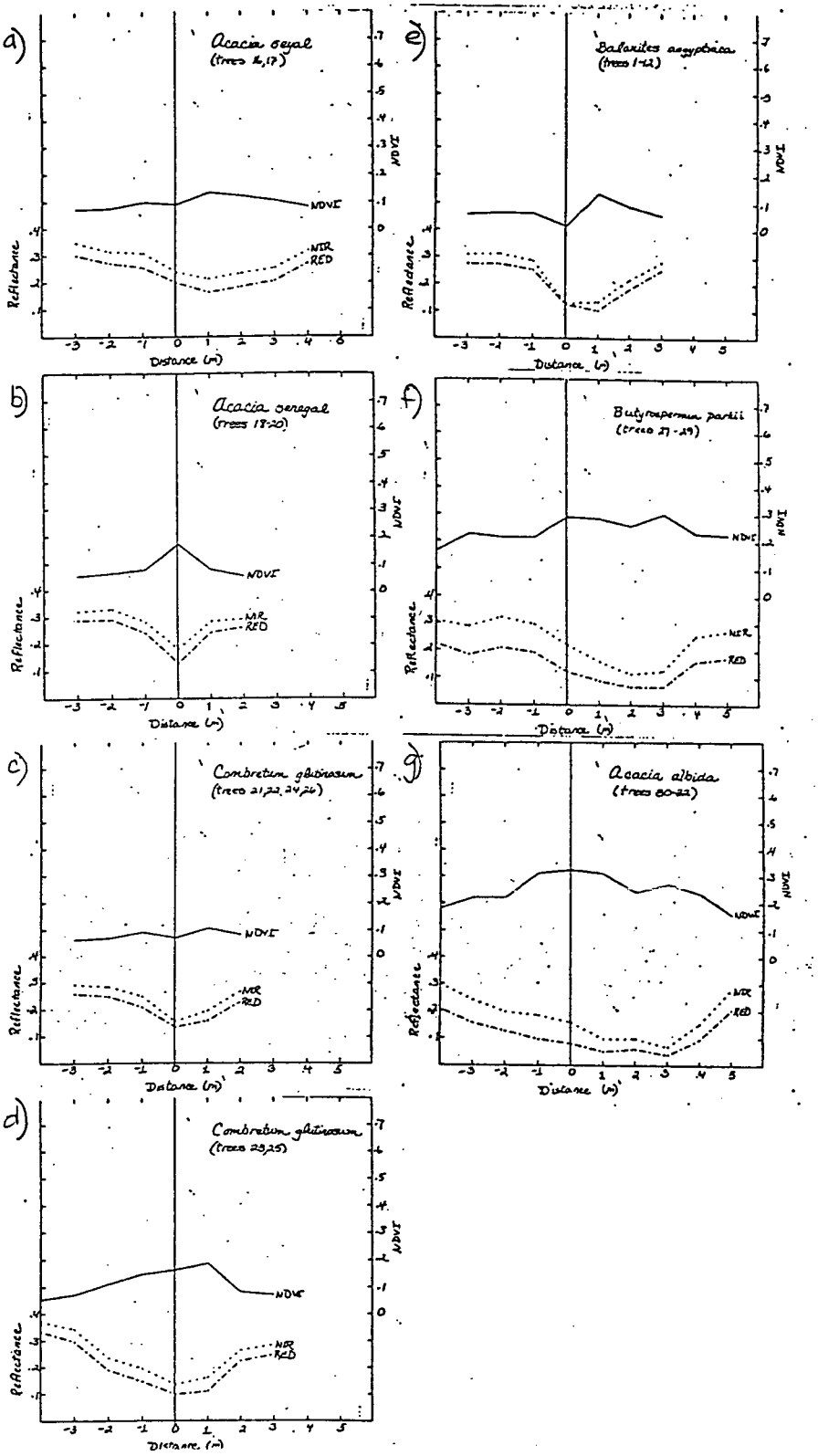

Figure 3. Reflectance of the ground, below the tree canopy canopy (1.5 m), down-looking (15 ° field of view), in TM Bands 3 (.63-.69 μm) and 4 (.79-.90 μm), and calculated NDVI for trees averaged by species. a. *Acacia seyal* (trees 16-17), b. *Acacia senegal* (trees 18-20), c. *Combretum glutinosum* (trees 21, 22, 24 and 26), d. *Combretum glutinosum* (trees 23 and 25), e. *Balanites aegyptiaca* (trees 1-12), f. *Butyrospermum parkii* (trees 27-29), g. *Acacia albida* (trees 30-32).

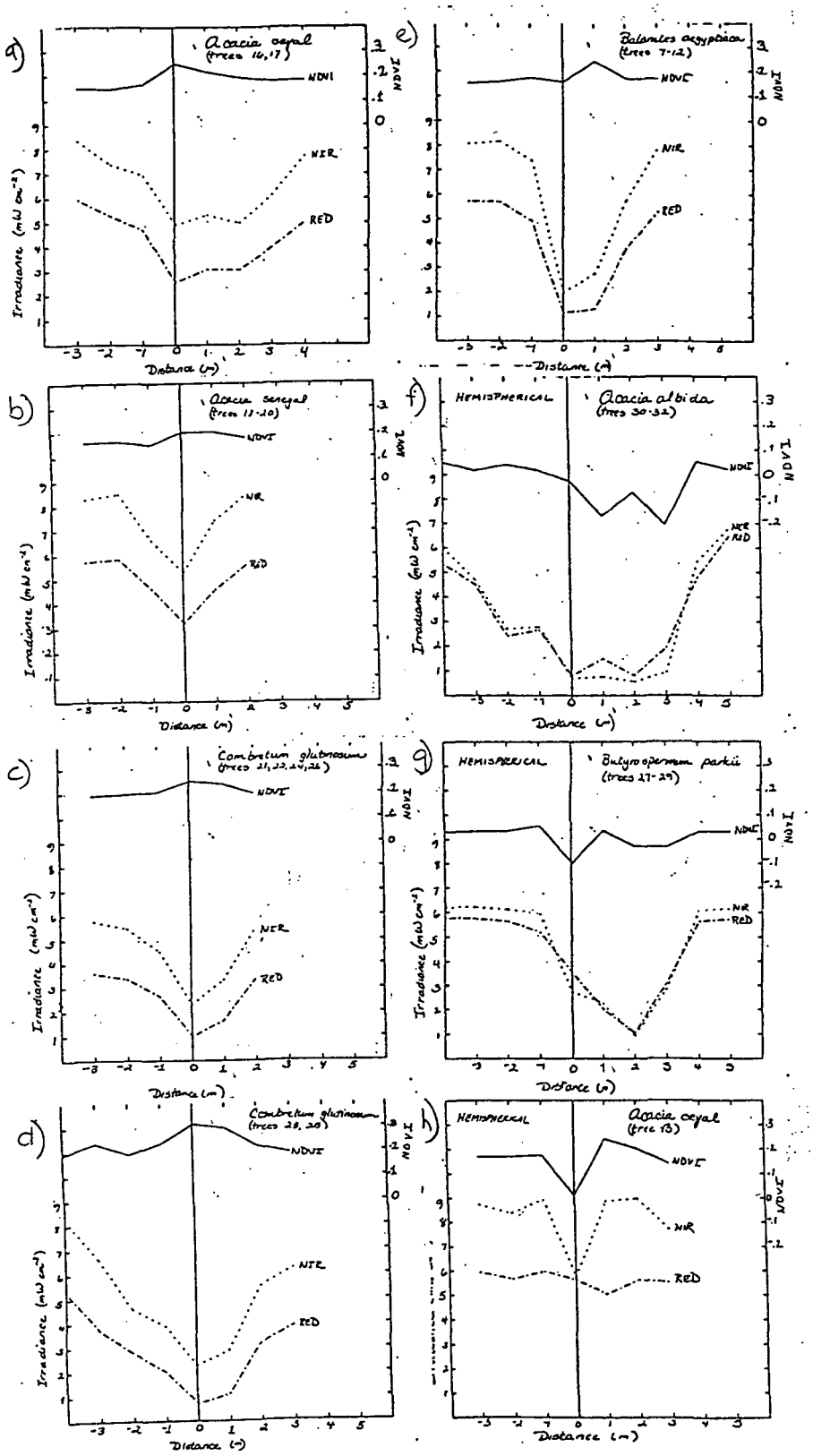

Figure 4. Irradiance ($mW\ m^2$) under a tree canopy calculated from a gray card in TM Bands 3 (.63-.69 μm) and 4 (.79-.90 μm), and calculated NDVI for trees averaged by species. a. *Acacia seyal* (trees 16-17), b. *Acacia senegal* (trees 18-20), c. *Combretum glutinosum* (trees 21, 22, 24 and 26), d. *Combretum glutinosum* (trees 23 and 25), e. *Balanites aegyptiaca* (trees 7-12). Irradiance calculated from a hemispherical radiometer. f. *Butyrospermum parkii* (trees 27-29), g. *Acacia albida* (trees 30-32), h. *Acacia seyal* (tree 13).

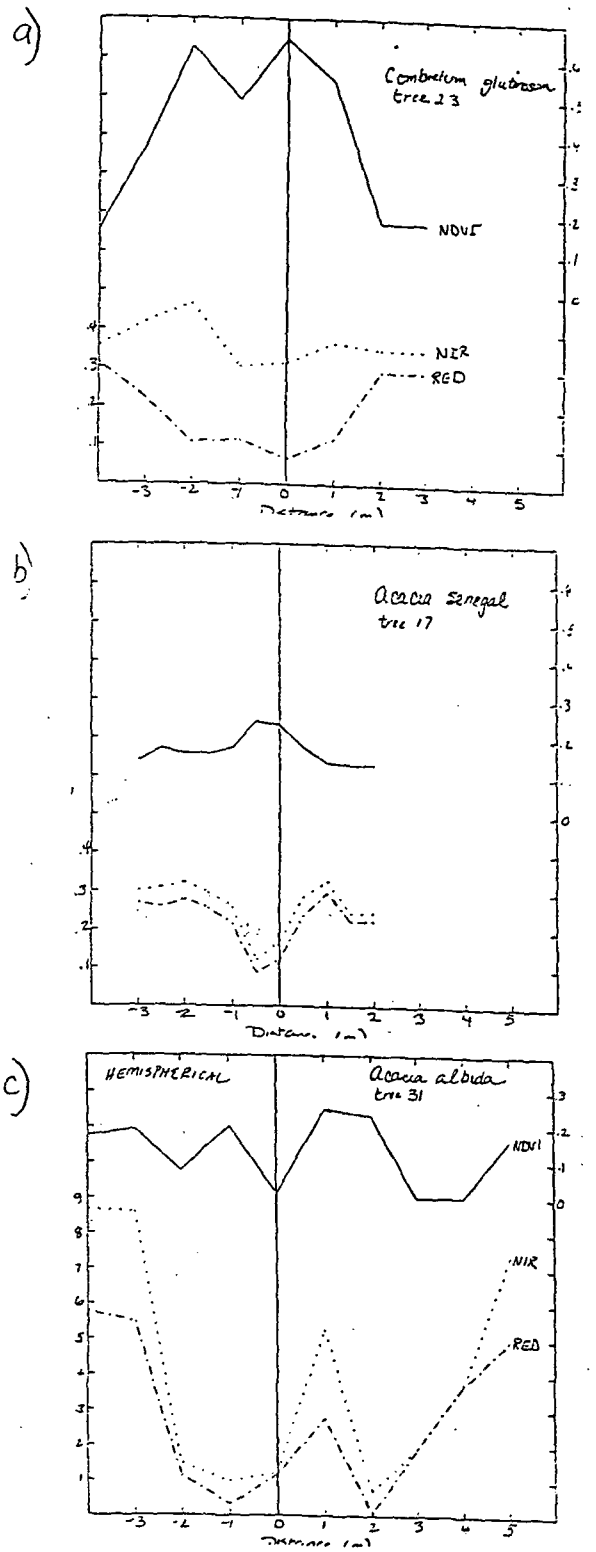

Figure 5. Samples of individual canopy reflectance (tree 23), ground reflectance under the canopy (tree 17) and hemispherical irradiance under the canopy (tree 31), showing the variability of the measurements for individual trees.

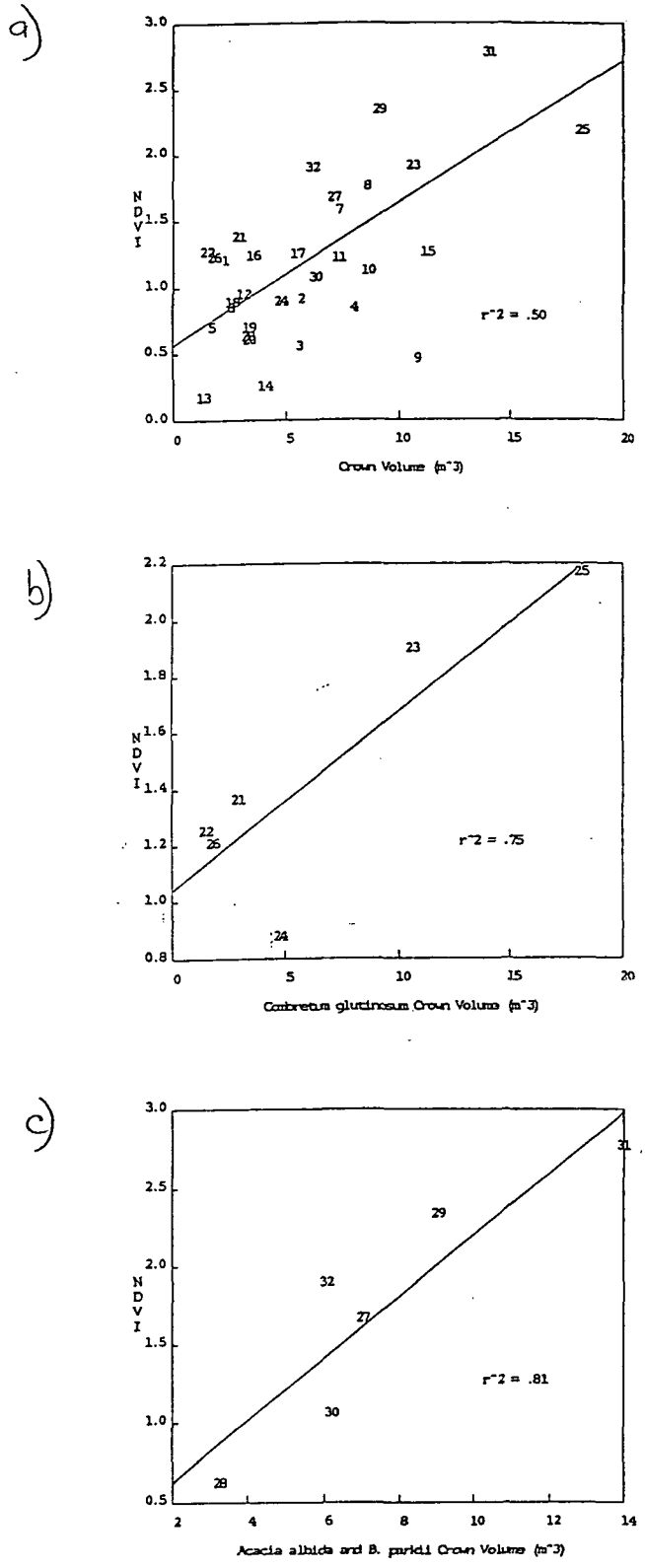

Figure 6. Scatterplots of crown volume (m^3) versus integrated NDVI for (*a*) all trees, $r^2 = .50$ (9 was considered an outlier); (*b*) *Combretum glutinosum*, $r^2 = .75$; and (*c*) *Acacia albida* and *Butyrospermum parkii*, $r^2 = .81$. Regression lines are shown.

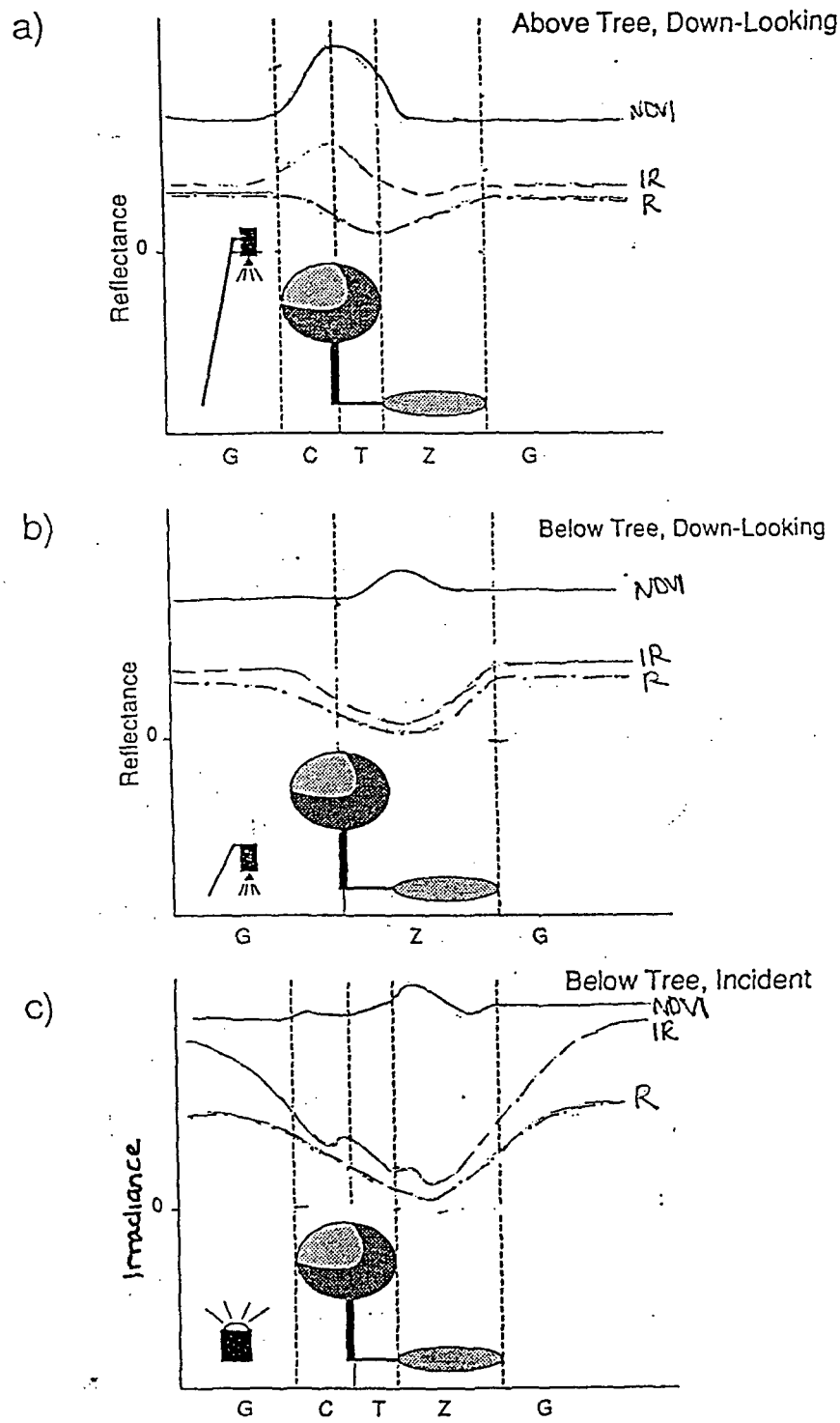

Figure 7. Generalized patterns for red and infrared reflectance and incident radiation, and NDVI, (*a*) above the tree canopy, down-looking, (*b*) below the canopy, down-looking (at the soil background), (*c*) below the canopy, incident hemispherical radiation. The sketch shows the position of the tree and the radiometer relative to these measurements. The x axis shows the location of the spectral components used in the Li-Strahler simple model: shadowed (Z) and sunlit (G) background, and shadowed (T) and sunlit (C) tree crown.

Chapter 3

ESTIMATING LEAF AND WOOD BIOMASS IN SAHELIAN AND SUDANIAN WOODLANDS USING A REMOTE SENSING MODEL

Abstract

Predictions of tree size and density from a remote sensing model were used with allometric equations from the literature to estimate woody and foliage biomass in sparse woodlands. Study sites were located in the Sudanian and Sahelian bioclimatic zones in Mali, West Africa, with cover ranging from ten to fifty percent. Our estimates are compared to independent measurements made in the Sahelian sites, and to typical values from the literature for these regions and for similar woodlands. If combined with a vegetation stratification at the appropriate scale, this approach could provide regional estimates of woody biomass for fuelwood inventory. Estimates of foliage biomass could be used in forage production modeling and inventory. Both could be used in regional and global scale models of biogeochemical cycling.

INTRODUCTION

Predictions of tree size and density from a remote sensing model were used to estimate wood and foliage biomass in sparse woodland sites in Mali, West Africa. When combined with a vegetation stratification at the appropriate scale, this approach could provide estimates of foliage and woody biomass for large areas. Regional estimates of biomass are important for fuelwood inventory, for forage production modeling and inventory, and as input to regional and global scale models of the biogeochemical cycles.

One way to measure biophysical vegetation parameters over large areas is with satellite reflectance data (NASA 1983, NAS 1986). Photosynthetic biomass and intercepted photosynthetically active radiation (IPAR) have been inferred from satellite spectral measurements at continental and regional scale (Goward *et al.* 1985, Tucker *et al.* 1985a), and vegetation has been stratified into physiognomic classes on a continental scale (Tucker *et al.* 1985b, Nelson *et al.* 1986). Remote sensing techniques that use spectral greenness indices to predict biomass, productivity and other ecosystem characteristics are based on theory which holds true only for vegetation whose canopy is composed of homogeneous photosynthetic biomass such as agricultural crops, natural grasslands and dense forests (Sellers 1986). In this paper we show how structural characteristics of vegetation, estimated from remotely sensed data using a reflectance model, can be used to predict two parameters of the woody component of an ecosystem, its foliage biomass and above ground woody biomass. This technique was applied to two types of sparse woody vegetation, sparsely wooded grassland (sometimes referred to as savanna) and open woodland.

Woody biomass must be quantified in semiarid regions for the purpose of fuelwood inventory. Wood and charcoal derived from these woodlands are the primary energy source for most of the developing worlds' population in Africa, South America, India and throughout Asia (Gillet 1980, Le Houérou 1980, Earl 1975, Arnold and Jongma 1978, Dunkerley *et al.* 1981). Although change in forest area in developing countries has been shown to be related to population growth and agricultural expansion (Allen and Barnes 1985), as well as climatic change (Livingston 1978), there is little agreement on the current distribution or magnitude of changes in these woodlands (Allen 1985, UNEP/FAO 1982).

It is also important to measure foliage biomass in sparse woodlands. Estimates of foliage biomass can be used in forage production modeling and inventory (Justice and Hiernaux 1986, Hiernaux and

Justice 1986, Hiernaux *et al.* 1984). In regions like the Sahel, foliage biomass production can be of the same order of magnitude as grass biomass production for woodland sites. Areas with high tree density may cover only a small fraction of areas of pastoralism and transhumance (e.g. probably less than ten percent of a 2,000 km^2 area in our Sahelian study region), and not all foliage biomass is available to animals as browse (because they can't reach it, Hiernaux 1980, Pellew 1980). However, browse may be the only available fodder during the very long dry season (Hiernaux and Cissé 1983, Penning de Vries and Djitéye 1982, Okafor 1980), and during drought or poor growing seasons (Diarra and Hiernaux 1987).

Estimates of woody and foliage biomass in major biomes are parameters in regional and global scale models of biogeochemical cycling (Woodwell *et al.* 1978). Most of the carbon and nutrients tied up in terrestrial vegetation are in the woody structures. Although sparse woodland has considerably fewer trees than dense forest, these woodlands cover more area than any other vegetation type on the earth's surface (Ajtay *et al.* 1979, Houghton *et al.* 1983), and they are rapidly changing. Photosynthetic biomass is also a critical component of regional nutrient cycling. In West Africa, virtually all nitrogen fixation takes place during regrowth of natural vegetation in grazed or fallow savanna woodlands or grasslands (Robertson and Rosswall 1986).

In this study, the regional averages of the structural parameters (tree size and density) derived from the remote sensing model were used with allometric equations from the literature to estimate above ground woody and foliage biomass for the test sites. The two types of woodland investigated were Sahelian *Acacia* woodland and Sudanian parkland (crop/woodland) in West Africa. We compared our estimates to independent measurements made in the Sahelian sites (Hiernaux and Justice 1986, Diarra and Hiernaux 1987), and to typical values from the literature for these regions and for structurally similar woodland types.

BACKGROUND

A canopy reflectance model based on a simplified geometric model of trees and their projected shadows predicts tree size and density from satellite reflectance data in open stands of woody vegetation (Li and Strahler 1986). The model assumes that the soil background is bright, and the presence of trees

reduces reflectance, particularly in the visible and middle infrared wavebands. Within the range of cover considered, multispectral brightness recorded by the satellite is inversely and linearly proportional to vegetation cover. Similar remote sensing models have been used by Colwell (1981), Ustin *et al.* (1986), Pech *et al.* (1986), Pech and Davis (1987), and Otterman and Tucker (1985) to estimate vegetation cover in semiarid regions. Further, by modelling the trees as a simple geometric shape with a given size distribution, the area of shadow can be predicted if the sun angle is known. Thus the estimate of canopy cover can be refined. The satellite records radiance over a particular field of view (approximately 812 m^2 for the data used in this study) and these measurements are arranged in a regular array. Therefore, a number of measurements falling within a woodland stand are replicate samples of reflectance. The mean is related to average cover, and the variance is related to the size and density of the plants. A stand of small trees at high density will have low variance, and large trees at low density will have high variance. These parameters (size and density) can be solved for if they can be assumed to be independent.

The Li-Strahler model was applied to Thematic Mapper data from the Landsat satellite for study sites in Mali, West Africa. Predictions of canopy cover and density were reasonably accurate, but crown size was not predicted well. Site specific predictions were not very accurate because this simple model does not account for all the factors contributing to reflectance, in particular, variance in background brightness due to leaf litter, shadowing from microscale topography, and so forth. However, the errors were not systematic. Therefore, when predictions for sites within bioclimatic regions (Sahelian versus Sudanian) were averaged, crown size as well as density were estimated with greater success. (See Franklin and Strahler, 1988, for a detailed discussion of the model and its performance in these study sites.)

The strength of the model is that it uses the shadowing geometry of the vegetation to derive structural information about tree size and density from covariance analysis. A well-calibrated empirical remote sensing model that accurately predicted canopy cover from reflectance data could also be used to estimate biomass. However, average tree size would have to be known from some independent source or cover and biomass would have to be directly related (see Hellden 1987). An empirical relationship between cover and biomass will only hold for a particular vegetation formation, and therefore direct estimates of size and density will probably yield more accurate biomass estimates. In other words, within a particular

vegetation type, a stratum with many small trees will have different biomass parameters than one with few large trees, even though the cover may be the same.

PREVIOUS WORK IN THE STUDY AREA

Average tree size (crown area) and density were sampled in the field and predicted using the remote sensing model for ten sites in two regions. This work was presented in Franklin and Strahler (1988), and only a few key points will be repeated for clarity. Sites ranged in size from 10 to 100 ha. Field sample plots ranged from 0.1 to 1.1 ha, depending on woodland stand density. Plot size was fixed within a site, and four to eight plots per site were sampled. In each plot each tree was enumerated and the crown dimensions measured. Six of the sites were located in the Sudanian bioclimatic zone in crop/woodland type of vegetation, near Ségou, Mali (average rainfall roughly 800 mm). These sites were dominated by *Butyrospermum parkii* (G.Don) Hepper (nomenclature follows Von Maydell 1983, and Hutchinson *et al.* 1963) and *Acacia albida* Del. at very low density with crops grown under them. Four Sahelian zone sites were located in woodland dominated by *Acacia seyal* Del. and *A. nilotica* (L.) Willd. Del. in the Gourma region of Mali (average rainfall, 250 mm). These sites are monitored as part of an ongoing study by the International Livestock Centre for Africa (see Diarra and Hiernaux 1987). Tree cover is generally less than ten percent in the Sahel, but was twenty to fifty percent in the low-lying, seasonally inundated sites used in this study.

Table 1 (modified from Franklin and Strahler, 1988) shows the averaged predicted and sampled values of crown area and density that were used to estimate average biomass for the sites. The Sudanian sites have fewer larger trees, and the Sahelian sites have smaller trees at higher density. Because the equations predicting biomass from crown or basal area describe an area-to-volume relationship, errors in the estimation of tree size for individual sites would be magnified. Therefore, we did not attempt to estimate biomass for individual sites but only for these averaged values.

BIOMASS EQUATIONS

Data on crown area and tree density are needed to predict foliage and woody biomass using allometric equations from the literature. These parameters are predicted from the remote sensing model. Sometimes stem (trunk) size and/or height are used to predict biomass, especially in more mesic forest types. In semiarid woodlands, trunks and crowns increase in diameter as the tree gets older (but not necessarily taller; see Poupon 1977). Therefore, crown area can often be used as the independent variable to predict biomass. However, existing biomass equations and common sense both indicate that crown area will be a better indicator of leaf biomass than of wood biomass, and this will be discussed further below.

Foliar Biomass

Table 2 presents regression equations from the literature predicting leaf biomass from structural parameters for several of the species occurring in our sites. Cissé (1980) related crown area to biomass for *Acacia seyal*, *A. albida* and *A. nilotica* (Equations 2.1, 2.2, and 2.3), and for several other Sahelian species using a sample stratified by size class. Trees were sampled at the Niono field station in Mali (average rainfall about 580 mm). Bille (1977) calculated multipliers relating basal circumference to different components of biomass for *Acacia seyal* (Equation 2.4) at the Fété Olé study area in Senegal, an area with average rainfall similar to our Sahelian sites (250 mm). Bille's equations could not be used with the parameters predicted from the model, because the model predicts crown area, not stem circumference, and we could not establish a strong relationship between crown area and basal area for the trees in our sample. We did use the equations from Bille to predict biomass from average stem diameter sampled in the field, in order to compare these biomass figures to those predicted from other equations, or sampled at the sites.

According to Bille (1980), who reviewed allometric equations established at savanna sites throughout Africa, the relationship between the log of foliage biomass and the log of trunk diameter is fairly constant for Sahelian tree and shrub species, with a y-intercept less than one and a slope of about two. However, the equations he presents from Cissé (1980) are incorrect. Bille identifies diameter as the independent variable, and Cissé actually used circumference, so the slope is wrong by a factor of (log π), and is

actually closer to one. In spite of this error, there does seem to be a similar pattern in Cissés data relating crown area to biomass, where the y-intercept is again less than one, and the slope is between 1.2 and 1.8. If this holds true, it will be possible to estimate biomass for species that have not been sampled, or in stands of unknown or mixed composition. Leaf biomass equations for *Butyrospermum parkii* could not be found. Although this tree is a source of browse, it is more commonly managed as a tree crop (its fruit is the source of a valuable cooking oil) or a timber resource, if it is managed at all.

In Table 3, the equations from Table 2 are used to predict leaf biomass per tree and per hectare from the regionally averaged crown area and tree density sampled for the sites or predicted from the reflectance model. For comparison, leaf biomass was predicted from stem circumference measured in the field using equation 2.4. It should be noted that this equation was based on measurements of *Acacia seyal*, and may not be applicable to the other two species. For the Sahelian sites the predicted biomass values can be compared to the range of biomass values observed in three of the four sites over several growing seasons (1984-86) by Diarra and Hiernaux (1987). They measured biomass by clipping a stratified subsample of branches and weighing leaves wet and dry. The figures shown in the table (observed foliage biomass) represent the interseasonal variation in maximum standing crop. The number chosen was the maximum foliage biomass at one sampling interval during the growing season. We used these figures for comparison because the allometric equations were established by weighing all the leaves on the tree at the time of sampling. This does not actually take into account all production during the growing season, some of which is lost to herbivory.

Our estimates based on sampled and predicted crown area and density compare favorably with measured values for the Sahelian sites for both species (*Acacia nilotica* and *A. seyal*). The sampled versus predicted values may differ by a factor of two due to error in the prediction of crown area by the remote sensing model, but they are of the same order of magnitude. This is well within the spatial and interannual variability in biomass one would expect in woodland sites of this type. For comparison, the estimates based on the measured trunk circumference fall within the same range of values.

Predictions for the pooled Sudanian sites are based on Cissés equation for *Acacia albida* (because there were none available for *Butyrospermum parkii*). There were no measurements of foliage biomass

made in the Sudanian sites, so these figures can only be compared in a general way to values from the literature. Table 4 shows ranges of values found for foliage biomass in West African savanna and woodland. The first part shows volume per tree for different Sahelian species. The second part shows estimates or measures of annual production for woodland types similar to our sample sites.

Our estimates based on crown area for the Sudanian sites (24-29 kg/tree) seem high compared to Cissé highest of biomass values for *Acacia albida* (14 kg/tree), but our sample had a much larger average basal diameter (54 cm) than the largest size class sampled at Niono (30 cm). This may be because the *Acacia albida* we measured were located near the village and in the flood plain of the river and may have been receiving more water and nutrients than the trees measured at Niono. The estimate based on measured trunk circumference is very high, and probably an overestimate, indicating that equation 2.4, developed for Sahelian *Acacia seyal* cannot be extrapolated to these large Sudanian *Acacia albida*.

Woody Biomass

Dimensional analysis refers to the destructive sampling of woody plants to develop allometric regressions relating biomass to non-destructive measures (crown area or trunk diameter). There have been very few of these studies done for Sahelian species (Table 5). Olsson (1985) destructively measured biomass for 39 trees and shrubs in the Kordofan region, Sudan. She calculated a log-log regression equation predicting the wet weight of woody biomass from crown area for a mixture of species (Equation 5.1). Studies in temperate forests have shown that equations for different species in the same genus have very similar regression slopes; therefore equations can be cautiously applied to species with similar growth forms for which equations do not exist (Gholz *et al.* 1979). However, some of the species sampled by Olsson (1985) have very different growth forms (for example, baobab versus *Leptadenia sp.*), so her equation is probably not valid. The equation presented by Hellden (1987) may be more useful. Hellden used 32 of the trees from Olsson's sample and added nine trees measured in Ethiopia (Equation 5.2). The regression is based primarily on *Acacia* species with similar growth forms although it includes *Balanites aegyptiaca* which is quite different. In addition, Hellden calculated a regression for crown cover and biomass based on seven one-hectare plots in Ethiopia (Equation 5.3). He felt that this relationship should hold for *Acacia-*

dominated shrub and woodlands. If this is the case, an empirical relationship between remotely-sensed reflectance and canopy cover could be used to estimate biomass. Also included in this table is an equation from Bille (1977) predicting wood biomass from trunk circumference for Sahelian species (Equation 5.4).

Table 6 shows the biomass values calculated for our sample sites using the regression equations. Biomass is also predicted from crown cover using Equation 5.3. There are no measures of woody biomass for our field sites, but the figures can be compared to values from the literature (Table 7). Again, values based on predicted versus sampled crown size and density differ by no more than a factor of two. Predictions based on the equations using basal circumference as the independent variable are about the same (slightly higher for the Sudanian sites) than estimates based on crown area. This gives some independent evidence that our predictions are of the right order of magnitude.

DISCUSSION AND CONCLUSIONS

Our estimates indicate that a remote sensing model predicting average tree size and density in sparse woodland (ten to fifty percent cover) can be used to estimate foliage biomass using allometric equations from the literature. Although results based on modelled versus sampled size and density differ by almost a factor of two in some cases, they are of the same order of magnitude. This is probably as precise as biomass estimates based on extensive field sampling due to the inherent spatial variability of biomass in savanna. For example, leaf area index varied from 0.6 to 1.1 between adjacent transects in southern African savanna (Walker 1980). Cover, or the number and size of trees, is only one of the factors determining potential leaf biomass. Actual productivity is controlled by the amount and pattern of annual rainfall. Modeling of forage production from cover and rainfall has been conducted on a very limited basis in the Sahel, the work of Diarra and Hiernaux (1987) being one of the few examples.

Results regarding wood biomass are encouraging but inconclusive. Further work must be done to verify our findings by testing our approach in more sites where biomass is known by independent measurements. Although Hellden (1987) found a strong relationship between crown area and above ground wood biomass for a small sample of trees, we would expect trunk diameter and height to be better predictors of wood volume. In some studies trunk diameter, height and crown area are all intercorrelated (for example

in Cissé 1980, r^2 was greater than 0.8). In this case, woody biomass would be proportional to crown area. However, in our sites correlation between height and crown area was much lower (r^2 ranging from 0.3 to 0.5). This is probably because the trees are lopped. Crown diameter and height are limited by cutting, while the girth may continue to increase. The trees in our sample were not stratified by size class, and a proper sample design might improve the correlation.

Better allometric equations are needed for Sahelian and other African woodland species. Equations for fruit production are also important for *Acacia albida* (Le Houerou 1980) and *Butyrospermum parkii*. Allometric relationships should be based on a sound sampling scheme, such as the stratified sample used by Cissé (1980). Our approach must be used in conjunction with a vegetation stratification or land cover inventory indicating the areal extent of vegetation strata. This could be produced using remotely sensed imagery (Hellden 1980, Adeniyi 1985, USAID-TAMS 1983, Franklin 1988) or a reliable existing land cover map could be used.

Other remote sensing techniques for quantifying herbaceous biomass in the field layer rely on the spectral properties of green vegetation in the red and infrared wavebands. However, the red to infrared contrast is not a good indicator of vegetation amount when cover is incomplete. In semiarid areas with sparse vegetation on a bright soil background, canopy cover is strongly related to brightness in all wavelength bands. We used a model based on this principal that predicts cover and then divides it into its components of average tree size and density based on a few simple assumptions about stand character (tree size distribution and spatial pattern). These assumptions are generalizable and need not be calibrated at each site. From tree size, average biomass per tree can be calculated from existing biomass equations, and when multiplied by the density estimate, gives an estimate of biomass per unit area. This stratified approach, using existing field data and a remote sensing model, provides a viable method for estimating biomass on a regional scale. This technique may provide a useful input to forage production modelling.

REFERENCES

Adeniyi, P. O., "Digital analysis of multitemporal Landsat data for land-use/land-cover classification in a semi-arid area of Nigeria," *Photogrammetric Engineering and Remote Sensing*, vol. 51, pp. 1761-1774, 1985.

Ajtay, G. L, Ketner, P., and Duvigneaud, P., "Terrestrial primary production and phytomass," in *The Global Carbon Cycle*, ed. E. Bolin, E.T. Degens, S. Kempe and P. Ketner, pp. 129-181, SCOPE 13, John Wiley and Sons, New York, 1979.

Allen, J. C., "Wood energy and preservation of woodlands in semi-arid developing countries," *Journal of Development Economics*, vol. 19, pp. 59-84, 1985.

Arnold, J. E. M. and Jongma, J., "Fuelwood and charcoal in developing countries," *Unasylva*, vol. 29, pp. 2-9, 1978.

Barnes, D. F. and Allen, J. C., "The causes of deforestation in developing countries," *Annals of the Association of American Geographers*, vol. 75, pp. 163-184, 1985.

Bille, J. C., "Etude de la production primaire nette d'un écosystème sahélian," Travaux et documents de l'O.R.S.T.O.M. No. 65, O.R.S.T.O.M., Paris, 1977.

Bille, J. C., "Mesure de la production primaire appetée des ligneux," in *Browse in Africa, the Current State of Knowledge*, ed. H. N. Le Houerou, pp. 183-193, International Livestock Centre for Africa, Addis Ababa, Ethiopia, 1980.

Cissé, M. I., "Effets de divers regimes d'effeuillage sur la production foliare de quelques buissons fourragers de la zone Soudano-Sahelienne," in *Browse in Africa, the Current State of Knowledge*, ed. H. N. Le Houerou, pp. 209-212, International Livestock Centre for Africa, Addis Ababa, Ethiopia, 1980.

Colwell, J. E., "Landsat feature enhancement or, can we separate vegetation from soil?," *Proceedings of the 15th International Symposium on Remote Sensing of Environment*, pp. 599-621, Ann Arbor, Michigan, 1981.

Diarra, L. and Hiernaux, P., "Evolution de la végétation sahélienne après la sécheresse bilan du suivi des sites du Gourma en 1986," Programme des Zones Aride et Semi-aride, Document du Programme,

Centre International pour l'Elevage en Afrique (CIPEA), Bamako, Mali, 1987.

Dunkerley, J., Ramsay, W., Gordon, L., and Cecelski, E., *Energy Strategies for Developing Nations,* Resources for the Future, Johns Hopkins University Press, Baltimore, 1981.

Earl, D. E., *Forest Energy and Economic Development,* Clarendon, Oxford, 1975.

Franklin, J., "Land cover stratification using Landsat Thematic Mapper data in the Sahelian and Sudanian zones in Mali, West Africa," *in preparation,* 1988.

Franklin, J. and Strahler, A. H., "Invertible canopy reflectance modeling of vegetation structure in semiarid savanna," *IEEE Geoscience and Remote Sensing,* 1988. Accepted for publication.

Gholz, H. L., Grier, C. C., Campbell, A. G., and Brown, A. T., "Equations for estimating biomass and leaf area of plants in the Pacific Northwest," Research Paper 41, Forest Research Lab Oregon State University, School of Forestry, Corvallis, Oregon, 1979.

Gillet, H., "Observations on the causes of devastation of woody plants in the Sahel and their resistance to destruction," in *Browse in Africa, the Current State of Knowledge,* ed. H. N. Le Houérou, pp. 127-129, International Livestock Centre for Africa, Addis Ababa, Ethiopia, 1980.

Goward, S. N., Tucker, C. J., and Dye, D. G., "North American vegetation patterns observed with the NOAA-7 advanced very high resolution radiometer," *Vegetatio,* vol. 64, pp. 3-14, 1985.

Hellden, U., A Test of Landsat-2 Imagery and Digital Data for Thematic Mapping, Illustrated by an Environmental Study in Northern Kenya, Lund University Department of Physical Geography, 1980.

Hellden, U., "An assessment of woody biomass, community forests, land use and soil erosion in Ethiopia — A feasability study on the use of remote sensing and GIS-analysis for planning purposes in developing countries," *Lund Studies in Geography,* vol. 14, Department of Geography, University of Lund, Lund, Sweden, 1987.

Hiernaux, P., "L'inventaire du potentiel fourrager des arbres et arbustes d'une region du Sahel Malien. Méthods et premiers résultats," in *Browse in Africa, the Current State of Knowledge,* ed. H. N. Le Houerou, pp. 195-201, International Livestock Centre for Africa, Addis Ababa, Ethiopia, 1980.

Hiernaux, P. and Cissé, M. I., "Les ressources naturelles de système de production animale du Gourma," Programme des Zones Aride et Semi-aride, Document du Programme, Centre International pour l'Elevage en Afrique (CIPEA), Bamako, Mali, 1983.

Hiernaux, P., Cissé, M. I., and Diarra, L., "Bilan d'une saison d'es pluies 1984 très déficitaire dans la Gourma (Sahel Malien). Première campagne de suivi et télédetection expérimentale, Annexe: Fiches descriptives des sites," Programme des Zones Aride et Semi-aride, Document du Programme, Centre International pour l'Elevage en Afrique (CIPEA), Bamako, Mali, 1984.

Hiernaux, P. H. Y. and Justice, C. O., "Suivi du développement végétal au cours de l'été 1984 dans le Sahel Malien," *International Journal of Remote Sensing*, vol. 7, pp. 1515-1531, 1986.

Houghton, R. A., Hobbie, J. E., Melillo, J. M., Moore, B., Peterson, B. J., Shaver, G. R., and Woodwell, G. M., "Changes in the carbon content of the terrestrial biota and soils between 1860 and 1980: A net release of carbon to the atmosphere," *Ecological Monographs*, vol. 53, pp. 235-262, 1983.

Hutchinson, J., Dalziel, J. M., and Hepper,, *Flora of West Tropical Africa*, Crown Agents for Oversea Governments and Administrations, London, 1963.

Justice, C. O. and Hiernaux, P. H. Y., "Monitoring the grasslands of the Sahel using NOAA AVHRR data: Niger 1983," *International Journal of Remote Sensing*, vol. 7, pp. 1475-1497, 1986.

Kelly, R. D. and Walker, B. H., "The effect of different forms of landuse on the ecology of a semi-arid region in south-eastern Rhodesia," *Journal of Ecology*, vol. 64, pp. 553-576, 1976.

Lanley, J. P. and Clement, J., "Tropical Forest Resources Assessment Project (in the framework of GEMS - Global Environmental Monitoring System)," in *Forest Resources of Tropical Africa, Part 1- Regional Synthesis*, UN FAO/UNEP (United Nations Food and Agricultural Organization/ United Nations Environmental Programme), Rome, 1982.

Le Houérou, H. N., "The role of browse in the Sahelian and Sudanian zones," in *Browse in Africa, the Current State of Knowledge*, ed. H. N. Le Houérou, pp. 83-100, International Livestock Centre for Africa, Addis Ababa, Ethiopia, 1980.

Li, X. and Strahler, A. H., "Geometrical-optical bidirectional reflectance modeling of a coniferous forest canopy," *IEEE Transactions on Geoscience and Remote Sensing*, vol. GE-24, pp. 906-919, 1986.

Livingston, D.A. and Hammen, T. Van der, "Paleogeography and paleoclimatology," in *Tropical forest ecosystems: A state of knowledge report*, pp. 61-90, Unesco/UNEP/FAO, Paris, 1978.

Martin, R., "Structure, biomass and utilization in the Mopane and miombo woodlands of the Sengwa Wildlife Research Area.," Certificate in Field Ecology Report, University of Rhodesia, 1974.

Menaut, J. C., "Analyse quantitative des ligneux dans une savane arbustive préforestière de Côte d'Ivoire," *Proceedings of the Fourth Tropical Ecology Symposium Geo-Eco-Trop*, vol. 1, pp. 77-94, Lubumbashi, 1977.

NASA, "Land-Related Global Habitability Science Issues," NASA Technical Memorandum 85841, National Aeronautics and Space Administration, July, 1983.

National Academy of Sciences (NAS) Committee of Planetary Biology, "Remote Sensing of the Biosphere," Space Sciences Board Commission on Physical Sciences, Mathematics and Resources, National Research Council, National Academy Press, Washington, D.C., 1986.

Nelson, R., Case, D., Horning, N., Anderson, V., and Pillai, S., "Continental land cover assessment using Landsat MSS data," *Remote Sensing of Environment*, vol. 21, pp. 61-81, 1987.

Okafor, J. C., "Trees for food and fodder in the savanna areas of Nigeria," *The International Tree Crops Journal*, vol. 1, pp. 131-141, 1980.

Olsson, K., "Remote sensing for fuelwood resources and land degradation studies in Kordofan, the Sudan," Ph.D. Dissertation., The Royal University of Lund, Department of Geography, Lund, Sweden , 1985. 182 pp.

Otterman, J. and Tucker, C. J., "Satellite measurements of surface albedo and temperatures in semi-deserts," *Journal of Climate and Applied Meteorology*, vol. 24, pp. 228-235, 1985.

Pech, R. P. and Davis, A. W., "Remote sensing of semi-arid woodlands: Reflectance modelling and calibration," *Remote Sensing of Environment*, 1987. In press.

USAID-TAMS, *Le Ressources Terrestres au Mali: Mali Land and Water Resources,* Government de la Republique du Mali Ministere Charge du Development Rural, 1983.

Ustin, S. L., Adams, J. B., Elvidge, C. D., Rejmanek, M., Rock, B. N., Smith, M. O., Thomas, R. W., and Woodward, R. A., "Thematic mapper studies of semiarid shrub communities," *BioScience,* vol. 36, pp. 446-452, 1986.

Von Maydell, H. J., *Arbres and Arbustes du Sahel,* 1983.

Walker, B. H., "A review of browse and its role in livestock production in southern Africa," in *Browse in Africa, the Current State of Knowledge,* ed. H. N. Le Houérou, pp. 7-24, International Livestock Centre for Africa, Addis Ababa, Ethiopia, 1980.

Woodwell, G. M., Whittaker, R. H., Reiners, W. A., likens, G. E., Delwiche, C. C., and Botkin, D. B., "The biota and the world carbon budget," *Science,* vol. 199, pp. 141-146, 1978.

Table 1

AVERAGED REGIONAL ESTIMATES OF TREE SIZE AND DENSITY										
Region	Species	n	Crown Area (m^2)				N ($per\ ha$)			
			Sampled		Predicted		Sampled		Predicted	
			mean	σ	mean	σ	mean	σ	mean	σ
Sahelian	*Acacia seyal* *Acacia nilotica*	4	30.32*	10.15	40.50	16.49	130.57†	38.83	123.97	44.40
Sudanian	*Butyrospermum parkii* *Acacia albida*	6	72.76*	22.93	86.14	32.17	26.10†	13.69	38.22	25.80

n is the number of sites that were averaged

* — Average crown area (sampled) is actually based on $\approx$ 60 trees per site.

† — Average density (sampled) is actually based on 4 to 8 plots per site.

Table 2

FOLIAGE BIOMASS EQUATIONS						
No.	Study	Site	Species	(n)	Equation	r^2
2.1	Cisse 1980	Niono, Mali	*Acacia nilotica*	30[1]	$FB\ (g/tree) = .0021\ CA\ (dm^2)^{1.91}$	.94
2.2	Cisse 1980	Niono, Mali	*Acacia seyal*	50[1]	$FB\ (g/tree) = .21\ CA\ (dm^2)^{1.22}$	.92
2.3	Cisse 1980	Niono, Mali	*Acacia albida*	50[1]	$FB\ (g/tree) = .32\ CA\ (dm^2)^{1.26}$	.96
2.4	Bille 1977[2]	Fete Ole, Senegal	*Acacia seyal*	?	$FB\ (kg/tree) = .0032\ BC^2(cm^2)$	-

Notes:

1 — Sample stratified by diameter class.

2 — In Penning de Vries and Djiteye 1982, p. 295.

FB = Foliar Biomass

CA = Crown Area

BC = Circumference at breast height (1.3 m).

Table 3

PREDICTED FOLIAGE BIOMASS							
Species	Equation from Tbl. 2	Independent Variable			Foliage Biomass		
		Source	*CA* (dm^2)	*BC* (*cm*)	predicted *kg /tree*	predicted *kg /ha*	observed[4] *kg /ha*
Acacia nilotica	2.1	sampled[1]	3031.6		8.5	1111.8	
	2.1	predicted[2]	4049.5		14.8	1829.0	554-1133
	2.4	measured[3]		66.4[5]	14.1	1848.2	
Acacia seyal	2.2	sampled[1]	3031.6		3.7	484.9	
	2.2	predicted[2]	4049.5		5.3	654.9	141-1034
	2.4	measured[3]		42.8[5]	5.9	767.9	
Acacia albida	2.3	sampled[1]	7275.9		23.5	613.4	
	2.3	predicted[2]	8614.3		29.1	1111.2	—
	2.4	measured[3]		170.0	92.5	2413.0	

Notes:

1 — Independent variable is the average for the field sites based on sample measurements (see Table 1).

2 — Independent variable is the average for the field sites predicted from the reflectance model (see Table 1).

3 — Independent variable is based on sample measurements from each field site.

4 — Foliage biomass (maximum standing crop) was measured (sampled) in the field sites in 1984, 1985, and 1986, and the range is given.

5 — Basal Circumference was multiplied by 0.8 to estimate circumference at breast height (1.3 m).

CA = Crown area
BC = Circumference at Breast Height (1.3 m).

Table 4

MEASUREMENTS AND ESTIMATES OF FOLIAGE BIOMASS IN SAVANNA WOODLAND					
Study	Location, Annual ppt.	Species or type	(*n*)	Basal Diam. (cm)	Biomass *kg /tree*
Poupon 1977	Fete Ole, Senegal	*Acacia senegal*	292	2.0-26.0	.14-1.36
Bille 1980	Fete Ole, Senegal	*Acacia seyal*	3	8.4-15.9	.58- 3.34
		Balanites aegyptica	6	5.1-27.3	.05- 5.58
	250 mm (*)	*Commiphora africana*	4	13.4-21.5	.28- .91
		Guiera senegalensis	6	3.8-10.2	.55- 2.85
		Adansonia digitata	4	100-320	14.3-99.0
Bille 1980	Oursi, Burkina Faso	*Acacia laeta*	?	0-25	.15- 3.5
		Acacia seyal	?	0-30	.60- 8.0
	440 mm	*Acacia tortilis*	?	0-30	.50- 1.6
		Balanites aegyptica	?	0-30	.50-10.5
		Guiera senegalensis	?	0-15	.04- .90
Cisse 1980	Niono, Mali	*Acacia albida*	50[1]	1.8-29.7	.04-14.01
		Acacia seyal	45[1]	2.3-26.6	.05-13.44
	580 mm	*Pterocarpus lucens*	45[1]	2.6-26.9	.05- 4.32
		Ziziphus mauritiana	40[1]	1.9-23.8	.05- 6.62
		Commiphora africana	50[1]	2.1- 3.2	.06- 3.92
		Balanites aegyptica	50[1]	2.0-30.2	.07- 9.44

ANNUAL PRODUCTION OF LEAVES					
Study	Location	Type	Density	Cover	*kg /ha /yr*
UNESCO 1979[2]	Sahel, 200-600 mm	literature review			60-300
Penning de Vries and Djiteye, 1982[3]	Mali, 400-1100 mm	Sahelian transect			60-1,100
Hiernaux 1980	Niono, Mali	*Acacia laeta* mixed	?	?	668
		Acacia seyal mixed	?	?	528
	580 mm	*A. seyal, B. aegyptica*	?	?	2,250
Hiernaux 1980	Sahel, 500 mm	regional average	-	-	500-700
	Sud-sahelian, 600 mm	regional average	-	-	750-860
Menaut 1977[4]	Ivory Coast, 1000 mm	Guinea savanna	300	20	1,700

Notes:

* — Annual precipitation figures are long term averages. Actual rainfall during sampling season may be quite different. For example, rainfall at Fete Ole was 33 mm in 1972.

1 — Stratified sample; numbers are mean for each size class.

2 — p. 133.

3 — p. 293.

4 — In UNESCO 1979, p. 134.

LAI = Leaf Area Index
CC = Crown Cover

Table 5

WOODY BIOMASS EQUATIONS						
No.	Study	Site	Species	(n)	Equation	r^2
5.1	Olsson 1985	Kordofan, Sudan	mixed[1]	39	$WW\,(kg\,/tree\,) = 1.55\,CD^2(m^2)^{1.28}$	.94
5.2	Helden 1987	Sudan, Ethiopia	mixed[2]	41	$WW\,(kg\,/tree\,) = 1.01\,CD^2(m^2)^{1.44}$	.98
5.3	Helden 1987	Sudan, Ethiopia	?	7	$WW\,(tonnes\,/ha\,) = -5.58 + .143\,CC\,(\%)$	.99
5.4	Bille 1977[1]	Fete Ole, Senegal	*Acacia seyal*	?	$WB\,(kg\,/tree\,) = .054BC^2\,(cm^2)$	-

Notes:

1 — *Acacia albida, A. mellifera, A. tortilis, Albizzia amara, Balanites aegyptica, Adansonia digitata, Boscia senegalensis, Commiphora africana, Guiera senegalensis, Leptadenia sp.*

2 — *Acacia albida, A. mellifera, A. tortilis, Albizzia amara, Balanites aegyptica,* 32 trees from Olsson 1985 and nine from Ethiopia.

3 — *Aacia seyal, Commiphora africana, Sclerocarya birrea, Ximenia americana, Grewia bicolor, Balanites aegyptiaca.*

4 — In Penning de Vries and Djiteye 1982, p. 295.

WW = Woody Biomass, Wet weight
CD = Crown Diameter
CC = Crown Cover
BC = Circumference at Breast Height (1.3 m).

Table 6

PREDICTED WOODY BIOMASS								
Region/ Species	Eqn. Tbl. 5	Independent Variable			Woody Biomass			
					kg /tree		*kg /ha*	
		Source	Variable	Value	wet	dry[1]	wet	dry[1]
Sahelian	5.1	sampled[2]	*CD (m)*	6.2	166.3	123.1	21,719	16,072
		predicted[3]	*CD (m)*	7.2	241.0	178.3	29,876	22,108
Sahelian	5.2	sampled[2]	*CD (m)*	6.2	194.5	143.9	25,468	18,846
		predicted[3]	*CD (m)*	7.2	295.1	218.4	36,583	27,071
Sahelian	5.4	measured	*BC (cm)*	50.6[5]		138.3		18,112
Sahelian	5.3	sampled[2]	Cover (%)	29-56			28,449[4]	21,052
		predicted[3]	Cover (%)	29-54			47,697[4]	35,296
Sudanian	5.1	sampled[2]	*CD (m)*	9.6	506.9	377.1	13,300	9,842
		predicted[3]	*CD (m)*	10.5	633.0	468.4	24,192	17,902
Sudanian	5.2	sampled[2]	*CD (m)*	9.6	685.3	507.1	17,885	13,235
		predicted[3]	*CD (m)*	10.5	847.5	647.1	33,424	24,734
Sudanian	5.4	measured	*BC (cm)*	141.6		1082.7		28,259

Notes:

1 — Conversion factor: dry=0.74 wet (in Olsson 1985, quoted from Lamprey 1974).

2 — Independent variable is the average for the field sites based on sample measurements (see Table 1).

3 — Independent variable is the average for the field sites predicted from the reflectance model (see Table 1).

4 — Biomass was predicted from cover for each of the four sites and the results averaged.

5 — Basal Circumference was multiplied by 0.8 to estimate circumference at breast height (1.3 m).

BC = Basal Circumference
CD = Crown Diameter

Table 7

MEASUREMENTS AND ESTIMATES OF WOODY BIOMASS IN SAVANNA WOODLAND					
Study	Location, Annual Ppt.	Vegetation type	Density (*per ha*)	Cover (%)	Biomass *kg /ha*
Bille and Poupon 1972[1]	Fete Ole, 250 mm	mixed[2]	133	8	3,500
		dune summits	-	2.8	2,000
		depressions	-	40	24,000
Olsson 1985[3]	Sudan, 150-450 mm	forest reserve	34-109	18	4,692-15,042
		agricultural	4-34	6	552-4,692
Cisse 1983	Niono, 580 mm	mixed[6]	?	?	17,000-54,000
Kelly and Walker 1976[5]	Zimbabwe 500 mm	mopane	?	?	21,367
Martin 1974[5]	Zimbabwe 600 mm	mopane	?	?	67,783
Martin 1974[5]	Zimbabwe 600 mm	dry miombo	?	?	21,161
Rutherford 1979[5]	N. Transvaal 700 mm	*Burkea, Terminalia*	?	?	16,237
Menaut 1977[1]	Ivory Coast, 1000 mm	shrub savanna	300	20	32,600
Hellden 1987	Ethiopia, 1000-2300 mm	*Acacia* woodland	?	15[4]	18,000[4]
			?	35[4]	40,000[4]
			?	65[4]	90,000[4]

Notes:

1 — In UNESCO 1979, p. 133-134.

2 — *Acacia senegal, Balanites aegyptica, Boscia senegalensis, Commiphora africana, Guiera senegalensis, Grewia bicolor, Acacia albida, A. mellifera, A. tortilis, Albizzia amara, Balanites aegyptica.*

3 — For 36 sites cover and density were measured from air photos, crown size was calculated, and biomass calculated from equation 5.3.

4 — These values were interpolated from a graph, p. 27.

5 — Reviewed in Walker (1980).

6 — *Pterocarpus lucens, Anogeissus leiocarpus, Combretum micranthum, Boscia angustifolia, A. seyal, Commiphora africana, Sclerocarya birrea, Ximenia americana, Grewia bicolor, Balanites aegyptiaca* and others.

Chapter 4

LAND COVER STRATIFICATION USING LANDSAT THEMATIC MAPPER DATA IN THE SAHELIAN AND SUDANIAN ZONES IN MALI, WEST AFRICA

ABSTRACT

Natural vegetation in two regions of semiarid Africa were classified using Landsat Thematic Mapper data. The method used was unsupervised classification of multi-date principal components images. While initial classification results were poor, accuracy was comparable with results reported in the literature for Level III land cover classes when a lenient accuracy criterion was used. When sample points identified as being one density class higher or lower that classified were counted as correct, overall accuracy was around 90 percent, and class accuracy was greater than 80 percent for most classes. The methodology could be improved by applying the lessons learned from biophysical remote sensing and thematic mapping in other areas with partial vegetation cover and complex landscape patterns. Contextual classification or spatial/spectral image segmentation will be more powerful techniques than per-pixel classification for stratification of complex vegetation patterns when they are commonly available as part of image processing systems. However, my results based on conventional digital image processing techniques are nonetheless useful. The accuracy achieved is adequate for stratification of woody biomass at a regional scale. Stratification will reduce variance in estimates of biophysical variables based on traditional field sampling, or remote sensing models.

1. Introduction

Remote sensing has long been promoted as a tool for monitoring natural resources in developing countries, including Africa (Deutsch 1975). Several studies have employed manual interpretation of Landsat satellite data (Ackerson 1985, Jacobberger 1986, Makhanya 1986, Cooley and Turner 1982, USAID-TAMS 1983, Parry and Williams 1986, Mushala 1986, Schultz 1979), and digital analysis of agricultural land (Adeniyi 1986). However, few have applied digital image classification techniques to Africa semiarid shrub and woodland (Adeniyi 1985, Negri 1985, Kihlblom and Johansson 1980, Hellden 1980). (Justice 1986). Ultimately, in Africa as in other places, comprehensive resource analysis must be based on data integrated from different satellite sensors (Malingreaux *et al.* 1987) and other environmental data, analyzed in a geographic information system (Hellden 1987). A thematic map of vegetation cover derived from satellite reflectance data may be an important layer of information in such a system. Land cover must be known to predict soil erosion and runoff (Hellden 1987). Vegetation and soils must be stratified for regional woody biomass inventory by conventional methods (Strahler 1981, Franklin *et al.* 1986) or using a remote sensing model (Franklin and Strahler 1988).

It has been argued that direct correlation of satellite spectral measurements with the biophysical variable of interest, for example, herbaceous biomass, is a better use of environmental satellite data than thematic mapping (Jensen 1983). In semiarid Africa the land cover consists of varying mixtures of woody and herbaceous vegetation cover and different soil backgrounds. Complex land-use practices (dryland farming in small fields, bush fallow rotation, and grazing) impose their own pattern on the landscape. While Landsat data are clearly not of sufficient temporal resolution (or affordable cost) for capturing the dynamics of the herbaceous layer, they are adequate for assessing woody cover and soil brightness in semiarid areas. This is particularly true in the dry season when herbaceous vegetation does not confuse the picture (see Olsson 1985). A woody cover stratification based on Landsat data may assist in calibrating biophysical remote sensing models of herbaceous biomass production (Prince and Astle 1986, Townshend and Justice 1986).

In this paper I have applied several conventional image classification procedures for stratifying woody vegetation classes to Landsat Thematic Mapper data in two study regions in Mali, West Africa.

The level of land cover categoric resolution (species groupings and density) corresponds to level III land cover classes (Anderson *et al.* 1976). In previous work in the study area, a remote sensing model successfully predicted tree size and density from spectral measurements when data from woodland stands were aggregated by region (Franklin and Strahler 1988). Effectively, the woodland sites were stratified into two tree cover classes, one with 5-25 percent cover and one with 25-45 percent cover. Therefore, if an area were stratified into broad cover and soil brightness classes, the model could be used to predict average tree size and density for a stratum over a region by applying the model to woodland stands from within the stratum. In the future, advanced landscape and image analysis techniques could be used to further automate the application of this type of model at a regional scale. These include spatial/spectral image segmentation, and applying the model to a digital image using a moving window. However, the present study shows that a reasonable stratification, useful for many purposes, can be achieved using conventional procedures available on most image processing systems. This is critical for applied geographical analysis in developing countries that must use methods that are accessible and affordable.

2. Study Area

The study area included sites dominated by savanna woodland and wooded grassland in the Sahelian and Sudanian bioclimatic regions of Mali, West Africa. Woodland and wooded grassland cover ten to twenty percent of the land surface, greater than any other vegetation type (Ajtay *et al.* 1979). Dry woodlands and wooded savanna (with tree cover greater than ten percent) are estimated to cover more than 20 percent of the continent of Africa (Lanley and Clement 1982).

The Sahel is usually defined with reference to mean annual isohyets and corresponds to the 200-600 mm annual precipitation zone (Le Houerou 1980). Rain falls in the summer months (primarily June through August). The vegetation of the Sahel ranges from an open annual grassland with less than ten percent woody cover in the north to perennial grasses with 25 percent or more tree cover in the south. In the Sahelian zone in northern Mali, two study areas were located in the Gourma region, one near the town of Gossi (15° 50′ N, 1° 20′ W) and one near Hombori (15° 15′ N, 1° 45′ W). These study areas encompass nine of the thirty sites along a trans-Sahelian transect being monitored by ILCA/Mali (The

International Livestock Centre for Africa) in collaboration with the GIMMS Project[1] (Hiernaux and Justice 1986, Hiernaux and Diarra 1986, Diarra and Hiernaux 1987).

The Sudanian zone is the region to the south of the Sahel, where the rainfall is 600 to 1000 mm, the rainy season lasts up to four or five months, and there is extensive dryland agriculture. The vegetation is a mosaic of open woodland savanna, with trees up to 15 m tall, closed woodland, and edaphic bush thickets and grasslands (Schnell 1977). The Sudanian study area is located within the administrative region of Ségou, Mali, and includes the town of Konodimini (13° 20′ N, 6° 20′ W). The "parkland" type of vegetation prevelent in this area is formed when crops are grown under a woodland of useful trees that are preserved when land is cleared (Nielsen 1965). The land is cultivated using a bush fallow rotation system. Fields near the villages are cultivated continuously, but distant fields are rotated, with a fallow period varying in length from five to 50 years. This creates a landscape of woodland patches in varying stages of succession.

3. Methods

For the Gourma region, a 9 September 1984 TM quarter scene was first chosen for analysis because it coincided with field data collection by Hiernaux *et al.* (1984). Also, I presumed that an early dry season image would provide the greatest spectral contrast between the dry herb layer and green tree canopy. However, a rainfall event in the study area just prior to scene acquisition caused patchy greening up of the grass layer. Therefore, a late dry season image (7 May 1985) was also acquired. Areas with high near infrared (NIR) reflectance in September 1984 (green vegetation growth) had lower NIR reflectance in May 1985 (e.g., the dune area northwest of Gossi). A single date (17 November 1984) TM image was used for the Ségou study area. On that date the fields beneath the tree canopy had been harvested.

The two-date data set for the Gourma subimages was registered, and image principal components were calculated from a subset of the bands. The principal components images were used in the classification. The classification of the Ségou subimage was based on five of the TM bands. Subimages

[1] Global Inventory, Monitoring and Modeling System; NASA (National Aeronautics and Space Administration), Goddard Space Flight Center, Greenbelt, Maryland, USA.

corresponding to the three study areas were selected and iteratively clustered, classified and labeled using unsupervised clustering and a minimum distance classifier.[2] Because principal components and clustering are both data-dependent, empirical procedures, the subimages were processes separately (Franklin *et al.* 1986). Dimensions and locations of subimages are given in Table I.

3.1. Registration of the Gourma subimages

For relative registration of the two-date images, the May 1985 image was selected as the reference, and the September 1984 image was registered to it. Five of the TM bands were processed during registration, Bands 1-4 and 7. Band 6 was not used because of its coarser spatial resolution, nor Band 5 because it was of poor quality in the 1984 image.

The ERDAS program GCP creates the file containing control points, and then COORD2 is used to compute a transformation matrix for rectification using the control points and least squares regression. The *rms* (root mean square) error is computed for each control point. If the sum of the *rms* errors for all control points is greater than the user-specified tolerance (1.0 pixel in this case), the control point having the largest *rms* error is eliminated. The coefficients are recomputed using the remaining control points until the total *rms* error is less than the tolerance entered. For the Gossi image, with 27 control points input, 21 control points were used, and the total *rms* error was 0.85977. For the Hombori image, with 18 control points input, 10 control points were used, and the total *rms* error was 0.97810.

The data were transformed with a first order (linear) transformation matrix using the program RECTIFY. A nearest neighbor resampling algorithm was used, that takes the DN[3] value from the closest input pixel, and assigns it to the computed output pixel location. Subimages of the registered images were used in further analysis.

---

[2] Image processing was done using ERDAS software at the UCSB Geography Remote Sensing Research Unit (RSRU) and Maps and Imagery Laboratory (MIL).

[3] Digital Number or brightness value, scale 0-255 representing 8-bit data.

3.2. Principal Components Images

The program PRINC creates an output image whose bands are the principal components of the spectral bands in the input file. A covariance matrix and eigenvectors are computed from the input image. Once the linear combinations needed to transform the image from the original spectral axes to the transformed principal components axes are identified, each pixel is converted into the new system.

Bands 3 (red, .63-.69 μm), 4 (near infrared, .76-.90 μm) and 7 (mid infrared, 2.08-2.35 μm) from the September and May scenes were used to create a six-band multitemporal image for input to PRINC. These bands were chosen because they are from relatively uncorrelated spectral regions, and each has a characteristic response to vegetation amount and soil moisture.

In the Gossi subimage, 99.5 percent of the variance in the six-band multitemporal image was contained in the first four principal components (see Table II). The transformed data channels resulting from principal components analysis are described below:

1) The first Principal Component (PC1) has positive loadings in all spectral bands, a common result for multispectral scanner data, and is a measure of overall image brightness in both dates.

2) The second Principal Component (PC2) has negative loadings in Bands 3 and 4 and positive in Band 7 for both dates. A low value in PC2 indicates bright (herbaceous) vegetation on both dates.

3) The third Principal Component (PC3) has negative loadings in Bands 3 and 7 for September 1984, positive loadings in 3 and 7 for May 1985. This emphasizes difference in herbaceous cover between seasons. A low value in PC3 indicates that soil moisture was high (or vegetation present) in September 1984, and low in May 1985.

4) The fourth principal component (PC4) has a high negative loading in Band 4 for September 1984, and a positive loading in Band 3 for May 1985. This is similar to PC3 in that a low value for PC4 indicates an area that had green vegetation in 1984, and were bright in Band 3 in May 1985 (low vegetation).

The third and fourth principal components both emphasize herbaceous vegetation differences between the two dates. This helped separate areas where herbaceous growth saturated the reflectance signal in the

September image from areas of varying woody cover density.

The first four principal components resulting from the Hombori subimage contained 99.6 percent of the spectral variance (see Table II) and are as follows:

1) The first Principal Component is again measure of overall scene brightness (positive weightings in all spectral bands).

2) The second principal component has negative loadings in all bands for September 1984, and positive in all bands for May 1985, emphasizing areas that are brighter (less vegetation or greater soil moisture) in the late dry season.

3) The third principal component is similar to the Gossi PC2. It emphasizes the difference between red/IR and mid-IR reflectance. A low value in PC3 indicated bright (herbaceous) vegetation.

4) The fourth principal component has positive loading in Band 4 (NIR) in September 1984 and a large positive loading in Band 3 in May 1985 (similar to PC4 in Gossi but the scale is reversed).

These transformed spectral channels capture the important multitemporal spectral features in the scene; these are overall scene brightness, woody cover, and the differences in herbaceous cover and soil moisture between early and late dry season.

In a classification test using small (256 x 256) single-date (1985 Bands 3, 4, and 7) imagery versus PC1-4 as input, visual inspection of the resulting clusters showed clearly that woody cover classes were better discriminated using the PC image. September 1984 data alone were not useful at all for discriminating woody cover classes because of confusion caused by the flush of green vegetation that occurred in response to the early September rainfall event.

3.3. Classification

Classification was performed using iterative unsupervised clustering and a minimum distance classifier. Clustering is an empirical procedure which divides spectral measurement space according to user-specified parameters. This technique for thematic mapping assumes that spectral classes are homogeneous with respect to ground cover types. In iterative clustering, large spectral classes that consist of

mixtures of land cover classes are again input to the clustering algorithm. In this way, spectral space is more finely divided.

The program CLUSTR is a two-pass sequential clustering algorithm. The first pass accumulates the cluster means. The second pass applies a minimum-distance classifier using the cluster means that were acquired in the first pass. In the first pass, cluster accumulation is controlled by several parameters, the maximum number of clusters (NMAX), the minimum distance between clusters (C), the maximum allowable cluster radius (R1), and the number of points until merger (M). A pixel cannot be included in a cluster if the distance between the pixel and the current cluster mean is greater than R1. Every M points, the cluster means are compared to determine if any are within distance C of each other. If so, the two clusters are merged to form a single new cluster. The image was subsampled (every 10th line and 10th pixel) to speed up processing. The default parameters were used in clustering each of the subimages except in cases where a large percentage of the image was reclustered. Then, NMAX was set to 50, C to 4 and R1 to 6.

For Gossi, there were 27 classes in the output of the first clustering. There were several large, heterogeneous spectral classes that contained more than one information (vegetation) class. Twenty-one percent of the image was labeled, and the remaining classes were further subdivided into fifty classes. For Hombori, 74 percent of the image was labeled after the first clustering, and the remaining 24 percent (in eight classes) was re-clustered and classified into 27 classes. In the Ségou subscene, 32 percent of the image was labeled in the first iteration, and 67 percent (in seven classes) was reclustered.

Itterative clustering was accomplished by using the program MASK to set all the labeled pixels to zero, and re-clustering the image spectral data only for the pixels falling in the un-labeled classes. The second clustering successfully separated the woody cover classes. RECODE assigns a new class value number to classes, creating an output file with the new class numbers. Finally, OVERLAY combines the recoded images to produce the final classified image where the DN corresponds to the class number.

The final step in the classification procedure was image smoothing, or reassigning isolated pixels to the classes surrounding them by a simple majority rule. This was a quick and dirty way of achieving a minimum mapping unit greater than a pixel. A more desirable procedure would have been to spatially

C-2

filter the image using a specified minimum mapping unit and class weightings (Franklin *et al.* 1986) but this type of filter was not available on the image processing system used.

Spectral classes were assigned information class labels using the 1956 air photos, the ILCA photos where available, a color composite of the image itself, and based on knowledge of the study area and the spectral properties of the vegetation. In addition, for Hombori and Gossi, sample points were photointerpreted and labeled by a local expert (P. Hiernaux) who was not involved in the image processing, and these points were used in clustering labeling. These were the same points used in accuracy assessment (see below), which introduces a bias to the accuracy figures, but it was the best information at hand for labeling.

The land cover classification system used (Table III) was modified from Kuchar (1979) for this study to include a soil label. The classes for Ségou are slightly different; the soil label only indicates the brightness of the soil background as light (sandy, silty and clayey loams under cultivation) or dark (lateritic gravels and outcrops, dark clayey alluvium). This was necessary in the absence of an accurate soils map or more detailed understanding of the lithology in the Ségou study area.

3.4. Accuracy Sampling

Accuracy was assessed based on a sample of points located in each subimage according to a stratified, systematic, unaligned sample design. Sample points were photointerpreted as to their actual (true) class. Hiernaux (for the Gourma sites). Crosstabulations were made of the labeled and photointerpreted classes for all the sample points in each subimage. This is referred to as a confusion table, and was analyzed by several methods for overall and per class accuracy.

Initially, the number of sample points in each sample class was chosen using the method of Rosenfeld *et al.* (1982) based on the binomial distribution (a pixel can be correctly or incorrectly classified). The cumulative binomial probability determines the minimum sample size, n, required for each map category given an allowable error E and an *a priori* estimate of the probability of correct classification p_o.

$$P_B = \sum_{r=K(n)-1}^{n} C_r^{\,n} \; p_o^{\,r} \; (1-p_o)^{n-r}$$

where $k(n) = [n(p_o + E)]$ is the largest integer greater than or equal to $n(p_o + E)$, and $r = x_1 + \ldots + x_n$ where $x = 1$ or 0 (correctly or incorrectly classified). The minimum sample size is the smallest integer $k(n)$ such that P_B is greater than or equal to 0.05 (if 95 percent confidence intervals are required). If allowable error (E) is set to 10 percent, and p_o (with no former experience in this area) set to 0.80 (0.85 for the water class) then 24 sample points are needed for each class (19 for water). In retrospect, it appears that 80 percent was an overestimate of classification accuracy for some classes, and therefore more sample points should have been used, but it was not possible within the time frame of this project to add points and have them interpreted by the local expert in Africa.

In addition, for the Gourma region, the sample points were divided between the Gossi and Hombori subimages proportional to the area of the class in each subscene. Although the sample points were originally allocated among the fourteen cover types assigned by the image analyst (Franklin) in class labeling, the classification was subsequently modified and classes were re-labeled based on the response of the local expert (Hiernaux). The final classification consists of 29 vegetation/soil classes, so the 270 samples (allocated before the final classification) are wholy inadequate for a statistically sound accuracy assessment of this area. However, they do give some indication of the thematic map accuracy when the land cover classes are pooled. In Ségou there were better quality, more recent air photos available, and therefore the image classification and accuracy analysis could be done by the same person.

3.5. Accuracy Assessment

Accuracy assessment for this type of thematic map is difficult, because it is impossible to know the "true" category for every point on the landscape. In addition to classification error, there can be photointerpretation error of the "true" class. Even if every point were visited in the field, there is the problem of spatial sampling or cartographic generalization. A label must be assigned to a pixel or group of pixels, and a category chosen for the equivalent area on the ground. Accuracy was assessed by four different measures to demonstrate the variability in different estimates of error. The measures uses were commission error (diagonals divided by row totals, for confusion tables arranged as described below), omission error (diagonals divided by column totals), errors adjusted for marginal sums (by the method of Card

1982), and the Kappa coefficient of agreement (Congalton and Mead 1983, and see Hudson and Ramm, 1987, for the correct formula).

4. Results

The land cover statistics resulting from image classification of the study areas are shown in Table IV and Table V. For the Gourma study area the types were aggregated by vegetation class (the soils classes are lumped). The classification error matrices are shown in Table VI and Table VII. The columns represent the "true" (photointerpreted) category, and the rows the "mapped" (by image classification) category. The diagonal represents points that were correctly classified. The row totals for the Ségou subimage are not all equal to 24 (the original number of points allocated to each class). In assessing the accuracy, a sample pixel was considered correctly classified is one of its immediate neighbors was the same class as the photointerpreted class, so some points changed classes. In Ségou the Bare soil and Grassland classes (light soil) were lumped, because they could not be distinguished by the photointerpreter in dry season air photos. As explained above, the Gourma subimage was relabeled after the sample points were allocated, and so there are uneven numbers of sample points in the classes (more or less proportionate to the area of the stratum). Therefore, the accuracy results must be interpreted with caution.

The results from the different accuracy assessment measures are shown in Table VIII and Table IX. These tables include the lower and upper confidence limits for the omission errors (percent correct given mapped category), and for the percent correct given the true category (the accuracy adjusted for the marginal proportions). These confidence limits were calculated by the method given in Card (1982). The Kappa coefficient is supposed to take into account omission and commission errors, and has been recommended as a standard for thematic map assessment (Rosenfeld and Fitzpatrick-Lins 1986), but for these data it seems to be strongly related to commission error. The method adjusted for marginal totals gave the lowest estimates because for several classes the percent of the area in each category as estimated by the classification differed greatly from that estimated from the sample points (for example, classes 5 and 7 in Ségou, and class 7 in Gourma).

For Ségou, a woodland (classes 4-7) versus non-woodland classification would yield accuracies of .96 and .93 (omission), and .91 and .97 (commission), respectively. Individual class accuracies were low. Overall accuracy was between 80 and 90 percent and most class accuracies weer greater than 70 percent when the woodland classes were pooled (effectively aggregated to level II). Because level III classes were being resolved (woodland density on an ordinal scale), there was a large potential for error in both photointerpretation and class labeling. Due to the heterogeneity of the landscape, a sample point could easily have been assigned to the wrong density class if the woody cover was borderline between classes. However, the purpose of a stratification is to reduce the variance within classes of some variable that is subsequently sampled. Therefore, accuracy was also estimated in a more lenient way: a point was counted as labeled correctly if it fell in the correct class or one density class higher or lower than the "true" class. This gives an indication of the usefulness of the classification as a stratification. In Ségou, overall accuracy is close to 90 percent, and most class accuracies are greater than 80 percent using this accuracy measure.

For the Gourma subimage, the accuracy figures for classes 1 and 2 are meaningless, because of the small sample size. Overall and individual class accuracies are low by all measures. Using the lenient accuracy criterion, overall accuracy is about 90 percent, and most class accuracies are greater that 80 percent (Table 0). The greatest confusion that remains is between class 6 (Grassland) and class 4 (Wooded Grassland, sparse). Six of these 9 confused points occur on gravels, where the dark substrate is confused with tree cover.

5. Conclusions

Mapping of vegetation density classes in open shrub and woodland from Landsat satellite data is difficult using per-pixel multispectral image classification. At Landsat Thematic Mapper spatial resolution, pixel reflectance represents a variable mixture of vegetation and soil background. In some cases, different components (tree patch vs. bare area) of the same information class (open woodland) are resolved as different spectral classes. In this study, accuracy was poor unless the criterion for accurate classification of a sample point was relaxed to include adjacent tree density classes. Then results are

reasonable accurate. In this environment, the product of a multispectral classification might not be an accurate map, but it may provide a good stratification for inventory (of tree density, or biomass) and for application of biophysical remote sensing models. Spatial-spectral classification would presumably produce a more accurate map, but until the algorithms are commonly available on commercial image processing systems, it does not provide a viable alternative for environmental analysis in remote regions. For resource assessment over large areas, and research on macroscale biophysical processes, an accurate stratification is a very useful tool.

REFERENCES

Ackerson, V., "Multistage variable probability sampling of tropical dry woodlands for fuelwood resource assessment," Masters Thesis, Department of Geography, University of California, Santa Barbara, 1985.

Adeniyi, P. O., "Digital analysis of multitemporal Landsat data for land-use/land-cover classification in a semi-arid area of Nigeria," *Photogrammetric Engineering and Remote Sensing*, vol. 51, pp. 1761-1774, 1985.

Adeniyi, P. O., "Agricultural land use inventory and mapping in Nigeria: the application of remote sensing," in *Remote Sensing and Tropical Land Management*, ed. John Wiley and Sons, pp. 175-187, 1986.

Ajtay, G. L, Ketner, P., and Duvigneaud, P., "Terrestrial primary production and phytomass," in *The Global Carbon Cycle*, ed. B. Bolin, E.T. Degens, S. Kempe and P. Ketner, pp. 129-181, SCOPE 13, John Wiley and Sons, New York, 1979.

Anderson, J. R., Hardy, E. E., Roach, J. T., and Witmer, R. E., "A Land-use and Land Cover Classification System for Use with Remotely Sensed Dadta," U.S. Geologic Survey Professional Paper 964, p. 28, 1976.

Card, D. H., "Using known map category marginal frequencies to improve estimates of thematic map accuracy," *Photogrammetric Engineering and Remote Sensing*, vol. 48, pp. 431-439, 1982.

Congalton, R. G. and Mead, R. A., "A quantitative method to test for consistency and correctness in photointerpretation," *Photogrammetric Engineering and Remote Sensing*, vol. 49, pp. 69-74, 1983.

Cooley, M. E. and Turner, R. M , "Application of Landsat products in range- and water-management problems in the Sahelian zone of Mali, Upper Volta, and Niger," *U. S. Geologic Survey Professional Paper 1058*, p. 52, United States Government Printing Office, Washington, D.C., 1982.

Deutsch, M., *East African Seminar and Workshop on Remote Sensing of Natural Resources and Environment,* Geologic Survey Report No. IR-NC-41 Washington, D.C., Nairobi, Kenya, 1975.

Diarra, L. and Hiernaux, P., "Evolution de la végétation sahélienne après la sécheresse bilan du suivi des sites du Gourma en 1986," Programme des Zones Aride et Semi-aride, Document du Programme, Centre International pour l'Elevage en Afrique (CIPEA), Bamako, Mali, 1987.

Franklin, J., Logan, T. L., Woodcock, C. E., and Strahler, A. H., "Coniferous forest classification and inventory using Landsat and digital terrain data," *IEEE Transactions on Geoscience and Remote Sensing*, vol. GE-24, pp. 139-149, 1986.

Franklin, J. and Strahler, A. H., "Invertible canopy reflectance modeling of vegetation structure in semiarid savanna," *IEEE Geoscience and Remote Sensing*, 1988. Accepted for publication.

Hellden, U., A Test of Landsat-2 Imagery and Digital Data for Thematic Mapping, Illustrated by an Environmental Study in Northern Kenya, Lund University Department of Physical Geography, 1980.

Helldén, U., "An assessment of woody biomass, community forests, land use and soil erosion in Ethiopia — A feasability study on the use of remote sensing and GIS-analysis for planning purposes in developing countries," *Lund Studies in Geography*, vol. 14, Department of Geography, University of Lund, Lund, Sweden, 1987.

Hiernaux, P., Cissé, M. I., and Diarra, L., "Bilan d'une saison d'es pluies 1984 très déficitaire dans la Gourma (Sahel Malien). Première campagne de suivi et télédetection expérimentale, Annexe: Fiches descriptives des sites," Programme des Zones Aride et Semi-aride, Document du Programme, Centre International pour l'Elevage en Afrique (CIPEA), Bamako, Mali, 1984.

Hiernaux, P. and Diarra, L., "Pour une technique de télédetection appliquée au sui de l'evolution de la végétations sahélienne," Programme des Zones Aride et Semi-aride, Document du Programme, Centre International pour l'Elevage en Afrique (CIPEA), Bamako, Mali, 1986.

Hiernaux, P. H. Y. and Justice, C. O., "Suivi du développement végétal au cours de l'été 1984 dans le Sahel Malien," *International Journal of Remote Sensing*, vol. 7, pp. 1515-1531, 1986.

Hudson, W. D. and Ramm, C. W., "Correct formulation of the Kappa coefficient of agreement," *Photogrammetric Engineering and Remote Sensing*, vol. 53, pp. 421-422, 1987.

Jacobberger, P. A., "Geomorphology of the upper inland Niger delta," *Journal of Arid Environments*, 1986. Submitted for publication

Jensen, J., "Biophysical remote sensing," *Annals of the Association of American Geographers*, vol. 73, pp. 111-132, 1983.

Kihlblom, U. and Johansson, D., *Satellite Monitoring of Vegetation and Geology in Semi-Arid Environments*, p. 98, Vattenbyggnadsbyran Ltd., Stockholm, 1980.

Lanley, J. P. and Clement, J., "Tropical Forest Resources Assessment Project (in the framework of GEMS - Global Environmental Monitoring System)," in *Forest Resources of Tropical Africa, Part 1- Regional Synthesis*, UN FAO/UNEP (United Nations Food and Agricultural Organization/ United Nations Environmental Programme), Rome, 1982.

Le Houerou, H. N., "The rangelands of the Sahel," *Journal of Rangeland Management*, vol. 33, pp. 41-46, 1980.

Makhanya, E. M., "Agricultural land use mapping in Lesotho: Problems and limitations," in *Remote Sensing and Tropical Land Management*, ed. John Wiley and Sons, pp. 215-222, 1986.

Mushala, H. M., "Multistage remote sensing land systems and soil erosion in central Tanzania," in *Remote Sensing and Tropical Land Management*, ed. John Wiley and Sons, pp. 223-234, 1986.

Negri, D. S., *Vegetation mapping using Landsat in a semi-arid region of Africa*, University of California, Santa Barbara, 1985. Masters thesis

Nielsen, M., *Introduction to the Flowering Plants of West Africa,* University of London Press, London, 1965.

Olsson, K., "Remote sensing for fuelwood resources and land degradation studies in Kordofan, the Sudan," Ph.D. Dissertation., The Royal University of Lund, Department of Geography, Lund, Sweden , 1985. 182 pp.

Prince, S. D. and Astle, W. L., "Satellite remote sensing of rangelands in Botswana. I. Landsat MSS and herbaceous vegetation," *International Journal of Remote Sensing,* vol. 7, pp. 1533-1553, 1986.

Rosenfeld, G. H., Fitzpatrick-Lins, K., and Ling, H. S., "Sampling for thematic map accuracy testing," *Photogrammetric Engineering and Remote Sensing,* vol. 48, pp. 131-137, 1982.

Rosenfield, G. H. and Fitzpatrick-Lins, K., "A coefficient of agreement as a measure of thematic classification accuracy," *Photogrammetric Engineering and Remote Sensing,* vol. 52, pp. 223-227, 1986.

Schnell, R., *Introduction á la Phytogéographie des Pays Tropicaux: 3. La Flore et la Végétation de l'Afrique Tropicale.* Gauthiers-Villars, Paris, 1977.

Schultz, J., "Applications of Landsat satellite imagery for resource inventory and evaluation in developing countries," *GeoJournal,* vol. 3.1, pp. 53-62, 1979.

Strahler, A. H., "Stratification of natural vegetation for forest and rangeland inventory using Landsat digital imagery and collateral data," *International Journal of Remote Sensing,* vol. 2, pp. 15-41, 1981.

Townshend, J. R. G. and Justice, C. O., "Analysis of the dynamics of African vegetation using the normalized difference vegetation index," *International Journal of Remote Sensing,* vol. 7, pp. 1435-1445, 1986.

USAID-TAMS, *Le Ressources Terrestres au Mali: Mali Land and Water Resources,* Government de la Republique du Mali Ministere Charge du Development Rural, 1983.

Williams, M. G., "Landsat and the detectability of land systems in northern Kenya," in *Remote Sensing and Tropical Land Management,* ed. J. T. Parry, pp. 101-130, 1986.

Table I

Thematic Mapper Scenes				
Name	Date	Path	Row	Scene ID
Gourma	9 Sep 1984	195	49	5019209552
Gourma	7 May 1985	195	49	5043209552
Segou	17 Nov 1984	198	51	5026110142

Subimage Coordinates				
Name	Starting Sample	Starting Line	Number Samples	Number Lines
1984 Gossi *	1865	1	1536	1536
1985 Gossi *	1120	1	1536	1536
Gossi clas. †	256	1	1024	1280
1984 Hombori *	821	1	1536	1024
1985 Hombori *	70	1	1536	1024
Hombori clas. †	256	256	1280	768
Segou1 *	977	1905	1024	512
Segou2 *	2001	1629	512	512

* with reference to TM quadrat
† with reference to registered subimages

Table II

Summary of Principal Components Analysis — Gossi				
	Principal Components (first four)			
Spectral band	1	2	3	4
1984 Band 3	0.437	-0.582	-0.433	0.150
1984 Band 4	0.351	-0.249	0.118	-0.832
1984 Band 7	0.517	0.445	-0.558	0.088
1985 Band 3	0.355	-0.311	0.421	0.527
1985 Band 4	0.295	-0.082	0.430	-0.027
1985 Band 7	0.453	0.545	0.353	0.005
Eigenvalues	2275.727	204.561	73.779	26.199
Percent var.	87.769	7.889	2.845	1.010
Cumul. percent	87.769	95.695	98.504	99.514

Summary of Principal Components Analysis — Hombori				
	Principal Components (first four)			
Spectral band	1	2	3	4
1984 Band 3	0.391	-0.352	0.292	-0.402
1984 Band 4	0.339	-0.257	0.562	0.645
1984 Band 7	0.475	-0.562	-0.490	-0.120
1985 Band 3	0.384	0.417	0.236	-0.515
1985 Band 4	0.346	0.360	0.236	0.025
1985 Band 7	0.490	0.429	-0.498	0.377
Eigenvalues	1395.398	112.214	17.356	10.613
Percent var.	90.533	7.280	1.126	0.689
Cumul. percent	90.533	97.813	98.940	99.628

Vegetation Classification System										
Woody Cover			(dark) Background (light)							
Class	% Cover	Symbol	Water	Rock outcrops	Gravels, silts	Sand sht rck/grv	Clay, loams	Silt, loams	Loamy sands	Sand dunes
Woodland	20-80	W								
dense	40-80	Wd				g		g	g,h	
sparse	20-40	Ws			g	g	g	g,h	(s)	g
Wooded Grassland	3-20	WG								
dense	10-20	WGd			g	g	g,h	g,h	(s) h	g,h
sparse	3-10	WGs		g,h	g	g,h	g,h	g,h	(s) g,h	g,h
very sparse	1-3	WGvs		g,h	g	g,h	g,h	g,h	g,h	g,h
Woodland/Bush		WB								
thicket	80-100	WBt								
dense	40-80	WBd						(s)		
sparse	20-40	WBs						(s)		
Wood/Bush Grslnd	3-20	WBG								
dense	10-20	WBGd								
sparse	3-10	WBGs								
Bushland		B								
thicket	80-100	Bt						g,h		
dense	40-80	Bd	(s)							
sparse	20-40	Bs								
Bush Grassland	3-20	BG								
dense	10-20	BGd								
sparse	3-10	BGs								
Grassland	0-1	G	(s) g	g,h	g,h	g,h	g,h	g,h	g,h	
Water	0	H	(s) g,h							
Bare	0	S	(s)	g,h	g,h		(s)	g,h		
Riparian veg.	-	R	(s)							

g — class occurs in Gossi subimage
h — class occurs in Hombori subimage
(s) — class occurs in Segou (soil only differentialed as dark or light)

Table IV

Land Cover — Gourma				
Number	Symbol	Cover Type	Percent of subimg.	Area** (ha)
1.	Wd	Woodland, dense	0.23†	475
2.	Ws	Woodland, sparse	1.04	2147
3.	WGd	Wooded Grassland, dense	6.05	12490
4.	WGs	Wooded Grassland, sparse	12.24	25268
5.	WGvs	Wooded Grassland, very sprs	34.87	71985
*	Bt	Bushland thicket	0.40	826
6.	G	Grassland	40.43	83463
7.	S	Bare (soil)	2.13	4397
8.	H	Water (lake)	0.42	867
	Total		100.00	206438

Aggregated by vegetation class (soil classes not differentiated).
† sum of areas in Gossi and Hombori subimages
* — not sampled in accuracy assessment
** — estimate based on 30x30 m TM pixels

Table V

Land Cover — Segou					
Number	Symbol	Cover Type	Soil	Percent of subimg.	Area** (ha)
1	Gl	Grassland	light	6.31	4031
2	Sl	Bare	light	0.43	275
3	WGsl	Wooded Grassland, sparse	light	23.95	15299
4	Wsl	Woodland sparse	light	4.76	3041
5	WGdl	Wooded Grassland, dense	light	16.38	10463
6	WBsl	Woodland/Bush sparse	light	6.46	4127
7	WBdl	Woodland/Bush dense	light	25.67	16397
8	Bdd	Bushland dense	dark	6.72	4293
9	R	Riparian		4.05	2587
10	Sd	Bare	dark	0.42	268
11	H	Water		4.86	3105
	Total			100.00	63878

** — estimate based on 30x30 m TM pixels

Table VI

Classification Error Matrix — Gourma subimages

Classified	Reference (Photointerpreted) Data									
	Wd	Ws	WGd	WGs	WGvs	G	S	Water	Total	mmp
1. Wd	0	0	1	0	0	0	0	0	1	0.0
2. Ws	0	4	1	0	0	1	1	0	7	0.01
3. WGd	1	2	8	3	0	1	1	0	16	0.06
4. WGs	0	1	8	15	9	9	2	0	44	0.12
5. WGvs	0	2	2	12	35	24	11	0	86	0.35
6. G	0	0	3	7	13	43	7	0	73	0.40
7. S	0	0	0	0	1	6	15	0	22	0.02
8. Water	0	0	0	0	0	0	0	21	21	0.0
Total	1	9	23	37	58	84	37	21	270	1
tmp	0	0.03	0.08	0.16	0.3	0.39	0.12	0	1	0.0

mmp: mapped marginal proportions
tmp: true marginal proportions

Table VII

Classification Error Matrix — Segou subimage

Classified	Reference (Photointerpreted) Data											
	Gl/Sl	WGsl	WGdl	Wsl	WBsl	WBdl	Bdd	Sd	R	H	Total	mmp
1,2 Gl/Sl	50	0	0	0	0	0	0	0	0	0	50	0.07
3. WGsl	2	25	1	0	0	0	0	0	0	0	28	0.24
4. WGdl	0	4	10	1	2	3	2	0	0	0	22	0.16
5. Wsl	2	1	2	4	2	0	0	3	0	0	14	0.05
6. WBsl	0	0	2	0	23	1	1	0	0	0	27	0.06
7. WBdl	0	1	1	0	4	20	1	0	0	0	27	0.26
8. Bdd	1	0	0	0	0	1	14	1	4	0	21	0.07
9. Sd	0	0	0	0	0	0	0	24	0	0	24	0.004
10. R	2	2	0	1	1	0	0	2	18	0	26	0.04
11. Water	0	0	0	0	0	0	0	0	0	25	25	0.05
Total	57	33	16	6	32	25	18	30	22	25	264	1.00
tmp	0.1	0.24	0.14	0.04	0.13	0.24	0.08	0.04	0.05	0.05	1.00	

mmp: mapped marginal proportions
tmp: true marginal proportions

Table VIII

Accuracy of Classification — Gourma subimages

No.	Class	Commission	% Correct Mapped*	upper	lower	% Correct True	upper	lower	Kappa
1.	Wd	0.0	0.0	NA	NA	0.0	NA	NA	0.0
2.	Ws	0.57	0.44	0.41	0.48	0.18	0.15	0.22	0.56
3.	WGd	0.50	0.35	0.31	0.39	0.27	0.23	0.31	0.45
4.	WGs	0.34	0.41	0.36	0.45	0.30	0.26	0.35	0.24
5.	WGvs	0.41	0.60	0.53	0.68	0.69	0.62	0.77	0.24
6.	G	0.59	0.51	0.44	0.59	0.53	0.46	0.61	0.40
7.	S	0.68	0.41	0.38	0.43	0.07	0.05	0.10	0.63
8.	H	1.00	1.00	0.97	1.03	1.00	0.97	1.03	1.00
	Total	0.52	0.52	0.0	0.0	0.51	NA	NA	0.40

* — i.e., omission

Lenient Accuracy Criterion

No.	Class	Commission	Omission	Kappa
1.	Wd	0.0	0.0	0.0
2.	Ws	0.67	0.86	0.85
3.	WGd	0.74	0.81	0.93
4.	WGs	0.81	0.73	0.66
5.	WGvs	1.00	0.95	0.76
6.	G	0.87	0.96	0.97
7.	S	0.89	1.00	1.29
8.	H	1.00	1.00	1.00
	Total	0.91	0.91	0.87

Table IX

Accuracy of Classification — Segou subimage

No.	Class	Commission	% Correct Mapped*	upper	lower	% Correct True	upper	lower	Kappa
1,2	Gl/Sl	1.00	0.88	0.81	0.94	0.61	0.54	0.67	1.00
3	WGsl	0.89	0.76	0.62	0.90	0.74	0.60	0.88	0.88
4	WGdl	0.45	0.63	0.52	0.73	0.73	0.62	0.83	0.42
5	Wsl	0.29	0.67	0.59	0.75	0.73	0.65	0.81	0.27
6	WBsl	0.85	0.72	0.65	0.79	0.37	0.30	0.44	0.83
7	WBdl	0.74	0.80	0.64	0.96	0.85	0.69	1.01	0.71
8	Bdd	0.67	0.78	0.69	0.87	0.62	0.53	0.70	0.64
9	Sd	1.00	0.80	0.78	0.82	0.09	0.07	0.12	1.00
10	R	0.69	0.82	0.75	0.88	0.69	0.62	0.75	0.66
11	Water	1.00	1.00	0.91	1.09	1.00	0.91	1.09	1.00
	Total	0.81	0.81	0.0	0.0	0.76	0.70	0.83	0.78
				Pooled Classes					
1,2	Gl/Sl	1.000	0.877	0.813	0.942	0.686	0.621	0.750	1.000
3,4,5	WGd,sl/Wsl	0.762	0.873	0.857	0.889	0.758	0.742	0.774	0.699
6,7	WBd,sl	0.889	0.842	0.826	0.858	0.707	0.691	0.724	0.858
8	Bdd	0.667	0.778	0.772	0.783	0.218	0.213	0.224	0.642
9	Sd	1.000	0.828	0.477	1.178	0.714	0.363	1.064	1.000
10	R	0.692	0.818	0.409	1.228	0.817	0.408	1.227	0.664
11	Water	1.000	1.000	0.883	1.117	1.000	0.883	1.117	1.000
	Total	0.863	0.863	0.807	0.908	0.469	0.405	0.534	0.785

* — i.e., omission

Lenient Accuracy Criterion

No.	Class	Commission	Omission	Kappa
1,2	Gl/Sl	0.91	1.00	1.03
3	WGsl	0.88	1.00	1.02
4	WGdl	0.94	0.77	0.71
5	Wsl	0.83	0.57	0.45
6	WBsl	0.97	0.96	1.06
7	WBdl	0.84	0.89	0.82
8	Bdd	0.78	0.67	0.64
9	Sd	0.80	1.00	1.00
10	R	0.82	0.69	0.66
11	Water	1.00	1.00	1.00
	Total	0.89	0.89	0.87